GTSE1 regulates microtubule stability during mitosis through inhibition of the microtubule depolymerase MCAK

Inaugural-Dissertation zur
Erlangung des Doktorgrades
Dr. rer. nat.

der Fakultät für Biologie
an der
Universität Duisburg-Essen

vorgelegt von
Shweta Bendre
aus Pune, Indien

durchgeführt am
Max Planck Institut für molekulare Physiologie
Abteilung für mechanistische Zellbiologie
AG Bird

Juni 2017

Die der vorliegenden Arbeit zugrunde liegenden Experimente wurden am Max Planck Institut für molekulare Physiologie in der Abteilung für mechanistische Zellbiologie durchgeführt.

1. Gutachter: Prof. Dr. Andrea Musacchio
2. Gutachter: Prof. Dr. Stefan Westermann

Vorsitzender des Prüfungsausschusses: Prof. Dr. Christian Johannes

Tag der mündlichen Prüfung: 6th September 2017

Publications

Bendre, S., Rondelet, A., Hall, C., Schmidt, N., Lin, Y. C., Brouhard, G. J., & Bird, A. W. (2016). GTSE1 tunes microtubule stability for chromosome alignment and segregation by inhibiting the microtubule depolymerase MCAK. *The Journal of cell biology, 215(5)*, 631-647.

List of Tables

List of Figures

List of Abbreviations

ADP – Adenosine diphosphate

APC – Anaphase Promoting Complex

ATP – Adenosine triphosphate

BACs – Bacterial Artificial Chromosomes

bp – basepair

CBB – Coomassie Brilliant Blue

CCAN – Constitutive Centromere-Associated Network

Cdk – Cyclin Dependent Kinase

CIN – Chromosomal Instability

Co-IP – Co-immunoprecipitation

CPC – Chromosome Passenger Complex

CREST – Calcinosis, Raynaud's syndrome, Esophageal dysmotiliy, Sclerodactyly, Telangiectasia

DAPI – 4,6-diamidin-2-phenylindoldihydrochlorid

ddH_2O – double distilled water

DMEM – Dulbecco's Modified Eagle Medium

DMSO – Dimethyl sulfoxide

DNA – Deoxyribonucleic acid

D-TACC – Drosphila-Transforming Acid Coiled-coil Containing Protein 3

EB – End Binding

FDAPA – Fluorescence Dissipation After Photoactivation

FISH – Fluorescence *In Situ* Hybridization

FL – fulllength

FSG – Fish skin gelatin

GDP – Guanosine-5'-triphosphate

GTP – Guanosine-5'-triphosphate

GTSE1 – G2 and S phase expressed 1

ICIS – Inner Centromere KinI Stimulator

kDa – kilo Dalton

KMN – KNL, Mis12, and Ndc80 Network

KT – Kinetochore

KT-MT – Kinetochore-Microtubule attachment

LB – Luria-Bertani medium

M – Molecular weight marker

M-phase – Mitotic phase

mA – milli Ampere

MAPs – Microtubule Associated Proteins

Mad – Mitotic Arrest Deficient

MCAK – Mitotic Centromere Associated Kinesin

MCC – Mitotic Checkpoint Complex

MCRS1 – Microspherule protein 1

MT – Microtubule

NEBD – Nuclear Envelope Breakdown

NuSAP – Nucleolar and Spindle Associated Protein 1

Nup98 – Nucleoporin 98

PBS – Phosphate buffered saline

PCR – Polymerase Chain Reaction

Plk1 – Polo Like Kinase 1

S-phase – Synthesis phase

SAC – Spindle Assembly Checkpoint

SEC – Size Exclusion Chromatography

TACC3 – Transforming Acid Coiled-coil Containing Protein 3

TCEP – Tris-(2-carboxyethyl)-phosphine

TPX2 – Targeting Protein for Xklp2

V – Volts

wt – Wildtype

+TIP – Plus tip interacting proteins

Table of Contents

1. Introduction

The maintenance of genome stability is crucial for survival and propagation of progeny. Integrity of the genome is maintained by equally partitioning the duplicated set of chromosomes into two daughter cells during the process of cell division. The process of cell division is intricately regulated at multiple steps in time and cellular space to prevent any event of chromosome missegregation. Errors in segregation of chromosomes alter the cell ploidy, which is irreversible and can be the driving force of tumorigenesis (Compton, 2011). Frequent gain or loss of chromosomes during cell division leads to chromosomal instability (CIN), which has been reported to be a common feature of cancer cells and solid tumors (Mitelman et al., 2017). Recent reports show that CIN plays a causal role in tumour progression and that 90% of tumors are aneuploid (Duijf and Benezra, 2013; Schvartzman et al., 2010; Hassold and Hunt, 2001; Vanneste et al., 2009; Weaver and Cleveland, 2006). Aneuploidy and CIN are commonly observed in cancers, however, the exact molecular mechanisms underlying CIN are elusive and need further investigation.

1.1 The cell cycle

The eukaryotic cell cycle, consisting of a complex series of events, is essential for normal growth and development. It allows faithful duplication and segregation of chromosomes into two daughter cells and can be categorized into four phases: G1, S, G2 and M (Figure 1). In G1 (gap1) phase, the cell is metabolically active and prepares for the synthesis (S) phase (reviewed in Norbury and Nurse 1992). Chromosomes are duplicated in S-phase, which is followed by a G2 (gap2) phase, during which, the cell synthesizes proteins and prepares for mitosis (M phase). G1, S and G2 phases collectively are also referred to as interphase (Alberts 2002). In the M phase, the cell equally segregates its DNA and cytoplasm into two daughter cells (reviewed in Norbury and Nurse 1992).

The transition between different cell cycle phases is orchestrated in a highly organized and precise manner. The fidelity of cell cycle progression is maintained mainly by the cyclin dependent kinases (Cdks) and three major quality control checkpoints. The Cdks are Serine/Threonine kinases whose activity is regulated by binding to cyclins, their regulatory subunits. Cyclin protein levels oscillate during the cell cycle, periodically activating distinct Cdks that tightly control the transition from one cell cycle phase to the next in a timely manner (Morgan, 1995; reviewed in Norbury and Nurse, 1992; Pines, 1991; Evans et al., 1983).

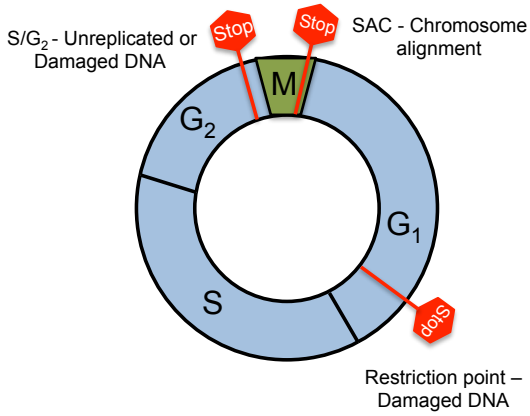

Figure 1. The eukaryotic cell cycle

The cell duplicates its DNA during the S phase. The two gap phases (G1 and G2) provide more time for the cell to prepare for the next steps and safeguard cell cycle progression at quality control checkpoints. The duplicated chromosomes and cytoplasm are segregated equally into two daughter cells during mitosis (M phase) and cytokinesis, respectively. The three cell cycle checkpoints; restriction point, DNA damage checkpoint and SAC are depicted in red.

Errors in any step of the cell cycle may lead to activation of checkpoints, thereby inducing cell cycle arrest. The first checkpoint is in the late G1 phase and is called the "restriction point" or "start" where the cell commits to genome duplication and a new round of cell division (Pardee, 1974; Hartwell, 1970). The second checkpoint is at the end of the G2 phase that ensures proper replication of DNA during S phase before the cell enters mitosis (reviewed in Lucas et al., 2004). The third checkpoint is called the spindle assembly checkpoint (SAC) that monitors proper chromosome attachments during metaphase and ensures accurate chromosome segregation (Musacchio and Salmon, 2007).

1.2 Mitosis

In 1882, Walther Flemming coined the term "mitosis", which refers to the "thread-like" appearance of chromosomes (Paweletz, 2001; Flemming, 1882). Today, the term mitosis is used to define the process of cell division, a highly complicated process involving multiple steps that are precisely controlled in time and cellular space. Mitosis is composed of two phases - karyokinesis and cytokinesis. During karyokinesis the duplicated set of chromosomes are equally distributed into two daughter cells. This phase can be further sub-divided into five distinct phases – prophase, prometaphase, metaphase, anaphase and telophase (Figure 2) (Alberts, 2002).

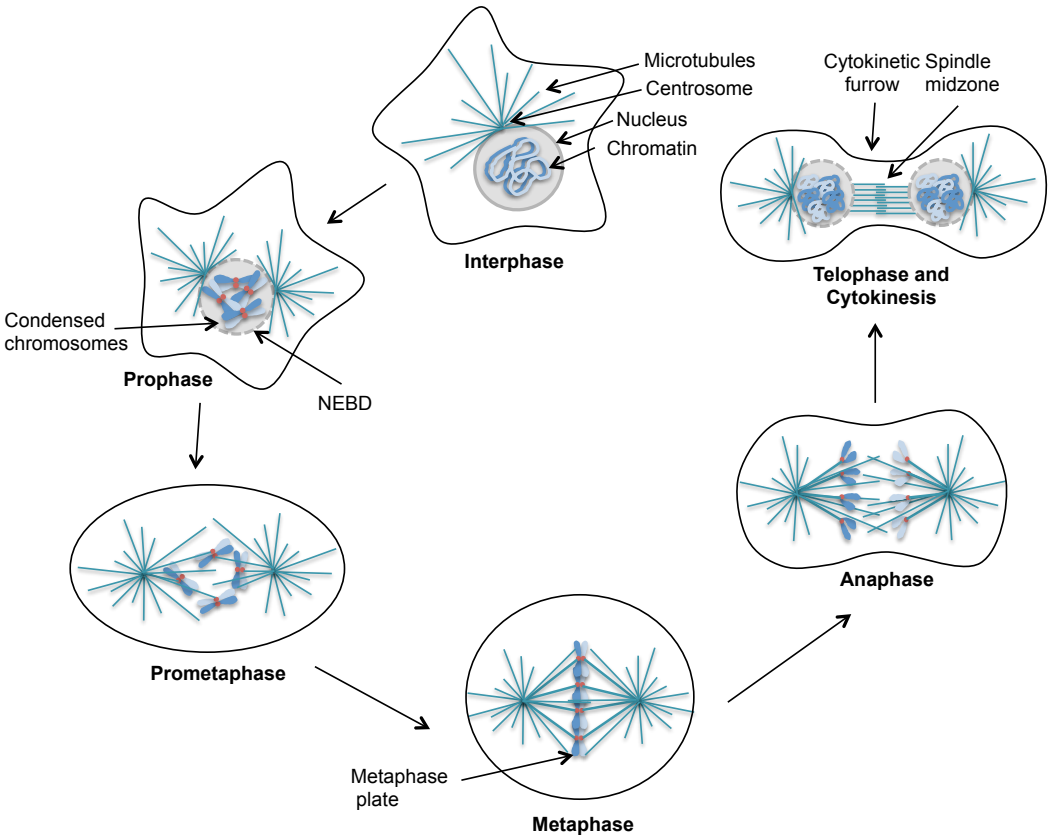

Figure 2. Schematic representation of the process of mitosis

The process of mitosis can be divided into five phases. During prophase, chromosomes condense and duplicated centrosomes begin to nucleate MTs and move to opposite sides of the nucleus. The transition from prophase to pro-metaphase is marked by nuclear envelope breakdown (NEBD). During prometaphase, the cell starts to build the mitotic spindle and MTs bind to specialized structures on chromosomes called kinetochores. During metaphase, chromosomes align at the metaphase plate and become bi-oriented. In anaphase, duplicated chromosomes are pulled towards opposite poles. In telophase, chromosomes decondense and the nuclear envelope reforms. Division of cytoplasm (cytokinesis) marks the end of mitosis.

During the first step of mitosis, DNA binding proteins like the condensin complex catalyze the condensation of duplicated DNA into discrete chromosomes (Schmiesing et al., 2000). Duplicated sister chromatids are bound to each other at a point called the “centromere” and are held together by the cohesin protein complex (Brooker and Berkowitz, 2014; Peters et al., 2008). In vertebrate cells, during prophase, duplicated centrosomes move to opposite sides of the nucleus and show an increase in nucleation of microtubules (MT), which are polar filaments required for building the mitotic spindle. During open mitosis in vertebrates, at the end of prophase the nuclear envelope disintegrates marking the beginning of prometaphase. This is accompanied by reorganization of the MT network to form the mitotic spindle. MTs

bind to kinetochores (KTs), which are specialized load-bearing protein assemblies fully built on the centromeric region of condensed chromosomes during late prophase. As the cell progresses into metaphase, a bipolar spindle is formed and chromosomes align at the metaphase plate. Following proper alignment of chromosomes at the metaphase plate, anaphase begins where cohesin is cleaved. This facilitates separation of sister chromatids, which are pulled towards the poles due to shortening of KT MTs. Segregated chromosomes, decondense in telophase and the nuclear envelope reforms. Cytokinesis marks the end of mitosis where the cytoplasm is equally distributed into two daughter cells. The cells are physically separated by formation of a contractile ring composed of actin and myosin at the spindle equator. This ring pinches the membrane at the cytokinetic furrow, ending the mitotic process.

1.3 Microtubules and the mitotic spindle

The interphase MT network undergoes an extensive rearrangement during mitosis to form a bipolar spindle. Proper assembly of a mitotic spindle depends on precise regulation of MTs, which are fundamental structural components of the cell division machinery (Petry, 2016; reviewed in Inoué and Salmon, 1995). MTs are hollow polymers composed of α- and β-tubulin heterodimers that polymerize in a head-to-tail fashion to form a polar protofilament (Amos and Klug, 1974; Weisenberg et al., 1968). Lateral association of 11 to 13 such protofilaments forms a MT, which is approximately 25 μm in diameter (reviewed in Desai and Mitchison, 1997). MTs are polar structures showing a dynamic fast growing plus end where the β-tubulin is exposed and a stable slow growing minus end where a α-tubulin is exposed (Allen and Borisy, 1974). MTs show rapid alternating phases of growth and shrinkage/catastrophe at the plus end that corresponds to rapid addition and removal of tubulin dimers, respectively. These alternating phases of MT growth and shrinkage are together termed as "dynamic instability", which is an intrinsic property of MTs (Mitchison and Kirschner, 1984a) (Figure 3A). Each tubulin subunit binds to two GTP molecules and hydrolysis of one of the GTP molecules is crucial for regulating 'dynamic instability' (Weisenberg et al., 1968). The GTP bound to α-tubulin is stable and is not hydrolyzed as it is trapped at the αβ-tubulin heterodimer interface. The GTP bound to β-tubulin however, is exposed and is hydrolyzed to GDP by an incoming tubulin dimer (MacNeal and Purich 1978; David-Pfeuty et al., 1977; Spiegelman et al., 1977; Weisenberg et al., 1976;). The dynamic instability of the plus end is controlled by stochastic loss and gain of a GTP cap (Duellberg et al., 2016; Mitchison and Kirschner, 1984b). MTs formed using non-hydrolysable GTP analogs are more stable; suggesting that hydrolysis of

GTP to GDP makes the MT lattice unstable inducing catastrophes (Mejillano et al., 1990). In cells the minus end is stably anchored at the microtubule organizing center and the plus end shows dynamic instability. MT dynamic instability in cells is differentially regulated by cellular factors during interphase and mitosis. Previous studies have shown that the plus end of MTs in solution containing only purified tubulin and GTP are less dynamic as compared to the plus ends of MTs in interphase (Desai and Mitchison, 1997). Furthermore, MTs during mitosis show markedly higher dynamic instability as compared to MTs during interphase (Zhai et al., 1996; Saxton et al., 1984). This distinct transition in the MT dynamics during mitosis is believed to be important for maintaining steady-state spindle structure required for chromosome attachment and segregation (Hyman and Karsenti, 1996).

During mitosis, a bipolar spindle is assembled by coordination between centrosome-, chromatin- and MT-mediated MT nucleation pathways. In most animal cells, the centrosomes, comprising of a pair of centrioles and pericentriolar matrix, act as master MT nucleators during interphase and mitosis (reviewed in Posser and Pelletier, 2017; Kapoor, 2017). In cells without centrosomes, a chromatin-mediated MT nucleation pathway plays a dominant role. A RanGTP gradient is formed around chromatin that drives chromatin-based MT nucleation (reviewed in Posser and Pelletier, 2017; Kapoor 2017). MT-mediated MT nucleation occurs when MTs are also nucleated from nucleation factors bound to the MT lattice (reviewed in Prosser and Pelletier, 2017; Kapoor, 2017). These pathways work together redundantly to ensure timely execution of mitosis, and manipulating either of the pathways has a minor effect on spindle formation (reviewed in Prosser and Pelletier, 2017; Kapoor, 2017).

A bipolar spindle is constructed with MTs nucleated by a combination of these pathways and broadly contains three types of MTs as shown in Figure 3B (reviewed in Howard and Hyman, 2003). Interpolar MTs have their minus ends embedded at the centrosomes and the plus ends overlap and crosslink with other interpolar MT plus ends. These MTs are necessary for maintaining spindle shape and size during prometaphase and metaphase (Sharp et al., 2000). Astral MTs have their minus ends embedded at the spindle poles and their plus ends are free to interact with the cell cortex. Astral MTs are required for proper orientation of the spindle, which is important for defining the subsequent axis for formation of the cleavage furrow (Stevermann and Liakopoulos, 2012). Third types of MTs, known as kinetochore microtubules (KT MTs), have their plus ends bound to KTs. These KT MTs form discrete

bundles of 20-25 KT MTs, which are further cross-linked and stabilized by formation of inter-MT bridges (Rieder et al., 2005; McDonald et al., 1992; Witt et al., 1981; Rieder et al., 1981; Hepler et al., 1970). In vertebrate cells, such a bundle of KT MTs is known as a K-fiber. The K-fiber reaches the centrosome and needs to be stably anchored to KTs for proper chromosome alignment and segregation.

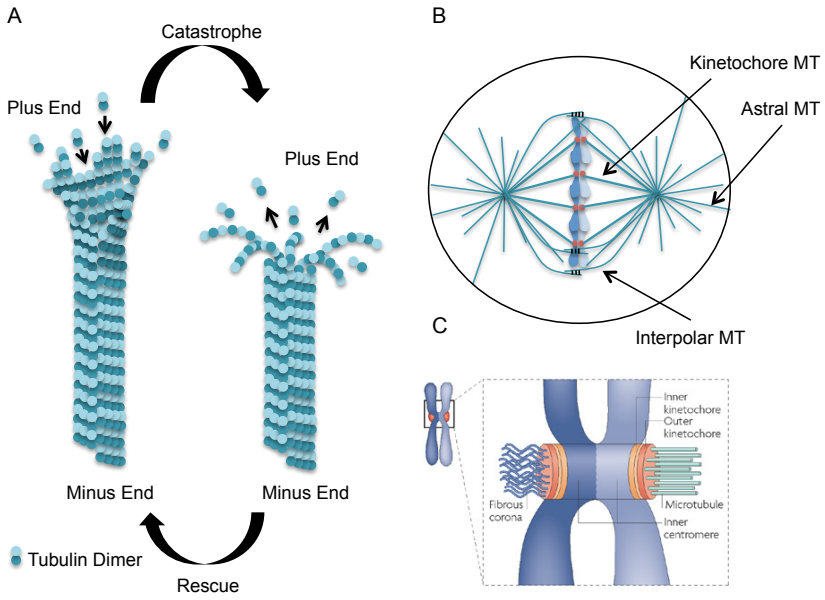

Figure 3. Microtubule dynamic instability, mitotic spindle and kinetochore

A. MTs are polar polymers made of αβ-tubulin heterodimers. MTs have a stable minus end and a dynamic plus end. MTs show phases of growth and shrinkage and this intrinsic property of MTs is called dynamic instability. Catastrophe happens when a MT starts shrinking. Rescue is when a shrinking MT plus end resumes growth by addition of tubulin dimers. **B.** Schematic representation of three types of MTs in a bipolar spindle. Interpolar MTs start from the centrosomes and overlap with other non-KT MTs. Astral MTs originate from the spindle pole and reach the cortex of the cell. K-fibers emanate from the centrosomes and bind to the KT. **C.** Schematic representation of the KT showing a dense inner and outer plate and a fibrous corona. (Image is taken from Santaguida and Musacchio, 2009.)

The KT is a highly conserved complex assembly of proteins, which appears as a trilaminar plate in vertebrates, and shows an electron-dense inner and outer plate and a translucent middle plate (Santaguida and Musacchio, 2009; Dong et al., 2007) (Figure 3C). The KT is built on tightly packed centromeric heterochromatin. The inner centromere is the centromeric region that connects two sister chromatids and harbours an error correction machinery including the CPC, which helps in correcting KT MT mal-attachments (Wang et al, 2010; Liu

et al, 2009). The inner KT contains the constitutive centromere associated network (CCAN) complex, which associates with centromeric DNA and provides a sturdy platform for building the outer KT (Weir et al, 2016; Basilico et al, 2014; Cheeseman and Desai, 2008; McClelland et al, 2007; Foltz et al, 2006; Okada et al, 2006). The outer KT contains the Knl1-Mis12-Ndc80 (KMN) complex, which binds to the inner KT on one hand and forms the MT-binding interface on the other hand (Foley and Kapoor, 2013; Przewloka et al, 2011; Screpanti et al, 2011; Cheeseman and Desai, 2008; Janke et al, 2001; Wigge and Kilmartin, 2001). In the absence of MTs, an outer corona layer is exposed that harbors several proteins that are part of the SAC, which plays a fundamental role in detecting proper kinetochore microtubule (KT-MT) attachments (Foley and Kapoor, 2013; Lara-Gonzalez et al., 2012; Musacchio and Salmon, 2007).

1.3.1 Kinetochore-microtubule attachments

For a diploid human cell, it is a challenging task to precisely align all 46 chromosomes at the metaphase plate followed by accurate segregation into two daughter cells in a short time-span. Therefore, it is important for the cell to rapidly establish (meta)-stable KT-MT attachments while also efficiently correcting erroneous ones. One of the earliest “search and capture” theories to explain rapid association of KTs with MTs at the onset of mitosis was proposed by Mitchison and Kirschner in 1984a. According to this theory, MTs ‘search’ for KTs and then ‘capture’ it to establish a (meta)-stable KT-MT interaction. This “search and capture” of KTs by MTs is a stochastic process that leads to several sporadic KT-MT mal-attachments during prometaphase. These mal-attachments include ‘monotelic’ attachments where the KT of one sister chromatid is attached to MTs coming from one spindle pole, whereas the other KT remains unattached (Figure 4B) (Rieder et al., 1995; Rieder et al., 1994). A second type of mal-attachment is ‘syntelic’ attachment, where KTs of both sister chromatids bind to MTs emanating from one spindle pole (Figure 4C). A third type of mal-attachment is the ‘merotelic’ attachment, where the KT of one sister chromatid is bound to MTs originating from one spindle pole but the other KT simultaneously binds to MTs emanating from both spindle poles (Figure 4D) (Cimini et al., 2003).

These mal-attachments are efficiently corrected by an error correction machinery to amphitelic attachments, where the KT of each sister chromatid binds to MTs emanating from respective spindle poles. This type of alignment, also known as bi-orientation, is a pre-requisite for proper chromosome segregation (Figure 4A). Centromere geometry and back-to-back orientation of

the sister chromatids inherently promotes the possibility of formation of amphitelic attachments (Lončarek et al., 2007; Indjeian and Murray, 2007). Amphitelic attachments lead to generation of tension due to pulling forces exerted at the KTs by depolymerizing KT MTs and the resistance created due to the presence of cohesin. This tension results in labile-to-stable transition of amphitelic KT-MT attachments. In presence of unattached KTs, the SAC is "activated" and transmits a "wait" signal that ultimately leads to a mitotic arrest due to formation of a mitosis inhibitory complex called the mitotic checkpoint complex (MCC). The MCC is a ternary complex composed of Cdc20, Mad2, Bub3 and BubR1 that prevents premature anaphase onset by inhibiting the anaphase promoting complex (APC/C) (Lara-Gonzalez et al. 2012). Once all the sister chromatids display amphitelic attachments, via a series of complex steps the MCC is disassembled, leading to release of Cdc20 and this subsequently associates with APC/C and activates the APC/C (Musacchio and Desai, 2017; Lara-Gonzalez et al. 2012). Activated APC/C then catalyzes the degradation of the Cdk1 regulatory subunit cyclin B, leading to a drop in Cdk1 activity. This releases separase from the inhibitory act of securin after which, separase is free to cleave cohesin thereby, allowing separation of sister chromatids and initiating anaphase.

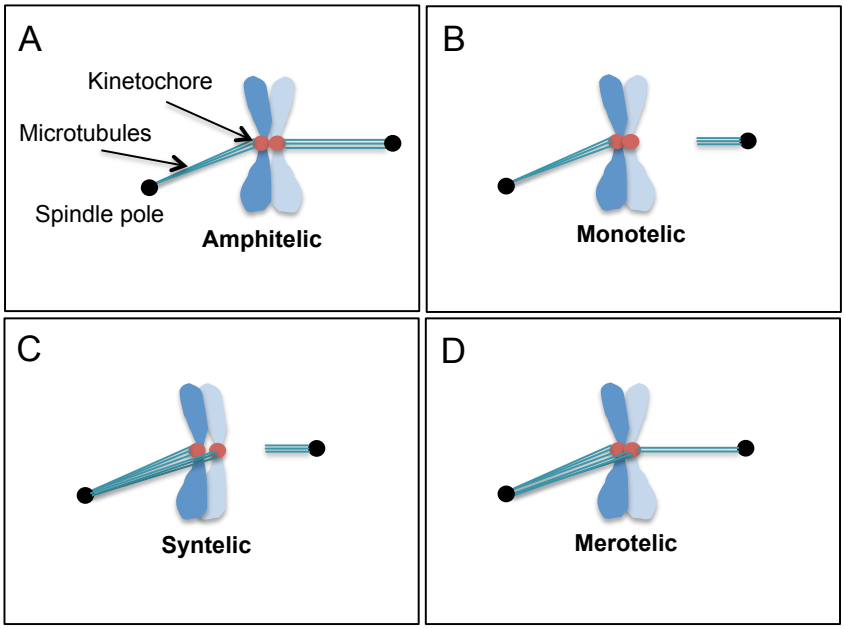

Figure 4. Kinetochore-microtubule attachments

Schematic representation of KT-MT attachments. **A.** Amphitelic attachment. Both KTs bind to MTs coming from the respective spindle poles leading to bi-orientation. **B.** Monotelic attachment. KT of only one sister chromatid is bound to MTs whereas the other one is unattached. **C.** Syntelic attachment. KTs of both sister chromatids are attached to MTs coming from one spindle pole. **D.** Merotelic attachment.

KT of one sister chromatid is bound to MT coming from one spindle pole but the KT of the other sister is bound to MTs coming from both spindle poles.

Of all the above-mentioned mal-attachments, merotelic attachments represent a particular challenging problem for the mitotic cell. In a merotelic attachment, both KTs are occupied by MTs and enough tension is generated within the KTs. If these KT-MT mal-attachments remain unresolved then they generally evade the SAC, leading to premature anaphase onset (Cimini and Degrassi, 2005; Cimini et al., 2001). This leads to so-called 'lagging chromosomes' during anaphase, where a chromosome lags behind at the spindle equator as it encounters equal forces from both spindle poles. Merotelic attachments are the most common cause of chromosome mis-segregation and are frequently observed in CIN cancer cell lines (Thompson and Compton 2008; Cimini et al., 2001). Therefore, it is critical for the cell to timely correct merotelic attachments to avoid chromosome mis-segregation. Central to this objective is the requirement to precisely regulate MT dynamics during mitosis, such that MTs are stable enough to allow formation of stable KT-MT attachments but at the same time dynamic enough for efficient repair of any mal-attachments (Bakhoum et al., 2009a, 2009b). This is made possible by the intrinsic dynamic instability of MTs and further modulation of MT dynamics by microtubule associated proteins (MAPs) that regulate the dynamic instability of MTs (discussed later). Errors in the regulation of MTs or perturbation in the levels of expression of MAPs influences MT dynamics, which escalates the possibility of KT-MT mal-attachments further enhancing the likelihood of developing CIN.

1.4 Chromosomal instability (CIN)

Chromosomal instability is defined as frequent and rapid loss or gain of whole chromosomes and is a common feature of cancerous cells and solid tumors. Cells that show high frequency of CIN develop aneuploidy, which is a state where the cells contain an abnormal number of chromosomes. More than a century ago in 1902 and 1914, Theodor Boveri proposed the relationship between aneuploidy and tumorigenesis while examining the effect of aneuploidy in fertilized sea urchin oocytes (Boveri, 1914; Boveri, 1902). However, until today, the exact molecular mechanisms that cause CIN and the interdependence of aneuploidy, CIN and tumorigenesis has remained elusive. Generally, cells that have undergone a chromosome mis-segregation event show reduced proliferation and are eliminated via the p53 apoptotic pathway (Thompson and Compton 2010; Thompson and Compton 2008). However, it is intriguing how some cells that undergo mis-segregation events overcome this barrier and

become tumorigenic. It is believed that CIN and aneuploidy provide several genetic variations that favour cells to adapt and competently survive in a changing environment (Thompson and Compton 2010; Thompson and Compton 2008). Moreover, it is also thought that inherited mutations in essential genes coupled with mis-segregation events further permit efficient propagation of aneuploid cells (Holland and Cleveland, 2009). Several proteins that play an important role during the mitotic cell cycle have been characterized as CIN genes (Stirling et al., 2011). Proteins of the cohesin complex and proteins that are required for cleaving cohesin at anaphase onset are commonly found mutated in cancers (Hill et al., 2016; De Koninck and Losada, 2016). Altered expression levels of SAC proteins like Mad1, Mad2, Bub1 and BubR1 are found to cause sporadic tumors in mouse models (Giam and Rancati, 2015). KT proteins and proteins responsible for maintaining proper KT-MT attachments like CenpA, CenpF, CenpE, Ndc80, Hec1, and components of the CPC complex have been found to be overexpressed in several cancers (Giam and Rancati, 2015). Cells showing over amplification of centrosomes are predisposed to chromosome mis-segregations (Levine et al., 2017). Despite the abundance of implicated proteins in this process, the exact molecular mechanisms causing aneuploidy and CIN are as yet to be fully elucidated.

Considering the central role played by MTs in mitosis, a mis-regulation of MT dynamics could potentially cause CIN. In line with this, few studies point towards hyper-stable KT-MT attachments as an important contributor to CIN (Bakhoum et al., 2009a; 2009b). Proper attachments of MTs at KTs play a crucial role in accurate segregation of chromosomes. K-fibers are MT bundles that are stably bound to KT proteins. Like other MTs, K-fibers show phases of polymerization, attachment to the KT followed by depolymerization and detachment from the KT. This dynamic nature of K-fibers permits release and correction of erroneous KT-MT attachments. It has been previously shown that several CIN cancer cell lines frequently mis-segregate chromosomes because of hyper-stable KT-MT attachments. These cells lack the ability to efficiently correct mal-attachments, which results in persistent merotely. Merotelic attachments evade the SAC and increase the frequency of lagging chromosome and chromosome mis-segregation events (Figure 5). In a recent study, where the fate of lagging chromosomes was determined by tracking them, showed that these chromosomes seldom mis-segregate and principally end up as micronuclei in the correct daughter cells (Huang et al., 2012; Thompson and Compton, 2011). On the other hand, chromosome mis-segregations are caused by multiple-merotelic attachments, where both KTs

bind to MTs emanating from one pole but one KT also weakly attaches to MTs coming from the other pole (Thompson and Compton, 2011). These chromosomes induce aneuploidy by segregating both sister chromatids to the same spindle pole without lagging behind at the spindle equator (Figure 5) (Thompson and Compton, 2011). Therefore, in order to prevent mis-segregation of chromosomes and CIN, these sporadic KT-MT mal-attachments should be precisely resolved before anaphase onset.

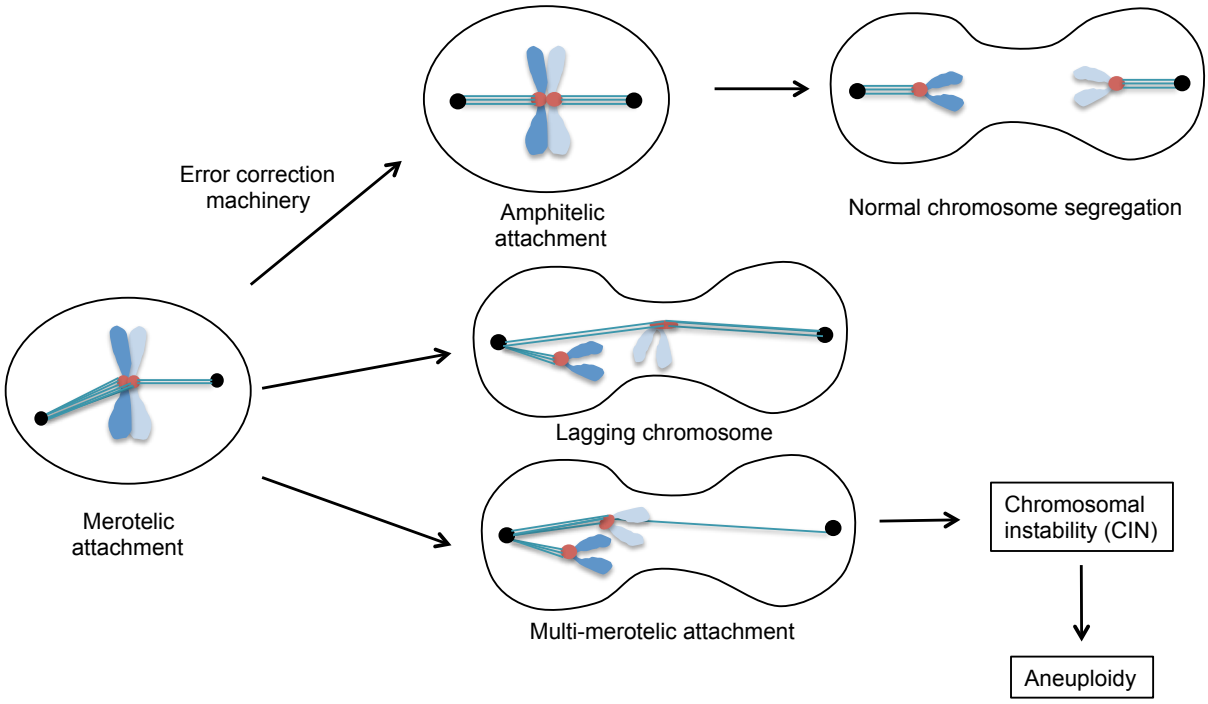

Figure 5. Consequences of merotelic attachments

Merotely is frequently seen during early phases of mitosis but is corrected by an error correction machinery to establish bi-orientation (amphitelic attachments) required for error free chromosome segregation. CIN cell lines show hyper-stable KT-MT attachments due to reduced intrinsic ability to correct these mal-attachments that causes persistent merotely. Persistent merotely leads to so-called "lagging chromosomes" where a chromatid lags behind at the spindle equator but in the end is segregated in to the desired daughter cell. On the other hand multi-merotelic attachments lead to mis-segregation of chromosomes altering ploidy and affecting genome stability.

It is known that proper regulation of MT dynamics is crucial for execution of error free mitosis and the key players that precisely control MT dynamics are microtubule-associated proteins (MAPs). MAPs are essential components required for balancing various parameters of MT stability and are generally seen up-regulated in solid tumors and cancers (Bhat and Setaluri, 2007). Some important MAPs that play a crucial role during mitosis are discussed in

the next section.

1.5 Microtubule associated proteins

MAPs are structurally and functionally diverse proteins that bind to MTs and regulate their dynamic behavior. MAPs influence the dynamicity of MTs during mitosis and are required in building a functional bipolar spindle by nucleating, stabilizing, polymerizing, and depolymerizing MTs (reviewed in Maiato et al., 2004). The expression level of several MAPs is highly regulated as the cell transits from interphase to mitosis. The activity and localization of MAPs is temporally and spatially controlled by multiple post-translational modifications during mitosis (reviewed in Maiato et al., 2004). As such, mis-regulation or altered expression levels of MAPs can have deleterious effects on cell division ranging from subtle defects in spindle morphology to a complete arrest of cells in mitosis. MAPs can be distinguished into several classes according to their function: polymerizing MAPs add tubulin dimers at the plus end of the MT; depolymerizing MAPs increase catastrophe frequency by removing tubulin dimers from the plus and minus ends; stabilizing MAPs bind to the MT lattice and cap plus ends of MTs and stabilize MTs; molecular motors use ATP to walk along MTs; and crosslinking MAPs that bind to MTs and crosslink them. Next section will address MAPs relevant for this study.

1.5.1 End Binding Proteins

End binding (EB) proteins are highly conserved plus tip interacting proteins (+TIPs) that autonomously track the growing plus ends of MTs and stabilize them. EBs help anchor MT plus ends to other cellular components and also influence MT dynamics (reviewed in Akhmanova and Steinmetz, 2008). EBs have a N-terminal calponin homology (CH) domain through which they bind MTs, and a C-terminal end binding homology (EBH) domain that mediates binding to a heterogeneous class of proteins including those that contain a ‘SxIP’ motif (reviewed in Akhmanova and Steinmetz, 2015; Akhmanova and Steinmetz 2008). Mammalian cells express three types of EB proteins namely, EB1, EB2 and EB3. EBs have a higher affinity for GTP tubulin explaining their comet like accumulation of 0.5-2 μm at the plus ends (Seetapun et al., 2012; Zanic et al., 2009; Bieling et al., 2007; Mimori-Kiyosue et al., 2000). EB proteins recruit several other +TIPs to MT plus ends and profoundly modulate MT dynamics during both interphase and mitosis. Numerous experiments on the most well studied member of this family EB1, comment on the role of EB1 in suppressing catastrophe frequencies in cells (Komarova et al., 2009). It has been reported that depletion of EB1 in

Drosophila reduces spindle size and leads to shorter astral MTs during mitosis (Rogers et al., 2002). In contrast to what has been observed in cells, *in vitro* reconstitution experiments using purified EB1 and MTs showed that EB1 increases not only rescue frequency but also catastrophe frequencies suggesting that they might alter the MT end structure (Vitre et al., 2008; Bieling et al., 2007).

1.5.2 Aurora A kinase

The Auroras are a family of Serine/Threonine kinases and in mammals this family consists of three members – Aurora A, Aurora B and Aurora C. Aurora kinases have a highly conserved C-terminal kinase domain and a diverse N-terminal domain through which these kinases interact with different protein partners and show distinct sub-cellular localization and function (reviewed in Hochegger et al., 2013; reviewed in Carmena and Earnshaw, 2003). Aurora A is activated by auto-phosphorylation of the activation loop, which is mediated by binding to proteins like TPX2, Ajuba, Bora and Pak1 (reviewed in Hochegger et al., 2013; Eyers et al., 2003). During mitosis Aurora A localizes to the spindle poles, MTs and the spindle midzone (reviewed in Hochegger et al., 2013; reviewed in Carmena and Earnshaw, 2003). At spindle poles, Aurora A is essential for centrosome separation and maturation (reviewed in Marumoto et al., 2005). Conditional knockout of Aurora A in chicken DT40 cells reduces spindle MT density and causes chromosome alignment defects (Hegarat et al., 2011). In Drosophila, Aurora A regulates MT dynamics by recruiting a stabilizing protein called D-TACC to the poles and phosphorylates it. Phosphorylated D-TACC then associates with the MT polymerase XMAP215 and antagonizes the activity of a MT depolymerase called MCAK further promoting MT growth (Kinoshita et al., 2005; Lee et al., 2001). Interestingly, Aurora A is an oncogene and is found overexpressed in several tumors. It has recently been reported that overexpression of Aurora A increases MT assembly rate. Increased MT assembly rate induces hyper-stabilization of KT-MTs, inducing CIN in colorectal cancer cells (Ertych et al., 2014).

1.5.3 Kinesin-13 family of motor proteins

Kinesins are molecular motors that translocate along MTs using energy released during ATP hydrolysis (Miki et al., 2005; Vale et al., 1985). All 14 families of kinesins in vertebrates, display two characteristic functional domains: a highly conserved motor domain through which kinesins can bind to MTs and hydrolyze ATP and a more divergent tail domain that modulates the kinesin activity (Miki et al., 2005; Lawrence et al., 2004; Miki et al., 2001).

Depending on the location of the motor domain on the protein, kinesins can be categorized into three distinct types: plus end directed kinesins have a N-terminally located motor domain; minus end directed kinesins possess a C-terminal motor domain; 'non-motile' kinesins have their motor domain placed in the center and are capable of depolymerizing MTs from the plus and minus ends (Hirokawa, 1998).

Kinesin-13 family members are 'non-motile' type of kinesins that diffuse along the MT lattice, bind to MT ends and induce a conformational change in the MT structure that leads to MT catastrophe. In humans and mouse, four kinesin-13 family members are known, namely Kif2A (Noda et al., 1995), Kif2B (Miki et al., 2001), Kif2C/mitotic centromere associated kinesin (MCAK) (Wordeman and Mitchison, 1995) and Kif24 (Kobayashi et al., 2011). Kinesin-13 members regulate MT dynamics by depolymerizing MTs and are important during both interphase and mitosis. Kinesin-13 members share a highly conserved ATP-hydrolyzing motor domain, however, the N- and C-termini show a high degree of divergence. All members of the kinesis-13 family perform different functions and show distinct sub-cellular localizations during mitosis.

Kif2A is mainly associated with spindle poles during mitosis and is required for determining spindle length and poleward MT flux (Ganem et al., 2005; Gaetz and Kapoor 2004). Kif2A plays a role in spindle scaling during embryonic development of *Xenopus laevis* (Wilbur and Heald, 2013). Kif2A is found enriched at the spindle midzone and controls MT length at the spindle midzone during anaphase (Uehara et al., 2013).

Kif2B is expressed at low levels in most somatic cells but shows high expression in testis (Manning et al., 2007). Kif2B when overexpressed localizes to KTs and centromeres and is required for bipolar spindle assembly, correcting KT-MT mal-attachments during prometaphase (Bakhoum et al, 2009a), chromosome movement (Hood et al., 2012) and cytokinesis (Manning et al., 2007).

Kif2C/MCAK is the most well characterized motor in this family and is discussed in detail below.

1.5.3.1 Kif2C/MCAK

MCAK localizes to the centromeres, centrosomes, midbody and MT plus tips during mitosis

(Figure 6A). It plays a crucial role in assembling a bipolar spindle, correcting improper KT-MT attachments, thus facilitating accurate chromosome segregation (Domnitz et al., 2012; Lan et al., 2004; Wordeman and Mitchison, 1995). MCAK is a potent MT depolymerase and can efficiently depolymerize MTs from both plus and minus ends *in vitro* (Hunter et al., 2003). In cells, it potently depolymerizes both ends of MTs and contributes to MT flux (Cross and McAnish, 2014; Wordeman, 2005; Waters et al., 1996). MCAK has a N-terminal domain that regulates its subcellular localization through binding to several protein partners. MCAK has a centrally located and well-conserved ATP-hydrolyzing motor domain required for MT binding and is the main MT depolymerizing domain (Figure 6B). MCAK shows a positively charged neck region that forms electrostatic interactions with the negatively charged MT lattice that facilitates diffusion along the MT lattice. The neck domain along with the motor domain is indispensible for MCAK's depolymerase activity. The C-terminus of MCAK facilitates dimerization and binding to tubulin dimers (Figure 6B). Similar to other motor kinesins the C-terminal part is known to regulate MCAK's depolymerase activity (Wordeman, 2005; Andrews et al., 2004; Lan et al., 2004; Ohi et al., 2004; Walczak et al., 2002; Ovechkina et al., 2002; Wordeman et al., 1999; Maney et al., 1998). The domain organization and regulation of MCAK's catalytic activity is well studied and reports have identified the region encompassing the neck and motor domain exists as a monomer and is the smallest functional unit that can efficiently depolymerize MTs (Maney et al., 2001). It has also been reported that intra-molecular interactions between the N- and C- termini of MCAK further coordinate its catalytic activity and this is required for proper spindle assembly (Ems-McClung et al., 2007).

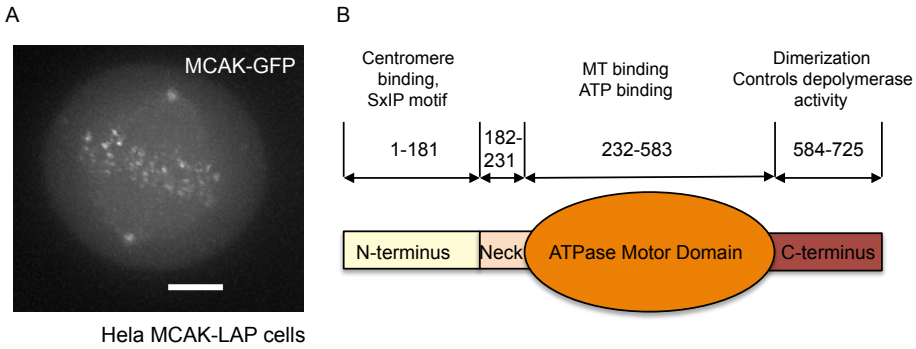

Figure 6. Subcellular localization and domain organization of MCAK

A. Live cell image of a metaphase Hela cell showing MCAK-GFP localization to centrosomes, centromeres and spindle MTs. Scale bar shows 5 μm. **B.** Schematic representation of different

domains of MCAK. The N-terminal domain extends from 1-181 amino acids (aa), has a SxIP motif and is required for centromere binding. The neck domain (182-231 aa) along with the motor domain (232-583 aa) is essential for MT depolymerization. The motor domain also binds to MTs. The C-terminal domain ranges from 584-725 aa and harbors the dimerization domain and modulates MCAK's depolymerase activity.

In cells, MCAK's activity is tightly regulated by intra-molecular interactions and phosphorylation by a plethora of kinases (Ritter et al., 2016; Tanenbaum 2011b). *In vitro* studies have helped understand the depolymerization cycle of MCAK which is shown in Figure 7A and B. Recent studies have shown that in solution, MCAK appears to be in the ''closed'' conformation, where the C-terminal tail folds back and interacts with the neck region (Ems-McClung et al., 2013). This "closed" conformation of MCAK corresponds to the 'active' state of MCAK. In another recent study, it was observed that one C-terminal tail of MCAK is bound to the interface between two motor domains when in solution (Talapatra et al., 2015). Interestingly, they showed that MCAK shifts to an "open" conformation upon an interaction between the motor domain of MCAK and the MT lattice. This leads to ATP hydrolysis and the C-terminal tail is released from the motor domain leaving MCAK in an "open" less active state (Wang et al., 2015, Talapatra et al., 2015; Asenjo et al., 2013; Ems-McClung et al., 2013). This "open" conformation of MCAK weakens its interaction with MTs due to electrostatic repulsion between the negatively charged C-terminal tail and E-hooks of tubulin further favoring MCAK's one-dimensional lattice diffusion (Talapatra et al., 2015). MT ends trigger a conformational change in MCAK from inactive "open" to the active "closed", which is accompanied by an exchange of ADP to ATP (Burns et al., 2014; Ems-McClung et al., 2013). At MT ends, ATP bound active MCAK strongly binds to tubulin dimers and alters the conformation of MT protofilaments by inducing an outward curvature and removes a tubulin dimer (Friel and Howard, 2011; Ogawa et al., 2004; Shipley et al., 2004). A second ATP is hydrolyzed during release of this detached tubulin dimer and MCAK shifts back to its open inactive conformation and begins another cycle of depolymerization (Wang et al., 2015).

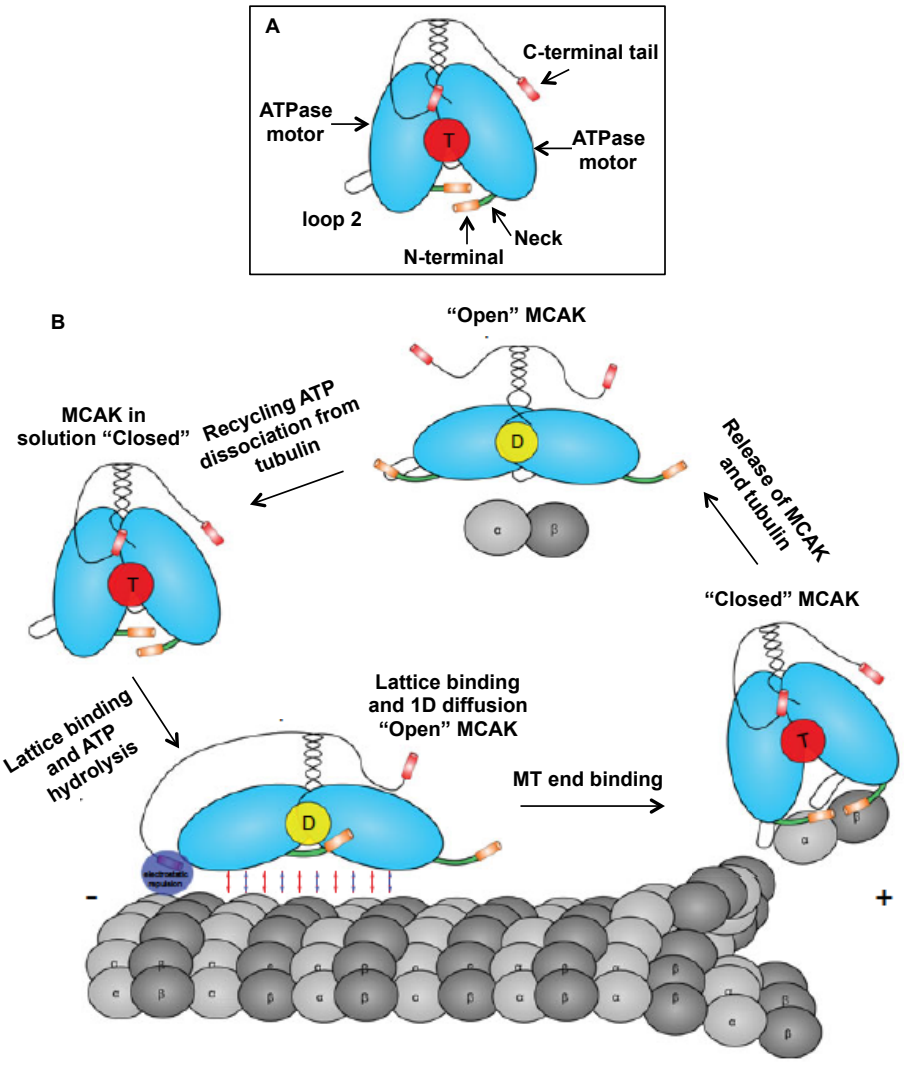

Figure 7. Schematic representation of the depolymerization cycle of MCAK

A. Representation of a "closed" ATP bound MCAK dimer in solution with one C-terminal tail bound to the interphase between two motor domains. **B.** Representation of the depolymerization cycle of MCAK. In solution, MCAK exists in a "closed" active conformation. On binding to MTs, the C-terminal tail is displaced and MCAK is converted into "open" conformation and ATP is hydrolyzed. This open conformation enfeebles its interaction with MTs due to electrostatic repulsion between the C-terminal domain and tubulin E-hooks. This facilitates diffusion of MCAK along the MT lattice. At MT tips, ADP is exchanged to ATP and the conformation of MCAK is switched from "open" to "closed" which enhances its affinity to tubulin dimers. Closed MCAK detaches with a tubulin dimer, which is released upon ATP hydrolysis. 'T' enclosed within a red circle represents ATP and 'D' enclosed in yellow circle represents ADP. Image is adapted from Ritter et al., 2016.

In cells, different pools of MCAK exist on KTs, spindle poles, astral MT plus tips and spindle MTs, where they depolymerize MTs. Increased MCAK activity in cells, leads to loss of astral MTs, spindle mis-orientation and problems in alignment of chromosomes (Zhang et al., 2011;

Walczak et al., 1996). In contrast, loss of MCAK activity results in longer astral MTs and hyper-stable KT-MT attachments that are a major cause of chromosome mis-segregation (Thompson and Compton, 2011; Rankin and Wordeman, 2010; Kline-Smith et al., 2004; Maney et al., 1998). MCAK is the only member of the kinesin-13 family that harbors a SxIP motif in its N-terminal domain and shows plus tip accumulation in both interphase and mitosis via interaction with EB1 (Domnitz et al., 2012; Tanenbaum et al., 2011; Honnappa et al., 2009; Moore et al., 2005). This plus tip tracking activity of MCAK is phospho-regulated and is required for maintaining MT length during bipolar spindle assembly (Domnitz et al., 2012; Tanenbaum et al., 2011a).

MT attachment at KTs is a stochastic process and leads to several KT-MT mal-attachments during early prometaphase, which are generally corrected before anaphase onset (Cimini et al., 2003). MCAK localizes to the KTs and assists in error correction of improper KT-MT attachments by depolymerizing KT MTs and destabilizing mal-attachments (Knowlton et al., 2006; Kline-Smith et al., 2004). Continuous cycles of MT growth and attachment followed by depolymerization and detachment are crucial for establishing bi-orientation and are orchestrated by the activity of MT depolymerases and polymerases (Nicklas and Ward 1994). KT-MT attachments are more dynamic during early phases of mitosis, which is suggestive of high error correction during prometaphase. Kif2B and MCAK localize to KTs during prometaphase and are involved in directly destabilizing mal-attachments (Bakhoum et al., 2009a). However, MCAK localizes to centromeres even during metaphase when the K-fiber turnover is reduced and KT-MT attachments are more stable (Kabeche and Compton, 2013; Bakhoum et al., 2009a; 2009b; Cimini et al., 2006Zhai et al., 1995). At the KT, MCAK maintains KT MT dynamics and corrects merotelic attachments during metaphase (Bakhoum et al., 2009a; Kline-Smith et al., 2004; Maney et al., 1998). It has been shown that depletion of MCAK causes hyper-stable KT-MT attachments leading to lagging chromosomes and mis-segregation of chromosomes (Bakhoum et al., 2009a; Kline-Smith et al., 2004; Maney et al., 1998).

Interestingly, several CIN cancer cell lines frequently display hyper-stable KT-MT attachments, which result in persistent merotely. When it remains uncorrected, this causes lagging chromosomes and drives CIN (Gregan, et al., 2011; Thompson and Compton, 2011; Cimini and Degrassi, 2005; Cimini et al., 2001). Intriguingly, artificially increasing MCAK's

activity in these CIN cancer cell lines destabilizes mal-attachments thus suppressing lagging chromosomes and CIN (Bakhoum et al., 2009a; Bakhoum et al., 2009b). The reason for this inherent stabilization of KT-MT attachments in CIN cancer cell lines that compromises the activity of the error correction machinery remains elusive.

Overexpression or reducing levels of MCAK in human cell lines affects the fidelity of chromosome alignment and segregation (Shao et al., 2015; Rankin and Wordeman 2010; Bakhoum et al., 2009a; Bakhoum et al., 2009b; Maney et al., 1998; Walczak et al., 1996; Wordeman and Mitchison, 1995). Therefore, the depolymerase activity of MCAK is fine-tuned spatially and temporally for proper execution of mitosis. In addition to control by intra-molecular interactions, several proteins are involved in positively or negatively regulating MCAK's depolymerase activity. Inner centromere KinI stimulator (ICIS) localizes to centromeres in an MCAK-dependent manner and is implicated in stimulating MCAK's depolymerase activity (Ohi et al., 2003). It has been proposed that prior to anaphase onset this complex is required for error correction by destabilizing KT-MT attachments (Ohi et al., 2003). Further, during mitosis, MCAK forms a complex with a kinesin-8 family member Kif18B at astral MT tips and promotes robust MT depolymerization (Tanenbaum et al., 2011a). Proteins Nup98 and MCRS1 have been implicated in impeding MCAK's depolymerase activity during mitosis (Cross and Powers, 2011; Meunier and Vernos, 2011). In a recent report, it has also been shown that MCAK and a protein called NuSAP directly interact in an Aurora B dependent manner and NuSAP stabilizes KT MTs by inhibiting MCAK's depolymerase activity (Li et al., 2016).

MCAK's depolymerase activity is also tightly regulated by several kinases. The most notable is its regulation by Aurora B. Aurora B is a component of the chromosome passenger complex (CPC) and localizes to chromosome arms, inner centromeres, and spindle midzone. Aurora B phosphorylates multiple residues on MCAK, which regulate its KT location and depolymerase activity (Ritter et al., 2015a; Shao et al., 2015; Zhang et al., 2007; Knowlton et al., 2006; Andrews et al., 2004; Lan et al., 2004; Ohi et al., 2004). MCAK and Aurora B are together a part of the error correction machinery and co-operatively destabilize improper KT-MT attachments (Kline-Smith et al., 2004; Hauf et al., 2003). Aurora B phosphorylation on S196 in the neck domain of MCAK is of particular importance, as this phosphorylation promotes its centromeric localization and reduces its depolymerization activity. Recent

reports have shown that this phosphorylation "opens" up *Xenopus* MCAK by reducing the affinity between the C-terminal tail and neck domain. This "open" MCAK shows reduced MT affinity and catalytic activity (Ems McClung et al., 2013). Aurora B also phosphorylates multiple residues in the N-terminal domain of MCAK and negatively regulates its binding to EB1 (Honnappa et al., 2009; Moore et al., 2005). Interestingly, MCAK appears to be linked to its own regulation by a negative feedback loop, as phosphorylation of MCAK on five N-terminally located residues by Aurora B enhances MCAK's interaction with NuSAP that attenuates its depolymerase activity (Li et al., 2016).

In addition to Aurora B, MCAK is also a substrate of Aurora A. Aurora A phosphorylates *Xenopus* MCAK at two residues namely S196 and S719. Phosphorylation on S196 attenuates its depolymerase activity whereas phosphorylation on S719 enhances binding of MCAK to MT asters and spindle poles further promoting bipolar spindle formation (Zhang et al., 2008). It has also been shown that depletion of Aurora A decreases MCAK centrosomal localization in mitotic human cancer cells, while it simultaneously increases centrosomal localization of a MT polymerase Ch-Tog, leading to an imbalance of forces further giving rise to multipolar spindles (DeLuca et al., 2008).

Another mitotic kinase called Polo-like kinase (Plk1) also phosphorylates MCAK. Plk1 localizes to centrosomes, KTs and central spindle during mitosis and phosphorylates multiple residues in the C-terminal domain of MCAK (Ritter et al., 2015b; Sanhaji et al., 2014; Zhang et al., 2011). Phosphorylation of MCAK by Plk1 stimulates its depolymerase activity as overexpression of phopsphomimetic mutants reduces MT density, increasing chromosome misalignment and multipolarity in Hela cells (Talapatra et al., 2015; Zhang et al., 2011). On the other hand expression of phosphonull mutants leads to increase in frequency of chromosome bridges during anaphase (Zhang et al., 2011). Recently, existence of an intertwined network between Plk1, Aurora B and MCAK has been suggested where Aurora B phosphorylates and activates Plk1, which further phosphorylates MCAK at S715 and stimulates its catalytic activity at KTs (Shao et al., 2015).

MCAK is also phosphorylated by Cyclin dependent kinase (Cdk1/Cyclin B1) that localizes to spindle poles and KTs during mitosis. Cdk1 reduces MCAK's depolymerase activity by phosphorylating it at a single residue in the ATP-binding motor domain. This

phosphorylation triggers re-localization of MCAK from poles to KTs in order to promote MT nucleation for formation of a bipolar spindle (Sanhaji et al., 2010).

1.5.4 GTSE1

The final MAP relevant for this study and the major focus of my Ph.D. is the protein GTSE1 (G2 and S-phase expressed 1). GTSE1 is a MAP found overexpressed in several tumors and its expression level correlates with metastasis and tumor grade (Scolz et al., 2012). Earlier reports have proposed a role of GTSE1 in down-regulation of p53 activity and p53 levels upon DNA damage (Monte et al., 2004; 2003). GTSE1 is an intrinsically disordered protein that exists only in vertebrates. In interphase, GTSE1 is enriched at the growing MT ends by interacting with EB1 via SxIP motifs, which is a short linear motif necessary for binding to the EBH homology domain of EB proteins (Jiang et al., 2012). GTSE1 accumulates at the growing tips of MTs and this MT tip tracking activity is necessary for cell migration (Scolz et al., 2012). GTSE1 also interacts directly with the MT lattice in an EB1 independent manner during interphase. Expression of GTSE1 peaks in mitosis where it is hyperphosphorylated, suggesting that GTSE1 might play distinct roles during mitosis and interphase. Interestingly, GTSE1 shows MT lattice binding and tracks growing MT plus ends throughout interphase, but stops in mitosis at the prophase-to-prometaphase transition, resuming again at anaphase onset (Scolz et al., 2012). Instead, during mitosis in a Cdk1 dependent manner, association between GTSE1 and MTs is abolished but GTSE1 is still seen associated with the mitotic spindle and spindle poles (Scolz et al., 2012 and our unpublished data).

Recent studies indicate that localization of GTSE1 on the mitotic spindle could be attributed to the TACC3-Ch-Tog-Clathrin complex (Nixon et al., 2015; Hubner et al., 2010). TACC3, clathrin and Ch-Tog are MT stabilizing proteins that localize slightly differently on the spindle during mitosis (Foraker et al., 2012; Royle et al., 2005; Gergely et al., 2003; Gergely et al., 2000a). TACC3 and clathrin are highly enriched on spindle MTs, spindle poles and a significant fraction is also present in the cytoplasm. Ch-Tog is enriched at spindle poles and also localizes to the mitotic spindle. TACC3 and Ch-Tog have been shown to +TIP track during mitosis (Gutiérrez-Caballero et al., 2015). TACC3 is considered to be a MT growth-promoting or stabilizing factor as depletion of TACC3 leads to shorter astral MTs and spindles in worms, flies and vertebrate cells (Kinoshita et al., 2005; O'Brien et al., 2005; Peset et al., 2005; Srayko et al., 2003; Gergely et al 2000b). On the other hand, overexpressing TACC3 causes longer astral MTs (Peset and Vernos 2008). Ch-Tog is a MT

polymerase that is necessary for robust MT nucleation from centrosomes and for formation of a bipolar spindle (Cassimeris et al., 2009; Brouhard et al., 2008; Popov et al., 2002). Ch-Tog and TACC3 together have been implicated in antagonizing MCAK's depolymerase activity in *Xenopus* egg extracts and vertebrate cells, which is crucial for maintaining centrosome integrity, spindle pole organization and bipolarity (Holmfeldt et al., 2004; Cassimeris et al., 2004; Gergely et al., 2003; Tournebize et al., 2000). During mitosis, clathrin binds to the spindle through its N-terminal domain and is important for maintaining K-fiber stability (Royle et al., 2005). Clathrin forms a triskelion consisting of three light chains and three heavy chains and this trimerisation of clathrin has been implicated in cross-linking KT-MTs (Royle and Lagnado, 2006; Royle et al., 2005).

Recently it has been reported that the TACC3-Ch-Tog-Clathrin complex stabilizes K-fibers by formation of inter-MT bridges (Cheeseman et al., 2013; Hood et al., 2013; Booth et al., 2011). During mitosis, a dileucine peptide and Aurora A phosphorylated S558 on TACC3 facilitate the binding between the TACC domain of TACC3 and the N-terminal domain of clathrin to form a composite MT binding interphase (Hood et al., 2013). Interestingly, the C-terminal part of GTSE1 shows five conserved LID motifs, which are putative clathrin-binding motifs (unpublished data). Preliminary results suggest that GTSE1 directly binds to clathrin and becomes a part the TACC3-Ch-Tog-Clathrin complex during mitosis. Depletion of TACC3 or clathrin leads to loss of GTSE1 from the spindle and spindle poles, which corroborates the interdependence of TACC3 and clathrin localization to spindle MTs and hence depletion of either of the two components leads to loss of GTSE1 from the spindle (Hood et al., 2013; Hubner et al., 2010). Furthermore, phosphorylation of TACC3 by Aurora kinase A is also important for GTSE1 localization to the spindle as inhibition of Aurora kinase A, using a small molecule inhibitor MLN8054 leads to loss of GTSE1 from the spindle (Hubner et al., 2010). This suggests that GTSE1 is a part of the K-fiber stabilizing complex. Despite all the evidence pointing towards GTSE1 being a part of the TACC3-Ch-Tog-Clathrin complex the exact role of GTSE1 on the spindle during mitosis is still not understood and needs to be investigated. Thus, the focus of my Ph.D. is to investigate the role of GTSE1 during mitosis.

1.6 Objective

GTSE1 is a cell cycle regulated protein that localizes to the mitotic spindle and poles via interaction with the TACC3-Ch-Tog-Clathrin complex. However, the role GTSE1 plays

while on the spindle needs to be elucidated. Preliminary results have shown that GTSE1 is necessary for proper execution of mitosis. Loss of GTSE1 in U2OS osteosarcoma cells negatively affects the stability of astral MTs during metaphase. It is also evident that cells depleted of GTSE1 have problems in congressing chromosomes and aligning them at the metaphase plate. A lesser percentage of cells also displayed multipolar spindles, detached spindle poles and defective cytokinesis. Our data suggests that GTSE1 is essential for proper execution of mitosis independent of EB1 as depletion of endogenous GTSE1 in cell lines stably expressing RNAi resistant GTSE1-GFP mutated at the SxIP motif (EB1 binding motif), do not display the above mentioned mitotic phenotypes (Bendre et al., 2016). Preliminary results imply that GTSE1 plays a significant role during mitosis, and the objective of this Ph.D. is to understand the molecular mechanisms by which GTSE1 influences mitosis. Previous studies in which GTSE1 was affinity purified followed by mass spectrometric analysis revealed that GTSE1 interacts with MCAK/Kif2C, the MT depolymerase (Hubner et al., 2010). Interestingly, the phenotypes observed after loss of GTSE1 i.e. loss of astral MTs, multipolar spindles, chromosome misalignments mimic those phenotypes seen after overexpression of MCAK in cell lines. This led us to hypothesize that GTSE1 might attenuate MCAK's depolymerase activity during mitosis. Thus, the goal of my Ph.D. thesis is to study the functional interplay between GTSE1 and MCAK and to elucidate the role played by GTSE1 during mitosis. The following aims have been addressed during my Ph.D.:

Aim 1: Define how GTSE1 controls MT dynamics necessary for the stability of astral MTs during mitosis.

Aim 2: Define how GTSE1 controls MT dynamics necessary for proper chromosome alignment and accurate segregation during mitosis

- Does depletion of GTSE1 affect KT MT stability?
- Does depletion of GTSE1 affect KT-MT attachments?

Aim 3: Are phenotypes observed after loss of GTSE1 through increased depolymerase activity of MCAK?

- Does GTSE1 interact with MCAK *in vivo* and *in vitro*?
- Does GTSE1 inhibit MCAK's depolymerase activity *in vivo*?
- Does GTSE1 inhibit MCAK *in vitro*?

Aim 4: Define how GTSE1 contributes to CIN

- Can overexpression of GTSE1 in diploid cell lines induce CIN?

2. Materials and Methods

2.1 Chemicals and Solutions

Table 01. List of chemicals and solutions

Chemical Name	Ingredients	Company
Agarose		Carl Roth GmbH, Karlsruhe, Germany
Ammonium persulfate (APS)		Max-Planck-Institute, Dortmund, Germany
Ampicillin sodium salt		GERBU Biotechnik GmbH; Heidelberg; Germany
Blasticidine		Invitrogen, California, U.S.A
Bradford Solution		Bio-Rad Laboratories GmbH, Munich, Germany
BRB80 Buffer	80 mM Pipes-KOH pH 6.9 1 mM EGTA 1mM $MgCl_2$ 150 mM KCl 10 μM ATP 1 mM TCEP	Sigma-Aldrich GmbH, Steinheim, Germany Thermo Fisher Scientific, Waltham, U.S.A J.T Baker Chemicals, Center Valley, USA Avantor Performance Materials (J.T. Baker), Center Valley, U.S.A. Sigma-Aldrich GmbH, Steinheim, Germany Biosynth AG; Staad; Switzerland
Buffer A	50 mM HEPES pH 7.5 300 mM NaCl 5% Glycerol	Sigma-Aldrich GmbH, Seelze, Germany VWR Chemicals, Darmstadt, Germany GERBU Biotechnik GmbH,

	2 mM TCEP	Heidelberg, Germany Biosynth AG; Staad; Switzerland
Cdk1 inhibitor (RO-3306)		Calibiochem
Cell Lysis Buffer	50 mM HEPES pH7.2 50 mM Na_2HPO_4, 150 mM NaCl 10% glycerol 1% Triton X-100 1 mM EGTA 1.5 mM $MgCl_2$	Sigma-Aldrich GmbH, Seelze, Germany Avantor Performance Materials (J.T. Baker), Center Valley, U.S.A VWR Chemicals, Darmstadt, Germany GERBU Biotechnik GmbH, Heidelberg, Germany Thermo Fisher Scientific, Waltham, U.S.A Thermo Fisher Scientific, Waltham, U.S.A J.T Baker Chemicals, Center Valley, USA
CO_2 Independent Medium		Thermo Fisher Scientific (Gibco), Waltham, U.S.A.
Coomassie Brilliant Blue staining solution	10% Acetic acid 2.5% Coomassie G250	Sigma-Aldrich GmbH, Hamburg, Germany Serva GmbH, Heidelberg, Germany
Destaining solution for ProQ Diamond staining	20% Acetonitrile 50 mM Sodium acetate	Fisher Scientific, UK Sigma-Aldrich GmbH, Steinheim, Germany
Dimethyl sulfoxide (DMSO)		SERVA Electrophoresis GmbH, Heidelberg, Germany
Disodium phosphate(Na_2HPO_4)		Avantor Performance Materials (J.T. Baker), Center Valley,

		U.S.A.
Dithiothreitol (DTT)		SERVA Electrophoresis GmbH, Heidelberg, Germany
DNA Loading Buffer (6x)	0.4% Orange G 30% Glycerol 10 mM Tris-HCl 25 mM Ethylenediaminetetraacetic acid (EDTA)	Sigma Aldrich, Hamburg, Germany GERBU Biotechnik GmbH, Heidelberg, Germany Carl Roth, Karlsruhe, Germany GERBU Biotechnik GmbH, Heidelberg, Germany
Dulbecco's Modified Eagle's Medium (DMEM)		PAN Biotech, Aidenbach, Germany
Dynabeads Protein G magnetic beads		Invitrogen GmbH, Karlsruhe, Germany
ECL prime Western blotting detection reagent		GE Healthcare, Freiburg, Germany
Effectene transfection reagent		QIAGEN GmbH, Hilden, Germany
Ethanol		Sigma-Aldrich GmbH, Seelze, Germany
Fetal Bovine Serum		Thermo Fisher Scientific (Gibco), Waltham U.S.A.
Fish skin gelatin		Sigma-Aldrich GmbH, Steinbach, Germany
Fixing solution for ProQ Diamond staining	50% Methanol 10% Acetic acid	Sigma-Aldrich GmbH, Steinheim, Germany Sigma-Aldrich GmbH, Steinheim, Germany
FuGENE® HD Transfection Reagent		Promega GmbH, Mannheim, Germany

GeneRuler 1 kb Plus DNA		Fermentas, Hennigsdorf, Germany
Gentamycin		Sigma-Aldrich GmbH, Seelze, Germany
GSH Amintra Glutathione Resin		Amintra, Cambridge, UK
GST-Binding buffer	25 mM HEPES pH 7.5 300 mM NaCl 1 mM EDTA 5% Glycerol 1% Triton X-100 DNase	Sigma-Aldrich GmbH, Seelze, Germany VWR Chemicals, Darmstadt, Germany GERBU Biotechnik GmbH, Heidelberg, Germany GERBU Biotechnik GmbH, Heidelberg, Germany Thermo Fisher Scientific, Waltham, U.S.A Sigma-Aldrich GmbH, Seelze, Germany
HEPES		Sigma-Aldrich GmbH, Seelze, Germany
Isopropyl β-D-1-thiogalactopyranosid (IPTG)		Carl Roth, Karlsruhe, Germany
Imidazole		Merck Millipore, Darmstadt, Germany
Kanamycin		GERBU Biotechnik GmbH; Heidelberg; Germany
L-Glutamine		Thermo Fisher Scientific, Waltham, U.S.A.
L-Glutathion reduced		Biochemica, Darmstadt, Germany
Laemmli SDS Sample loading buffer (5X)	4% Sodium dodecyl sulfate (SDS)	Sigma-Aldrich GmbH, Steinheim, Germany

	10% Glycerol 1% 2-Beta mercaptoethanol 0.02% Bromophenol Blue 50 mM Tris-HCl	GERBU Biotechnik GmbH, Heidelberg, Germany Thermo Fisher Scientific, Waltham, U.S.A Sigma Aldrich, Hamburg, Germany Carl Roth GmbH, Karlsruhe, Germany
Lipofectamine 2000 Reagent		Invitrogen GmbH, Karlsruhe, Germany
Luria-Bertani medium (LB medium)	1% Peptone 0.5% Yeast extract 0.5% NaCl	Sigma Aldrich, Hamburg, Germany GERBU Biotechnik GmbH, Heidelberg, Germany VWR Chemicals, Darmstadt, Germany
Methanol		Sigma-Aldrich GmbH, Steinheim, Germany
Midori Green DNA Stain		Nippon Genetics Europe GmbH, Düren, Germany
Milk powder		Carl Roth, Karlsruhe, Germany
MLN8054		Sigma-Aldrich GmbH, Seelze, Germany
Nickel-NTA-Superose Beads		GE Healthcare, Freiburg, Germany
BioTrace Nitrocellulose Membrane		Pall Life Sciences, Pensacola, Florida, USA
Nocodazole		Sigma-Aldrich GmbH, Steinheim, Germany
OptiMEM		Invitrogen GmbH, Karlsruhe, Germany
Oligofectamine		Invitrogen GmbH, Karlsruhe, Germany

Paraformaldehyde (PFA, 16%)		Thermo Scientific, Rockford, USA
Penicillin Streptomycin		PAN-Biotech GmbH, Aidenbach, Germany
Phenylmethylsulfonyl-fluorid (PMSF)		Serva Electrophoresis GmbH, Heidelberg, Germany
Phosphate buffered saline (PBS)	137 mM Sodium chloride 2.7 mM Potassium chloride 10 mM Di-Sodium hydrogen phosphate dihydrate 2 mM Potassium dihydrogen-phophate (0.2 g/l)	VWR Chemicals, Darmstadt, Germany J.T.Baker Chemicals, Center Valley, USA Merck Millipore, Darmstadt, Germany AppliChem GmbH, Darmstadt, Germany
Poly-L-Lysin		Sigma Aldrich, Hamburg, Germany
Potassium chloride (KCl)		Avantor Performance Materials (J.T. Baker), Center Valley, U.S.A.
Precision Plus Protein unstained standards		Bio-Rad, Munich, Germany
Precision Plus Protein prestained standards		Bio-Rad, Munich, Germany
ProLong® Gold antifade mounting solution with DAPI		Molecular Probes, Life technology
ProQ Diamond Phosphoproetin gel stain		Invitrogen, Molecular probes, Eugene, Oregon, USA
Protease Inhibitor mix (500X)		Serva GmbH, Heidelberg, Germany

Pull-down buffer	20 mM HEPES pH 6.9 150 mM NaCl 1 mM ATP	Sigma-Aldrich GmbH, Seelze, Germany VWR Chemicals, Darmstadt, Germany Sigma-Aldrich GmbH, Steinheim, Germany
Sf-900 III medium		Thermo Fisher Scientific Gibco, Waltham, U.S.A.
SDS PAGE electrophoresis buffer	25 mM Tris-HCl 200 mM Glycin 3.5 mM SDS	Carl Roth, Karlsruhe, Germany Sigma Aldrich, Hamburg, Germany Carl Roth, Karlsruhe, Germany
Size Exclusion Chromatography (SEC) buffer	20 mM HEPES pH 6.9 150 mM NaCl 5% Glycerol 1mM TCEP 10 μM ATP	Sigma-Aldrich GmbH, Seelze, Germany VWR Chemicals, Darmstadt, Germany GERBU Biotechnik GmbH, Heidelberg, Germany Biosynth AG; Staad; Switzerland Sigma-Aldrich GmbH, Steinheim, Germany
Taxol		Sigma-Aldrich GmbH, Steinheim, Germany
TCEP (tris(2-carboxyethyl)phosphine)		Biosynth AG; Staad; Switzerland
Tris-Acetate-EDTA (TAE) buffer (50X)	50 mM Tris-Base 57.1 ml Glacial acetic acid 0.5 M EDTA (pH 8)	Carl Roth, Karlsruhe, Germany Sigma-Aldrich GmbH, Hamburg,Germany GERBU Biotechnik GmbH, Heidelberg, Germany

Tetramethylethylenediamine (TEMED)		SERVA Electrophoresis GmbH, Heidelberg, Germany
Tertracycline		Sigma-Aldrich GmbH, Steinheim, Germany
Thymidine		Sigma-Aldrich GmbH, Steinheim, Germany
Triton X-100		Thermo Fisher Scientific, Waltham, U.S.A.
Trypan blue solution (0.4 %)		Thermo Fisher Scientific, Waltham, U.S.A.
Trypsin-EDTA		PAN-Biotech GmbH, Aidenbach, Germany
Tween-20		SERVA Electrophoresis GmbH, Heidelberg, Germany
Wash buffer for pull-downs	20 mM HEPES 500 mM NaCl 5% Glycerol 0.1% Triton X-100 1mM TCEP	Sigma-Aldrich GmbH, Seelze, Germany VWR Chemicals, Darmstadt, Germany GERBU Biotechnik GmbH, Heidelberg, Germany Thermo Fisher Scientific, Waltham, U.S.A Biosynth AG; Staad; Switzerland
Western transfer buffer	25 mM Tris 190 mM Glycin 10 % Methanol	Carl Roth, Karlsruhe, Germany Carl Roth, Karlsruhe, Germany Sigma Aldrich, Hamburg, Germany
X-Galactoside		Sigma-Aldrich GmbH, Steinheim, Germany
β-Mercaptoethanol		Serva Electrophoresis GmbH, Heidelberg, Germany

2.2 Instruments and devices

Table 02. List of instruments and devices

Device	Model	Company
-80° freezer	MDF-U5386S	SANYO Electric Co., Ltd.; Moriguchi, Japan
Cell Counter	Countess	Invitrogen GmbH, Karlsruhe, Germany
Cell Counter	Scepter Handheld Automated Cell counter 2.0	Merck Chemicals GmbH; Darmstadt; Germany
Centrifuge	Mini Spin plus	Eppendorf GmbH; Wesseling-Berzdorf; Germany
Centrifuge	5418	Eppendorf GmbH; Hamburg Germany
Centrifuge	5417 R	Eppendorf GmbH; Wesseling-Berzdorf; Germany
Centrifuge	5804 R	Eppendorf GmbH; Wesseling-Berzdorf; Germany
Centrifuge	Avanti J-20 XP	Beckman and Coulter GmbH; Krefeld, Germany
Centrifuge	Allegra J-30 I New	Beckmann and Coulter GmbH; Engelsdorf, Germany
Centrifuge (high speed)	Avanti J-30 I Old	Beckman and Coulter GmbH; Krefeld, Germany
Cryogenic Freezer	MDF-1156-PE Ultra Low Temperature Freezer	Panasonic Biomedical Sales Europe B.V
DNA Electrophoresis Unit	CRHU10, Min-Plus Horizontal	Carl Roth, Karlsruhe, Germany
Electrophoresis power supply	Power SourceTM 300V	VWR International GmbH; Langenfeld; Germany
Flake ice machine	AF 100	Scotsman Ice Systems; Milan; Italy
Fluorescence Microscope	EVOS® FL Imaging System	Life Technologies; Thermo Fisher Scientific, Waltham, U.S.A.

Freezer -20 °C	LGex 3410 MediLine	Liebherr-Elektronik GmbH; Lindau; Deutschland
Freezer -20 °C	LGUex 1500 MediLine	Liebherr-Elektronik GmbH; Lindau; Deutschland
Fridge 4 °C	LKexv 1800	Liebherr-Elektronik GmbH; Lindau; Deutschland
Fridge 4 °C	LKUexv 1610 MediLine	Liebherr-Elektronik GmbH; Lindau; Deutschland
Imaging System	ChemiDoc MP	Bio-Rad Laboratories GmbH, Munich, Germany
Incubator	Heraeus B6030	Thermo Electron LED GmbH; Langenselbold Germany
Incubator CO_2-DH Autoflow	NU-5500	NuAir
ibidi Imaging chamber	15 µ-Slide 8 well	iBidi, Martinsried, Germany
ibidi Imaging chamber	µ-Dish 35 mm dish	iBidi, Martinsried, Germany
Incubator shaker	Multitron Standard	Infors HAT AG; Bottmingen; Switzerland
Incubator shaker	Minitron	Infors HAT AG; Bottmingen; Switzerland
Mini Rocker Shaker	MR1	BioSan
PCR cycler	T3000 Thermocylcer	Biometra GmbH; Göttingen; Germany
Photometer	NanoDrop 2000	Thermo Electron LED GmbH; Langenselbold Germany
Photometer	Biophotometer 6131	Eppendorf GmbH; Wesseling-Berzdorf; Germany
SDS Page Electrophoresis Unit	Mini Protean Tetra Cell	Biorad, China
Scale	BL150 S	Sartorius
Scale	PE 3600	Mettler
See-saw rocker	SSL4	Bibby Scientific Limited; Staffordshire; UK

Sonicator	Sonifier 450	Branson Ultraschall- Emerson Technologies GmbH; Dietzenbach; Germany
Sterile bench	Herasafe™ KS	Thermo Electron LED GmbH; Langenselbold Germany
Sterile Bench	NU-437 (Nuaire)	Ibs tecnomara GmbH; Fernwald; Germany
Thermostat-Metal	Techne Dri-Block D13.3	Germany
Thermostat	BT 100	Kleinfeld Labortechnik, Germany
Thermostat	MBT 250	ETG-Ilmenau; Illmenau; Germany
Thermomixer	Thermomixer comfort	Eppendorf GmbH; Wesseling-Berzdorf; Germany
Thermomixer	Thermomixer 5436	Eppendorf GmbH; Wesseling-Berzdorf; Germany
Ultracentrifuge Optimal TL	TL361547	Beckman Coulter
Vortex	Vortex-Genie 2	Scientific Industries, Inc; New York; U.S.A.
Water bath	WNB7	Memmert (Shanghai) Trading Co. Ltd; Shanghai City; China
Waterbath	TW8	Julabo
Western Blot electrophoresis chamber	Mini Protean II ™	Biorad, Italy

2.3 Cloning and Plasmids

Table 03. List of plasmid constructs, vectors and primers

Construct name	Vector	Primers (5'-3')	Primer number
GTSE1-GFP-T2A-	EGFP-N2	GTSE1 Fwd - accggactcagatctcgagctcgccAccatggaaggaggcggcggc	SB50

BSD		GTSE1 Rev - gctcctcgcccttgctcacgaacttgaggagtggggaatcca	SB52
		(GFP amplification) Vector GTSE1 Fwd – tggattccccactcctcaagttcgtgagcaagggcgaggagc	SB53
		(GFP amplification) Vector T2A Rev – gacttcctctgccctcggccttgtacagctcgtccatgccg	SB55
		T2A Fwd – cggcatggacgagctgtacaaggccgagggcagaggaagtc	SB54
		T2A Rev – gatctagagtcgcggccgctttaaccctcccacacgtagcca	SB56
		Vector T2A Fwd - tggctacgtgtgggagggttaaagcggccgcgactctagatc	SB51
		Vector GTSE1 Rev - gccgccgcctccttccatggTggcgagctcgagatctgagtccggt	SB57
pFG-GTSE1-FL	pFastBac with GST (pFG)	Fwd – AAAGGATCCGAAGGAGGCGGCGGCCGCG	SB12
		Rev – AAAGAATTCTTAGAACTTGAGGAGTGGGG	SB13
pFG-GTSE1 1-460	pFastBac with GST (pFG)	Fwd – AAAGGATCCGAAGGAGGCGGCGGCCGCG	SB12
		Rev – AAAGAATTCTTATGTCTTGGAATTTAGAC	SB14
pFG-GTSE1 381-739	pFastBac with GST (pFG)	Fwd – AAAGGATCCCTGCGGCCAGCTCTGCCTGC	SB15
		Rev – AAAGAATTCTTAGAACTTGAGGAGTGGG	SB13
pFH-MCAK FL	pFastBac with His (pFH)	MCAK Fwd – ACCTGTATTTTCAGGGCGCCATGGGATCCGCCAT GGACTCGTCGCTTCAGGCCC	SB96
		MCAK Rev – GACTAGTGAGCTCGTCGACGTAGGCCTTTGAATT CTCACTGGGGCCGTTTCTTGCTGC	SB97
		pFH Vector Fwd – AAGCAGCAAGAAACGGCCCCAGTGAGAATTCAA AGGCCTACGTCGACGAGCTCACTAGTC	SB99
		pFH Vector Rev -	

		GGGCCTGAAGCGACGAGTCCATGGCGGATCCCAT GGCGCCCTGAAAATACAGGT	SB98
MCAK-FL-myc	pcDNA4/TO /mycHisA	Fwd - AAAGGATCCATGGCCATGGACTCGTCGCTTCAGG Rev – AAAGAATTCCTGGGGCCGTTTCTTGCTGC	SB1 SB2
MCAK 1-181-myc	pcDNA4/TO /mycHisA	Fwd – AAAGGATCCATGGCCATGGACTCGTCGCTTCAGG Rev – AAGAATTCAGAAGAGCTGCCTCGGATGG	SB1 SB5
MCAK 1-231-myc	pcDNA4/TO /mycHisA	Fwd – AAAGGATCCATGGCCATGGACTCGTCGCTTCAGG Rev – AAAGAATTCTTCCCAGTTTGGAAAACTAC	SB1 SB6
MCAK 182-583-myc	pcDNA4/TO /mycHisA	Fwd – AAAGGATCCATGGCAAACCCTGTGAACTCA Rev – AAAGAATTCGTCTGCATATCTCAGGGTGTTTAA	SB7 SB8
MCAK 232-583-myc	pcDNA4/TO /mycHisA	Fwd – AAAGGATCCATGTTTGCCCGAATGATTAAAG Rev – AAAGAATTCGTCTGCATATCTCAGGGTGTTTAA	SB9 SB8
MCAK 584-725-myc	pcDNA4/TO /mycHisA	Fwd – AAAGGATCCATGAGGGTCAAGGAGCTGAGCCC Rev – AAAGAATTCCTGGGGCCGTTTCTTGCTGC	SB10 SB2
GTSE1-GFP-FL	pEGFP-C1	Fwd - aaaGTCGACATGGAAGGAGGCGGCGGCCGCGAT Rev - aaaGGATCCAGAACTTGAGGAGTGGGGAATCCA	YC1 YC3
GTSE1-GFP 1-460	pEGFP-C1	Fwd - aaaGTCGACATGGAAGGAGGCGGCGGCCGCGAT Rev - aaaGGATCCTTGTCTTGGAATTTAGACAGGAA	YC1 YC4
GTSE1-GFP 1-338	pEGFP-C1	Fwd - aaaGTCGACATGGAAGGAGGCGGCGGCCGCGAT Rev –	YC1

		aaaGGATCCTCCCGCTCCAAACAGGCCCC	YC13
GTSE1-GFP 1-246	pEGFP-C1	Fwd - aaaGTCGACATGGAAGGAGGCGGCGGCCGCGAT Rev – aaaGGATCCTTCTTCCTCTAACAGAGGCCGC	YC1 YC14
GTSE1-GFP 1-187	pEGFP-C1	Fwd - aaaGTCGACATGGAAGGAGGCGGCGGCCGCGAT Rev - aaaGGATCCTGGAGGAGGCCAAGAGCCGAGGC	YC1 YC15
GTSE1-GFP 380-739	pEGFP-C1	Fwd - aaaGTCGACATGCTGCGGCCAGCTCTGCCTGCA Rev - aaaGGATCCAGAACTTGAGGAGTGGGGAATCCA	YC2 YC3
GST-GTSE1 1-460	pGEX-6p1	Fwd – aaaGGATCCATGGAAGGAGGCGGCGGCCGC Rev – aaaGTCGACTGTCTTGGAATTTAGACAGGAA	YC16 YC19
GST-GTSE1 463-739	pGEX-6p1	Fwd – aaaGGATCCATGCCTACTCCTACAAATC AA Rev – aaaGTCGACGAACTTGAGGAGTGGGGAA	YC18 YC17

2.3.1 Cloning using restriction enzymes

2.3.1.1 Polymerase Chain Reaction

PCR is a powerful molecular biology technique that allows us to modify genes and clone the gene of interest. The principle of PCR is to generate multiple copies of the gene of interest using a high fidelity DNA polymerase.

In this study three different DNA polymerases namely, Q5 DNA polymerase, Flash Phusion, and Taq polymerase were used depending on their purpose and availability. Q5 polymerase and Flash Phusion polymerase are high fidelity polymerases and were used for error free amplification of genes. Taq polymerase was used for confirming the results after cloning. Following are the standard procedures that were used for PCR amplification.

Table 04. Standard PCR reaction using Q5 polymerase

Component	Volume for 50 µL PCR reaction
Q5 2x Master Mix (contains dNTPs, Polymerase)	25 µL
10 µM Primer Mix	5 µL (2.5 µL Forward + 2.5 µL Reverse)
DNA	~ 10 – 100 ng
ddH_2O	X µL

Table 05. Standard program used for PCR amplification

Step	Temperature	Time	
Denaturation	98 °C	45 s	
	98 °C	10 s	30x
Annealing	52 °C – 65 °C	30 s	
Elongation	72 °C	3 -5 min	
	72 °C	3 – 5 min	
Pause	4 °C	~	

2.3.1.2 Restriction digestion and agarose gel purification

For cloning using restriction digestion enzymes, the amplified insert and vector DNA were digested with 2 Units of respective enzyme, 2X restriction digestion buffer and ddH_2O as per requirement. The restriction digestion was performed overnight at 37 °C and agarose gel electrophoresis was used to confirm the size of the digested insert and vector. The principle of agarose gel electrophoresis is to separate DNA fragments according to their size. Agarose gels were prepared by dissolving 0.8 or 1% agarose in 1X TAE buffer and 1:25000 Midori Green DNA stain was added to this solution. GeneRuler 1 kb plus DNA ladder was used as a reference for dsDNA molecular weight. Samples were prepared by adding 1/10 volume of Orange G DNA loading dye. Electrophoresis was performed in 1X TAE buffer for 20 min at 120 V. The insert and vector were purified using QIAgen gel extraction kit according to instructions mentioned in the user manual.

Table 06. List of restriction digestion enzymes used for cloning

Restriction enzyme	Company
*Dpn*I	New England Bio Labs Inc., New England, U.S.A.

High Fidelity *EcoR*I	New England Bio Labs Inc., New England, U.S.A.
High Fidelity *BamH*I	New England Bio Labs Inc., New England, U.S.A.
Sal1	New England Bio Labs Inc., New England, U.S.A.

GFP tagged GTSE1 FL, GTSE1 1-460, GTSE1 1-338, GTSE1 1-246, GTSE1 1-187 and GTSE1 380-739 were generated by cloning the constructs into pEGFP-C1 mammalian expression vector using *Sal1* and *BamH1* restriction enzymes. GST tagged GTSE1 FL, GTSE1 1-460 and GTSE1 463-739 constructs were generated by cloning these constructs in pGEX-6p1 bacterial expression vector using *BamH1* and *Sal1* restriction enzymes. For expression of GST tagged GTSE1 in insect cells, *GTSE1-FL, GTSE1 1-460* and *GTSE1 381-739* were cloned into pMultiBAC vector (pFG) using *BamH1* and *EcoR1* restriction enzymes. Myc-tagged *MCAK-FL, MCAK 1-181, MCAK 1-231, MCAK 182-583, MCAK 232-583* and *MCAK 584-725* were cloned in pcDNA4/TO/mycHisA mammalian expression vector using *BamH1* and *EcoR1* restriction enzymes.

2.3.1.3 Ligation

The appropriately digested insert and vector were recombined using T4 DNA ligase. Ligation was performed for 6-7 h at room temperature using the following scheme:

Table 07. Standard scheme used for ligation

Component	Volume for 10 μL ligation reaction
Vector:Insert	1:3
T4 DNA Ligase	2 μL
T4 Ligase Buffer	2 μL
ddH_2O	X μL

2.3.1.4 Transformation

Recombinant DNA was transformed into competent *E.coli* bacterial cells using heat shock method. Bacterial cells were incubated with recombinant DNA for 30 min on ice followed by incubation at 42 °C for 50 sec and then immediately transferred on ice for 5 min. These cells were then supplemented with fresh LB medium and incubated at 37 °C for 1 h before plating on LB agar plates containing the appropriate antibiotic.

Table 08. List of competent *Escherichia coli (E.coli)* cells used for transformation

Bacteria	Strain	Company
E. coli	Rosetta 2(DE3)	Max-Planck Institute, DPF, Dortmund, Germany.
E. coli	OmniMax (chemically competent cells)	Max-Planck Institute, DPF, Dortmund, Germany.
E. coli	Top10 (chemically competent cells)	Thermo Fisher Scientific (Gibco), Waltham, USA
E. coli	Max Efficiency DH10Bac™ Chemically competent cells (EMBACY)	Thermo Fisher Scientific (Gibco), Waltham, USA

2.3.2 Gibson Assembly

Gibson assembly is a technique used to seamlessly clone several genes in a vector (Gibson et al., 2009). It is a one step *in vitro* recombination that uses a combination of a 5' exonuclease, a DNA polymerase, and a DNA ligase. The 5' exonuclease creates 3' overhangs that are repaired by a DNA polymerase and a DNA ligase catalyzes the formation of phosphodiester bonds and ligates the DNA. The insert and vector both were PCR amplified using respective primer pairs and purified using agarose gel extraction. A mixture of vector and insert with a ratio of 1:3 respectively (100ng total DNA concentration) was mixed with the Gibson master mix and incubated at 50 °C for 1 h. Bacterial cells were transformed using 10 µL of this Gibson assembly reaction mix.

2.3.3 Plasmid extraction

Plasmids were extracted using the following kits according to manufacturer's protocol.

Table 09. List of kits used for plasmid/BAC extraction

Kit Name	Company
NucleoSpin Plasmid (NoLid)	Macherey-Nagel GmbH; Düren, Germany
Roti-Prep Plasmid MINI	Carl Roth GmbH, Karlsruhe, Germany
Zymoclean Gel DNA Recovery Kit	Zymo Research Corporation, Irvine, U.S.A.
GeneJET Plasmid Miniprep Kit	Thermo Scientific, Baltics, U.S.A
QiaQuick PCR Purification Kit	Qiagen, Hilden, Germany

Wizard SV Gel and PCR Clean-up system	Qiagen, Hilden, Germany

2.3.4 Preparation of bacterial glycerol stocks

Glycerol stocks of the bacterial cells containing recombinant DNA were prepared by mixing 400 µL of bacterial cell culture with 600 µL of 50% sterile glycerol. The mixture was frozen at -80 °C.

2.4 Cell culture and cell lines

All cell lines were grown in DMEM media containing 10% fetal bovine serum, 2 mM L-Glutamine, 100U/mL Penicillin and 0.1mg/mL streptomycin (PAN Biotech) at 37 °C in 5% CO_2.

Table 10. List of mammalian cell lines

Cell line	Species	Antibiotic resistance	Transgene	Cell line number
HCT116	Human	-	-	A00546
HCT116 Control Clone 1	Human	-	-	A00612
HCT116 Control Clone 4	Human	-	-	A00613
HCT116 GTSE1-GFP Clone 30	Human	BSD (4 µg/mL)	GTSE1-GFP-T2A-BSD	A00640
HCT116 GTSE1-GFP Clone 47	Human	BSD (4 µg/mL)	GTSE1-GFP-T2A-BSD	A00632
HCT116 $p53^{-/-}$	Human	-	-	A00445
HCT116 $p53^{-/-}$ Control Clone 1	Human	-	-	A00616
HCT116 $p53^{-/-}$ Control Clone 5	Human	-	-	A00617
HCT116 $p53^{-/-}$ GTSE1-GFP Clone 27	Human	BSD (4 µg/mL)	GTSE1-GFP-T2A-BSD	A00641
HCT116 $p53^{-/-}$ GTSE1-GFP Clone	Human	BSD (4 µg/mL)	GTSE1-GFP-T2A-BSD	A00642

46				
HEK 293T	Human	-	-	A00411
Hela Kyoto	Human	-	-	A00004
Hela MCAK-LAP (2257)	Human	G418 (200 μg/μL)	MCAK-LAP tag	A00763
MCF-7	Human	-	-	A00562
U2OS wt	Human	-	-	A00002
U2OS H2A.Z-mCherry (Clone 3)	Human	G418 (200 μg/μL)	Mouse Histone H2A.Z – mCherry tag	A00386
U2OS NFLAP-GTSE1 pool	Human	G418 (200 μg/μL)	NFLAP Tag-GTSE1 harboring resistance to RNAi #3	A00375
U2OS GTSE1-GFP siR3 212	Human	G418 (200 μg/μL)	GTSE1-LAP harboring resistance to RNAi #3	A00252
U2OS-PA-Tub	Human	G418 (200 μg/μL)	Tubulin tagged to photoactivatable GFP	A00430

U2OS cells stably expressing RNAi-resistant GTSE1 wild-type transgenes were described previously (Scolz et al., 2012). HCT116 $p53^{-/-}$ and U2OS-PA-GFP-tubulin cells were kind gifts from Duane Compton. U2OS cells expressing NFLAP-GTSE1, MCAK-LAP and mH2A.Z-mCherry were generated by transfecting the respective BACs using Effectene transfection reagent according to manufacturers protocol, and selecting for stable transfectants and were obtained from Antony Hyman. HCT116 and HCT116 $p53^{-/-}$ cells grown in 6 cm dishes were transfected with 1.5 μg of hGTSE1-GFP-T2A-BSD cDNA using 5 μL of Lipofectamine 2000 according to manufacturer's protocol. Stable line populations were selected on BSD (4 μg/mL), and individual clones isolated. HCT116 and HCT116 $p53^{-/-}$ control clones were isolated after treating the cells with Lipofectamine 2000 in absence of DNA.

2.5 Generation of GTSE1 knockout using CRISPR/Cas9 gene editing

This experiment has been performed by Dr. Rondelet and Ms. Nadine Schmidt. This has been taken from Bendre et al. 2016.

To generate GTSE1 knockout cells using the CRISPR-Cas9 system, two different target sites

were chosen in GTSE1 downstream of the ATG in exon 2 (GGCAGGCTGAAGGCTCATCG) and exon 9 (AAGGCCAGAGCAGCGCCGGC). Plasmids expressing the Cas9 nuclease and the corresponding guide RNAs were obtained by cloning the following primers pairs: (5'-CACCGAAGGCCAGAGCAGCGCCGGC-3' and 5'-AAACGCCGGCGCTGCTCTGGCCTTC-3') and (5'-CACCGGCAGGCTGAAGGCTCATCG-3' and 5'-AAACCGATGAGCCTTCAGCCTGCC-3') into the pX330 background (from Addgene), as described in Ran et al., 2013. U2OS cells were transfected with individual plasmids targeting a single site, or with two plasmids targeting both sites simultaneously, and clones were isolated by serial dilution 48 h after transfection. Genomic DNA was prepared using the DNeasy Blood and Tissue kit (Qiagen). The regions surrounding the CRISPR-Cas9 sites were amplified using the primers 5'-CGGCAATGAGTCTCCCTCAG-3' and 5'- AATCGCTTGAACCCGAAAGG-3' (for the site in exon 2) or 5'- CAGTCCACAGCAAATGCCAG-3' and 5'-CACGACTGAGGTGTGACTTC-3' (for the site in exon 9) and the corresponding PCR products were sequenced using primers 5'- CCCTGGGATGCGATCATTTC-3' or 5'-CCCTCAGCACTGCATTAGCAC-3', respectively. Heterozygous insertions and deletions were resolved using the TIDE software (http://tide.nki.nl) as described in (Brinkman et al., 2014).

2.6 Maintaining mammalian cell stocks

Mammalian cells are stored at -150 °C for long-term. Cell grown in 15 cm dishes were harvested by centrifugation at 1500 rpm for 5 min at room temperature. The cell pellet was resuspended in 10 mL freezing media (90% FBS an 10% DMSO) and distributed in cryo-vials and frozen in cryo-freezers for 2 days at -80 °C and then transferred to -150 °C.

2.7 Gene silencing using RNA interference (RNAi)

Table 11. Sequences of silencer RNA (siRNA)

Name	Sequence	Working concentration	Company
GTSE1	5′-GAUUCAUACAGGAGUCAAA-3′	80 nM	Ambion
MCAK	5′-GAUCCAACGCAGUAAUGGU-3′	12 nM	Ambion
Kif2A #2	5'-CUACACAACUUGAAGCUAU-3'	50 nM	Sigma-Aldrich
Kif2A #4	5'-GACCCUCCUUCAAGAGAUA-3	50 nM	Sigma-Aldrich
Silencer	-		Ambion

negative control #2			

Approximately 35,000-40,000 cells were added to prewarmed media in 24-well plates or 8-well imaging chambers. Transfection complexes containing 2.5 µL oligofectamine and siRNA were prepared and incubated at room temperature for 20 min and added immediately afterwards to the cells. Media was changed after 6–8 h. All experiments were performed 48 hours after siRNA transfection.

2.8 Antibodies

Table 12. List of primary and secondary antibodies

Primary antibody	Directed to	Made in	Dilution		Clone number and Company
			WB	IF	
DM1α (anti-alpha tubulin)	Human	Mouse Monoclonal	1:10,000	1:400	Sigma Aldrich
Anti-GTSE1 3753	Human	Rabbit	1:30,000	1:1000	MPI CBG, Dresden (Scolz et al., 2012)
Anti-CREST (human nuclear antibodies to nuclear antigens–centromere autoantibody)	Human	Human	-	1:500	CS1058; Europa Bioproducts Ltd.
Anti-EGFP	Human	Goat	1:10,000	1:5000	MPI CBG, Dresden (Poser et al., 2008)
Anti-c-myc	Human	Mouse	1:5000	1:500	Oncogene/Calibiochem
Anti-MCAK	Human	Mouse	1:800	1.50	Clone 1G2; Abnova Corporation
Anti-CEP135	Human	Rabbit	-	1:5000	MPI CBG, Dresden (Bird and Hyman, 2008)
488 conjugated	Human	Mouse	-	1:500	Kind gift from Andrea

to anti-Mad1					Musacchio
Anti-End Binding Protein 1 (EB1)	Human	Rat			Absea Biotechnology, Clone KT-51
Anti-alpha tubulin	Human	Rat		1:500	Santa Cruz Biotechnlogy, YL1/2
Anti-Kif2A	Human	Rabbit	1:10,000	1:10,000	Novus Biologicas NB500-180
Anti-TACC3	Human	Rabbit	1:5000	1:500	Santa Cruz Biotechnlogy, H-300
Anti-pTACC3	Human	Rabbit	1:1000	1:2000	Kind gift from Kazu Kinoshita
Anti-Ch-Tog	Human	Rabbit	1:2000		Abcam #86073
Anti-Aurora B	Human	Rabbit	1:1000	1:1000	Abcam #2254
Texas Red (594) dye-conjugated AffinityPure	Mouse	Donkey	-	1:500	Jackson ImmunoResearch Europe Ltd., UK
Texas Red (594) dye-conjugated AffinityPure	Rabbit	Donkey		1:500	Bethyl Laboratories, Inc. Montgomery, USA
Texas Red (594) dye-conjugated AffinityPure	Rat	Donkey		1:500	Bethyl Laboratories, Inc. Montgomery, USA
Texas Red (594) dye-conjugated AffinityPure	Human	Donkey		1:500	Jackson ImmunoResearch Laboratories
Alexa 488-conjugated AffinityPure	Mouse	Donkey		1:500	Bethyl Laboratories, Inc. Montgomery, USA
Alexa 488-conjugated AffinityPure	Rabbit	Donkey	-	1:500	Bethyl Laboratories, Inc. Montgomery, USA
Alexa 488-	Goat	Donkey		1:500	Bethyl Laboratories,

conjugated					Inc. Montgomery, USA
Alexa 488-conjugated AffinityPure	Rat	Donkey		1:500	Bethyl Laboratories, Inc. Montgomery, USA
Cy5-conjugated AffinityPure	Mouse	Donkey		1:300	Bethyl Laboratories, Inc. Montgomery, USA
Cy5-conjugated AffinityPure	Rabbit	Donkey		1:300	Bethyl Laboratories, Inc. Montgomery, USA
Cy5-conjugated AffinityPure	Rat	Donkey		1:300	Bethyl Laboratories, Inc. Montgomery, USA
Cy5-conjugated AffinityPure	Human	Donkey		1:500	Jackson ImmunoResearch Laboratories
HRP-conjugated	Mouse	Goat	1:5000	-	GE/Amersham
HRP-conjugated	Rabbit	Donkey	1:5000	-	GE/Amersham
HRP-conjugated	Goat	Donkey	1:5000	-	GE/Amersham

2.9 Immunofluorescence

2.9.1 Fixing using Methanol

Cells on coverslips were fixed using −20 °C methanol for 10 min and then blocked with 0.2% fish skin gelatin (FSG) in PBS for 15 min. Cells were incubated with primary antibodies in 0.2% FSG in PBS for 1 h at 37 °C in a humidified chamber. They were then washed for 30 min with 0.2% FSG, and the same process was repeated with secondary antibodies. Coverslips were mounted with ProLong gold containing DAPI.

2.9.2 Fixing using Paraformaldehyde (PFA)

Cells grown on coverslips were washed once with PBS and then incubated with PFA for 10 min at room temperature. Cells were washed three times with PBS and then incubated with 0.1% Triton X-100 for 5 min followed by washing with PBS. The cells were then stained using the same procedure as mentioned above.

2.10 Microscopy and live cell imaging

Fluorescence dissipation after photoactivation (FDAPA) analysis and images used for quantifying astral length, inner spindle intensity, spindle orientation, and TACC3 and MCAK spindle localization were acquired using a Marianas (3i) spinning disk confocal system based on an Axio Observer Z1 microscope (Zeiss) equipped with a Hamamatsu ORCA-Flash 4.0 Camera. Images were taken using 63x 1.4 NA Apochromat objective (Zeiss). Images for TACC3 spindle localization in U2OS cells were obtained using a 100x 1.4 NA Plan-Apochromat objective (Zeiss). The images were Z-projected using Slidebook software 5.5. All other images were acquired using a DeltaVision imaging system (GE Healthcare) equipped with an sCMOS camera (PCO edge 5.5). Images were taken using a 60x 1.42 NA PlanApo-N objective (Olympus) at room temperature. Serial Z-stacks of 0.2 μm thickness were obtained and deconvolved using SoftWoRx 6.1.1 software. For live cell imaging, media was changed to CO_2 independent media (Gibco) 12 h prior to imaging. Live cell image sequences were acquired at 1 min intervals for 12 h in 2 μm serial Z sections using a 40x 1.42 NA UPlanFL-N objective (Olympus) at 37 °C.

2.11 Image quantification and data analysis

Inner spindle tubulin intensity as well as TACC3 and MCAK spindle localization were quantified in three dimensions using the surface module in IMARIS software (Bitplane). The same surface area detail of 1.0 μm was used for all measurements. Absolute intensities were measured and the intensity sum for the respective channels was used for further calculations. Astral MT lengths were measured in three dimensions using IMARIS software. Astral MT length measurements using EB1 comets were performed as described in Stout et al., 2011. EB1 astral MT comets were quantified using IMARIS software. To measure spindle tilt, both spindle poles were located in the Z-series and then using the angle tool in Slidebook software 5.5, the angle made by the spindle to the substratum was measured. Images were processed with ImageJ and Photoshop (Adobe).

2.12 Determining kinetochore-MT half life by FDAPA

Fluorescence dissipation after photoactivation (FDAPA) in U2OS cells expressing Photoactivatable (PA)-GFP-tubulin was performed as described in Bakhoum et al 2009b. U2OS-PA-GFP-tubulin cells grown on poly-L-Lysine coated 3.5 cm glass bottom chamber were treated with either control or GTSE1 RNAi for 48 h. The medium was changed to CO_2-independent media 12 h prior to the experiment. PA-GFP-tubulin in a small area around the

KT-MT attachment region on the metaphase spindle was activated with a 405 nm laser and images were taken every 10 sec for 5 minutes using the 488 filter. Fluorescence intensity of the entire half spindle containing the activated area was measured at each time point using ImageJ. Fluorescence intensity of the other non-activated half spindle was used for background subtraction. Values were corrected for photobleaching by normalizing to values obtained from taxol-treated stabilized spindles. Following background subtraction and correction for photobleaching, values were normalized to the first time-point and were fitted to a double exponential decay curve $F = A1\times \exp(-k1\times t) + A2\times \exp(-k2\times t)$, using Prism, where A1 and A2 are the percent total fluorescence contribution of the non-KT and KT MTs, k1 and k2 are their respective decay rate constants and t is the time after photoactivation. The curve fitting was performed using Prism and MATLAB. The half-life of KT MTs was calculated using $T1/2 = \ln 2/k_2$.

2.13 KT MT stability assays and determining Mad1 positive kinetochores

U2OS cells treated with either control or GTSE1 RNAi were arrested using Cdk1 inhibitor (RO-3306; 9 μm) at 31 hours after RNAi transfection. Cells were arrested for 17 hours and then released in normal media for 1 h. After 1 h of release the cells were immediately transferred to ice cold media for 17 min and then fixed in -20 °C methanol. To determine the ratio of Mad1 positive KTs, U2OS cells treated with either control or GTSE1 RNAi were arrested using Cdk1 inhibitor (RO-3306) as mentioned for KT MT stability assay. After 1 h of release the cells were fixed with 4% PFA and permeabilized with 0.1% triton X-100. The number of Mad1 positive KTs was determined by quantifying the number of KTs showing Mad1 accumulation in aligned metaphase plates and then dividing it by the total number of KTs within a cell. KTs were detected using the spots module in IMARIS software using a threshold of 0.5 μm. Co-localization of Mad1 with CREST was checked at each z-stack using Coloc tool of IMARIS software. Only bright spots that showed a 100% co-localization with CREST were counted as Mad1 positive.

2.14 Measuring inter-kinetochore distance

To determine the inter-KT distance, U2OS cells treated with either control or GTSE1 RNAi were arrested using Cdk1 inhibitor (RO-3306) as mentioned in section 2.13. After 1 h of release the cells were fixed with 4% PFA and permeabilized with 0.1% triton X-100. The distance between the KTs of two sister chromatids was determined using CREST

immunofluorescence. Distances between the brightest CREST intensities of evident KT pairs were measured using the length tool of Slidebook 6.0 software.

2.15 K-fiber localization of GTSE1 in U2OS and HCT116 cell lines

U2OS cells expressing BAC based GTSE1-LAP$^{WT(303)}$ were arrested using Cdk1 inhibitor (RO-3306) for 17 h and then released in normal media for 1 h. After 1 h of release the cells were immediately transferred to ice cold media for 17 min and fixed using 4% PFA solution prepared using PIPES (50 mM PIPES pH 7.2m 10 mM EGTA, 1 mM $MgCl_2$, 0.2 % Triton X-100. GTSE1 localization to KT fibers was studied using a Marianas (3i) spinning disk confocal system based on an Axio Observer Z1 microscope (Zeiss). Images were taken using a 100x 1.4 NA Plan-Apochromat objective (Zeiss). HCT116 control clones and GTSE1-GFP overexpressing clones were treated in a similar way with an exception that these clones were incubated on ice for 60 min and fixed using -20 °C methanol. Cells were stained for GTSE1, CREST and tubulin and imaged using DeltaVision imaging system.

2.16 Immunoprecipitation

Cells at ~ 70% confluency were arrested in mitosis by adding 3.3 μM nocodazole for 16 h and then harvested by shake-off. Cells in S-phase were obtained by treating them with 2 mM Thymidine for 18 h. Cells were lysed using cell lysis buffer followed by centrifugation at 13,000 rpm for 10 min at 4 °C in order to clear the lysate. A part of the supernatant (100 μL) was taken as "input" and 1-2 μg of the indicated antibody was added to the remaining supernatant and incubated for 2 h at 4 °C with rotation. Dynabeads coupled to protein G were added to the extracts and incubated for 4 h at 4 °C. The beads were washed three times with 1 mL of cell lysis buffer each and once with 1X PBS and then resuspended in hot Laemmli buffer to be analyzed by Western blotting. To study the interdependence of GTSE1-MCAK interaction on phosphorylation the cell lysates were treated with either a phosphatase inhibitor (PPI) to prevent removal of any phosphorylation or with λ-phosphatase to obtain the above proteins in the dephosphorylated state.

2.17 Sodium dodecyl sulfate (SDS) electrophoresis

In order to perform western blotting after RNAi, cells were harvested by directly adding hot Laemmli buffer in 24 well plates. For comparing protein levels, cells were harvested by centrifugation at 1500 rpm for 5 min at 4 °C. Cells were lysed using cell lysis buffer and the protein concentration was determined using Bradford assay. Equal amount of protein (40-50

μg for GTSE1) was further used for SDS electrophoresis. SDS electrophoresis separates proteins according to their molecular weights. Proteins are denatured using Laemmli buffer, which contains a negatively charged detergent SDS that coats the polypeptide chains. Due to this the proteins obtain a net negative charge. These negatively charged proteins move with different speeds towards the anode. The speed at which they move depends on the molecular weight of proteins and the percentage of acrylamide in the gel. Smaller proteins move faster through the pores towards the anode, whereas, the motion of larger proteins is retarded due to the small pore size of the acrylamide gel. SDS PAGE gels were run using SDS-PAGE running buffer at 100-120 V for 1.5-2 h.

2.18 Western blot

Proteins separated on SDS-page gels were further processed for Western blot analysis. Western blotting is employed to detect specific proteins of interest using specific antibodies. Proteins from SDS-PAGE gels were transferred onto nitrocellulose membrane using Western transfer buffer at 300 mA for 3 h at 4 °C. The membrane was blocked with 5 % skimmed milk in 1X PBS containing 0.1% Tween20 (PBS-T) and incubated with primary antibodies overnight at 4 °C. The membrane was then washed three times for 10 min each using PBS-T followed by incubation with appropriate secondary antibodies for 1 h at room temperature. The membrane was washed three times for 15 min each with PBS-T. Protein signals were detected using enhanced chemiluminescence.

2.19 Purification of GST-GTSE1 from bacteria

The *hGTSE1* 1-460 and 463-739 fragments and GST were cloned into pGEX-6p-1rbs vector and expressed in bacteria. Bacteria were grown until they reached an $O.D_{600}$ of 0.8 and protein expression was induced using 1 mM IPTG and incubated overnight at 20 °C. The bacterial cells were pelleted by centrifugation at 4000 rpm for 20 min at room temperature. Cells were resuspended in GST binding buffer (25 mM HEPES pH 7.5, 300 mM NaCl, 1 mM EDTA, 5% glycerol, 1% Triton X-100, DNase), lysed by sonication and cleared by centrifugation at 29,000 rpm for 30 min at 4 °C. The cleared lysate was incubated with Glutathione resin (Amintra) overnight at 4 °C. The beads were washed with GST binding buffer and the purified protein was used for experiments.

2.20 Pull-downs using bacterial protein

In vitro GST pull-downs were performed in GST binding buffer by incubating equal amount

of purified FL-MCAK with GST alone or GST-hGTSE1 1-460 and 463-739 fragments (immobilized on Glutathione resin) for 1 h at 4 °C. The reactions were washed with GST binding buffer and resuspended in hot Laemmli buffer and analyzed by Western blotting.

2.21 Protein purification using insect cells

2.21.1 Generation of Baculovirus and protein expression in insect cells

Baculovirus protein expression system as explained in Trowitzsch et al., 2010 was used for production of GST tagged *GTSE1 FL, GTSE1 1-460, GTSE1 381-739* and His tagged *MCAK FL* proteins. The gene of interest was cloned into pFLMultiBAC vector and confirmed by sequencing. The recombinant DNA was transformed into EMBACY *E.Coli* competent cells using heat shock method. The only exception to the transformation protocol was that the cells were incubated at 37 °C for 6 h. Bacterial cells were plated onto LB agar plates supplemented with 10 g/mL Gentamycin, 7 g/mL Tetracycline, 50 g/mL Kanamycin, 40 g/mL IPTG and 100 g/mL X-Gal. The EMBACY cells contain a BAC that harbors the Baculovirus genome along with a helper plasmid containing the Tn7 transposon enzyme complex under an IPTG inducible promoter. In the pFLMultiBAC vector, our gene of interest is flanked by Tn7R and Tn7L transposon sequences. In EMBACY cells after induction with IPTG, Tn7 transposon enzyme complex allows integration of our gene from the pFLMultiBAC vector to a site on the BAC, which disrupts the *LacZα* gene. Bacteria containing the recombinant BAC were identified using blue/white screening. One white colony was grown in liquid culture containing 10 g/mL Gentamycin, 7 g/mL Tetracycline, 50 g/mL Kanamycin overnight at 37 °C. The purified BAC was precipitated using isopropanol for 30 min on ice and further washed twice using 70% ethanol. The ethanol was removed under sterile conditions and the BAC was resuspended in Tris-EDTA buffer. Transfections were performed in 6 well dishes containing Sf9 cells ($1*10^6$ cells/mL; immortalized cell line from *Spodoptera frugiperda*) using FuGENE transfection reagent. The cells after transfection were incubated for 3 days at 27 °C. After 72 h, cells were resuspended and added to a 10 cm dish containing $1*10^6$ Sf9 cells/mL and incubated for 4 days at 27 °C for amplification of the virus. After 96 h, the cells were harvested and centrifuged at 2500 rpm for 5 min at 27 °C. Thereafter, 5% FBS was added to the supernatant, which was then sterile filtered and stored at 4 °C as V0 (Virus0). The virus was further amplified by adding 1:50 of the V0 to 50 mL $1*10^6$ Sf9 cells/mL and incubated for 4 days at 27 °C. The 50 mL culture was harvested by centrifugation and the supernatant was stored at 4 °C as V1. Similarly, the V1 was further amplified to produce V2,

by adding 1:50 V1 in 50 mL Sf9 culture. This V2 was further used for large-scale expression of proteins in Tnao38 (*Trichoplusia ni*) cells.

2.21.2 Purification of untagged GTSE1, GTSE1 1-460, GTSE1 381-739 and GST-GTSE1

GST tagged *GTSE1-FL, GTSE1 1-460*, and *GTSE1 381-739* were expressed as described in section 2.21.1. GST-GTSE1-FL protein was expressed in Tnao38 insect cells at 27 °C for 72 h by inoculating the virus (V2) at a titer of 1:20. After 72 h, the cells were harvested by centrifugation at 1800 rpm for 15 minutes. The cell pellet was either stored at -80 °C or processed immediately. Cell pellet from 1 L culture was resuspended in 100 mL ice cold Buffer A (50 mM HEPES pH 7.5, 300 mM NaCl, 5% Glycerol, 2 mM TCEP and Protease inhibitors), lysed by sonication and clarified by centrifuging at 29,000 rpm for 50 minutes at 4 °C. The cell lysate was incubated with 1 mL Glutathione resin (Amintra) for 1 hour at 4 °C. The resin beads were loaded on gravity flow columns and washed with 150 mL Buffer A at 4 °C. GTSE1 was cleaved from the beads using GST Precision enzyme overnight at 4 °C. The protein was eluted and concentrated using Amicon concentrators, after which it was further purified by Size Exclusion Chromatography in a Superdex 200 10/300 column using gel filtration buffer (30 mM HEPES pH 8, 300 mM NaCl, 5% glycerol, 2 mM TCEP). The peak fractions were collected and concentrated in Amicon concentrators to give a final concentration of 5–10 μM.

Similarly, GTSE1 1-460 and GTSE1 381-739 were produced and purified from insect cells. Likewise, GST tagged GTSE1-FL was also purified from insect cells. However, instead of cleaving using GST Precision enzyme, the protein was eluted using 40 mL of 40 mM glutathione and directly concentrated and run through a gel filtration column as described above.

2.21.3 Purification of His-MCAK

Full-length human *MCAK* cDNA sequence was cloned into pFLMultiBac vectors and baculovirus was generated. His-MCAK-FL protein was expressed in Tnao38 insect cells at 27 °C for 48 hours using 1:20 V2 virus titer. The cells were harvested by centrifugation at 1800 rpm for 15 min. The cell pellet was either stored at -80 °C or processed immediately. Cell pellet from 1 L culture was resuspended in 100 mL ice-cold BRB80 buffer (80 mM PIPES-KOH pH 6.9, 150 mM KCl, 1 mM EGTA, 1 mM $MgCl_2$, 10 μM ATP and 1 mM TCEP) lysed by sonication and clarified by centrifuging at 29,000 rpm for 50 min at 4 °C.

The cell lysate was incubated with 6 mL Ni-NTA superose resin for 1 hour at 4 °C. The resin beads were loaded on gravity flow columns and washed with 150 mL BRB80 buffer containing 10 mM imidazole at 4 °C. The protein was eluted using BRB80 buffer with 250 mM imidazole and concentrated using Amicon concentrators. The protein was further purified by size exclusion in a Superdex 200 10/300 column using BRB80 buffer. The peak fractions corresponding to His-MCAK dimers were collected and concentrated in Amicon concentrators to have a final concentration of 5–10 μM.

2.22 Pull-down and Size Exclusion Chromatography using GTSE1 and MCAK purified from insect cells

2.22.1 Phosphorylation of GTSE1

GST-GTSE1-FL, GTSE1-FL, GTSE1 1-460 and GTSE1 381-739 purified from insect cells were phosphorylated by Cdk1 or Aurora A using a 1:100 (kinase: protein) ratio overnight on ice in pull-down buffer further supplemented with 10 mM $MgCl_2$, 1 mM sodium orthovanadate and 2 mM ATP. The phosphorylation reaction was stopped by adding 5 μM RO-3306 (Cdk1 inhibitor) or 500 nM MLN8054 (Aurora A inhibitor) for 10 min on ice. The proteins were then either used for GST pull-down or for gel filtration.

2.22.2 ProQ Diamond staining

Phosphorylation of GTSE1 was confirmed using ProQ diamond staining. Equimolar concentrations (2 μM) of all proteins phosphorylated and unphosphorylated were resolved on a SDS PAGE gel. The gels were incubated with fixing solution overnight following which they were washed three times with water to remove all traces of fixing solution. Next the gels were incubated with ProQ Diamond phospho-specific stain for 90 min with shaking in dark. Gels were destained thrice for 30 min each with destaining solution followed by washing with water for 10 min thrice. All the steps were performed at room temperature. The signal for ProQ was detected using the BioRad developer. The gel was then stained with Coomassie brilliant blue (CBB) to confirm equal protein loading.

2.22.3 Pull-down using GST-GTSE1-FL

In vitro GST pull-downs were performed by incubating 2 μM unphosphorylated GST-GTSE1, Cdk1 phosphorylated GST-GTSE1 and Aurora A phosphorylated GST-GTSE1 with 3 μM His-MCAK and 5 μL GSH resin in a final volume of 30 μL. From this reaction, 5 μL was collected as input. The pull-down was performed for 1 h on ice in pull-down buffer. The

GSH-beads were washed 3 times with 250 µL of wash buffer and then denatured by adding 20 µL of 2x Laemmli buffer. The pull-downs and inputs were analyzed using SDS PAGE gels and the gels were stained with CBB for 20 min and then destained with water.

2.22.4 Size Exclusion Chromatography (SEC)

SEC is used to study protein-protein interactions. The principle of SEC is to separate proteins according to their sizes. The chromatography column is filled with a matrix consisting of beads with pores of specific sizes. When a mixture of proteins is loaded onto the column smaller proteins move slowly through the column as they pass through all the pores, whereas, larger proteins cannot enter the pores and elute faster. This allows detection of an interaction between proteins by comparing the elution profiles of proteins alone and when they are in a complex. Depending on their size, single proteins elute at a specific volume, however if it forms a complex with another protein, then the complex elutes faster due to its higher molecular weight. Interaction between GTSE1 and MCAK was thus analyzed using SEC. Unphosphorylated GTSE1 (4.5 µM) and Aurora A phosphorylated GTSE1 (4.5 µM) were incubated with 4.5 µM MCAK for 1 h on ice and loaded on a S200 increase 5/150 SEC column. Similarly, SEC was performed to check the interaction between MCAK (5 µM) and unphosphorylated GTSE1 1-460 (5 µM), Aurora A phosphorylated GTSE1 1-460 (5 µM), unphosphorylated GTSE1 381-739 (5 µM) and Aurora A phosphorylated GTSE1 381-739 (5 µM). Interaction was studied by analyzing the same elution fractions for all conditions by CBB staining of SDS-PAGE gels. The phosphorylation of proteins was confirmed by ProQ staining.

2.23 Microtubule Pelleting Assays

Taxol stabilized MTs were prepared by incubating MTs with 1 mM GTP at 37 °C for 30 min followed by incubation at 37 °C for 5 min after addition of 50 µM taxol. 1.66 µM tubulin was added to a reaction mixture of MCAK (200 nM) and increasing concentrations of GTSE1. All reactions were performed in BRB80 buffer (80 mM Pipes pH 6.8, 1 mM EGTA, 1mM $MgCl_2$) supplemented with 70 mM KCl, 1.5 mM ATP, 10 µM taxol for 1 h at room temperature. The reaction was then layered onto a cushion buffer (80 mM PIPES, 1 mM EGTA, 1 mM $MgCl_2$, 50% glycerol) in a microcentrifuge tube and was centrifuged at 90,000 rpm in a TLA-120.1 rotor for 10 min at 25 °C. Supernatant and pellet fractions were separated by SDS–PAGE and stained with CBB for analysis.

2.24 Total internal reflection fluorescence microscopy assays for microtubule dynamics and MCAK activity

This experiment has been performed by Conrad Hall and can be referred to in Bendre et al., 2016.

2.24.1 Tubulin and microtubule preparation:

Tubulin was purified from juvenile bovine brains using a modified version of the high-PIPES method (Castoldi and Popov, 2003), wherein the first polymerization cycle was performed in 100 mM PIPES instead of 1 M PIPES. Labelling of tubulin with tetramethylrhodamine (TAMRA) and Alexa Fluor 546 succinimidyl esters (Life Technologies) was performed as described previously (Wieczorek et al., 2013). GMPCPP stabilized MTs were prepared as follows: A polymerization mixture was prepared with BRB80 (80 mM PIPES-KOH, pH 6.9, 1 mM EGTA, 1 mM $MgCl_2$)+ 2 mM tubulin, 1 mM GMPCPP (Jena Biosciences), 1 mM $MgCl_2$ and a 1:4 molar ratio of TAMRA-labelled/unlabelled tubulin. The mixture was incubated on ice for 5 min, followed by incubation at 37 °C for 2 h. The polymerized GMPCPP MTs were centrifuged at maximum speed in a Beckman Airfuge and resuspended in BRB80. GMPCPP seeds were prepared by polymerizing a 1:4 molar ratio of TAMRA-labelled/unlabelled tubulin in the presence of guanosine-5′-[(α, β)-methyleno]triphosphate (GMPCPP, Jena Biosciences) in two cycles, as described previously (Gell et al., 2010). GMPCPP seeds prepared in this way were stable for several months at −80 °C.

2.24.2 Total internal reflection fluorescence microscopy and preparation of microscope chambers:

The microscope set-up uses a Zeiss Axiovert Z1 microscope chassis, a ×100 1.45 NA Plan-apochromat objective lens, and the Zeiss TIRF III slider. A λ = 491 nm diode-pumped solid-state laser (Cobolt) was coupled to a fiber optic cable in free space and introduced into the Zeiss slider. Epifluorescence was achieved using a PhotofluorII excitation source (89 North) with wavelength-specific filter cubes (Chroma). Images were recorded using an Andor iXon + DV-897 EMCCD cameras. Microscope chambers were constructed using custom-machined mounts (Gell et al., 2010). In brief, cover glass was cleaned and silanized as described previously (Helenius et al., 2006). Cover glasses (22 × 22 mm and 18 × 18 mm) were separated by two layers of double-sided tape creating a channel for the exchange of solution. Image acquisition was controlled using MetaMorph (Molecular Devices).

Seeds or GMPCPP stabilized MTs depending on the experiment were adhered to silanized glass slides as described previously (Bechstedt and Brouhard, 2012). On the day of each experiment for the dynamic assay, aliquots of unlabelled and Alexa Fluor 546-labelled tubulin were thawed, mixed to a 1:3 molar labelling ratio, aliquoted again, and stored in liquid nitrogen.

MT growth from GMPCPP seeds was achieved by incubating flow channels with tubulin in standard polymerization buffer: BRB80, 1 mM GTP, 0.1 mg ml^{-1} BSA, 1% 2-mercaptoethanol, 250 nM glucose oxidase, 64 nM catalase, 40 mM D-glucose. Assays were performed with an objective heater set to 35 °C. Time-lapse image sequences were acquired at 5 sec intervals. MCAK depolymerization of GMPCPP stabilized seeds was achieved by incubating flow channels with MCAK and standard polymerization buffer plus ATP: BRB80, 1 mM GTP, 0.1 mg ml^{-1} BSA, 1% 2-mercaptoethanol, 250 nM glucose oxidase, 64 nM catalase, 40 mM D-glucose and 1mM ATP. Assays were performed with an objective heater set to 35 °C. Time-lapse image sequences were acquired at 5 sec intervals.

2.24.3 Microtubule growth and shrinkage rates:

MT growth rates were analyzed by manually fitting lines to kymographs of growing MTs using the Kymograph and Linescan features in MetaMorph (Molecular Devices).

2.25 Fluorescence in situ hybridization

HCT116 and HCT116 $p53^{-/-}$ cells grown on 22 mm coverslips were washed once with 1x PBS and fixed with (3:1) methanol-acetic acid solution at room temperature for 30 min. Cells on coverslips were dried at room temperature for 10 min and immersed in 2X SSC (0.3 M NaCl, 30 mM sodium citrate) for 5 min at room temperature. Cell were dehydrated using increasing concentrations of ethanol (70%, 85%, 100%) for 5 minutes each at room temperature and then air-dried for 10 minutes. Cells were processed for FISH by using specific α-satellite probes against chromosome 7 and 11 (Cytocell) according to the manufacturers protocol. Coverslips were mounted using ProLong gold with DAPI overnight at room temperature and sealed. Chromosome signals from approximately 1000 cells were scored using the criteria outlined in Van Stedum and King, 2002.

2.26 Statistical analysis

Statistical significance was determined by performing two-tailed Student's t-test with unequal-variance unless otherwise stated. Statistical analysis of all karyotype studies, quantification of lagging chromosomes in GTSE1-overexpressing clonal cell lines, and

phenotype quantification in GTSE1 knockout clonal cell lines were performed using chi-squared tests.

3. Results

GTSE1 is an intrinsically disordered protein that binds to the MT lattice and EB1 during interphase, which is necessary for cell migration (Scolz et al., 2012). As the cell enters into mitosis, GTSE1 is highly phosphorylated by Cdk1 and Aurora A and this abrogates its binding to EB1 and MTs (our unpublished data). GTSE1 stops tip tracking at the prophase to prometaphase transition (Figure 8A) and localizes to spindle MT and spindle poles via interaction with the TACC3-Ch-Tog-Clathrin complex. During anaphase, GTSE1 resumes plus tip tracking and accumulates strongly at the spindle poles (Figure 8A). Preliminary results suggest that GTSE1 is required for proper spindle assembly and for accurate chromosome alignment. Here I present a novel mechanism by which the protein GTSE1 inhibits MCAK's depolymerase activity *in vivo* and *in vitro* to regulate MT dynamics required for proper mitotic spindle assembly and precise chromosome segregation.

3.1 GTSE1 stabilizes astral MTs in mitosis and promotes correct spindle orientation.

To investigate the role of GTSE1 during mitosis, we depleted GTSE1 using RNA interference (RNAi) in U2OS cells and observed more than 90% depletion after 48 h (Figure 8B). Cells depleted of GTSE1 were fixed for immunofluorescence and looked at for mitotic phenotypes. Reducing GTSE1 levels in U2OS cells decreased the overall MT stability during mitosis. Immunofluorescence analysis showed that more than 50% of cells in prometaphase and metaphase lacked astral MTs or had dramatically shorter astral MTs (Figure 8C and D). Comprehensive analysis of astral MT stability was performed via three different methods. We measured the lengths of 10 longest astral MTs after control and GTSE1 RNAi using α-tubulin immunofluorescence in 3D using Imaris software. Astral MT lengths were radically reduced to 2.8 μm after depletion of GTSE1 as compared to 5.7 μm for control cells (Figure 8E). We then quantified the astral MT lengths using EB1 immunofluorescence (Analysis was performed by Dr. Rondelet, Bendre et al., 2016). Astral MT lengths were determined by calculating the distance between EB1 labeled astral MT plus ends and EB1 maximum intensity at the centrosomes. Consistently, reducing GTSE1 levels showed a significant reduction in average astral MT lengths (Figure 8F). Next we quantified the number of growing astral MTs using EB1 plus end localization with Imaris software (Analysis was performed by Dr. Rondelet; Bendre et al., 2016). In line with our previous observation, the

total number of astral MTs was reduced nearly by 50% after depletion of GTSE1 (Figure 8G).

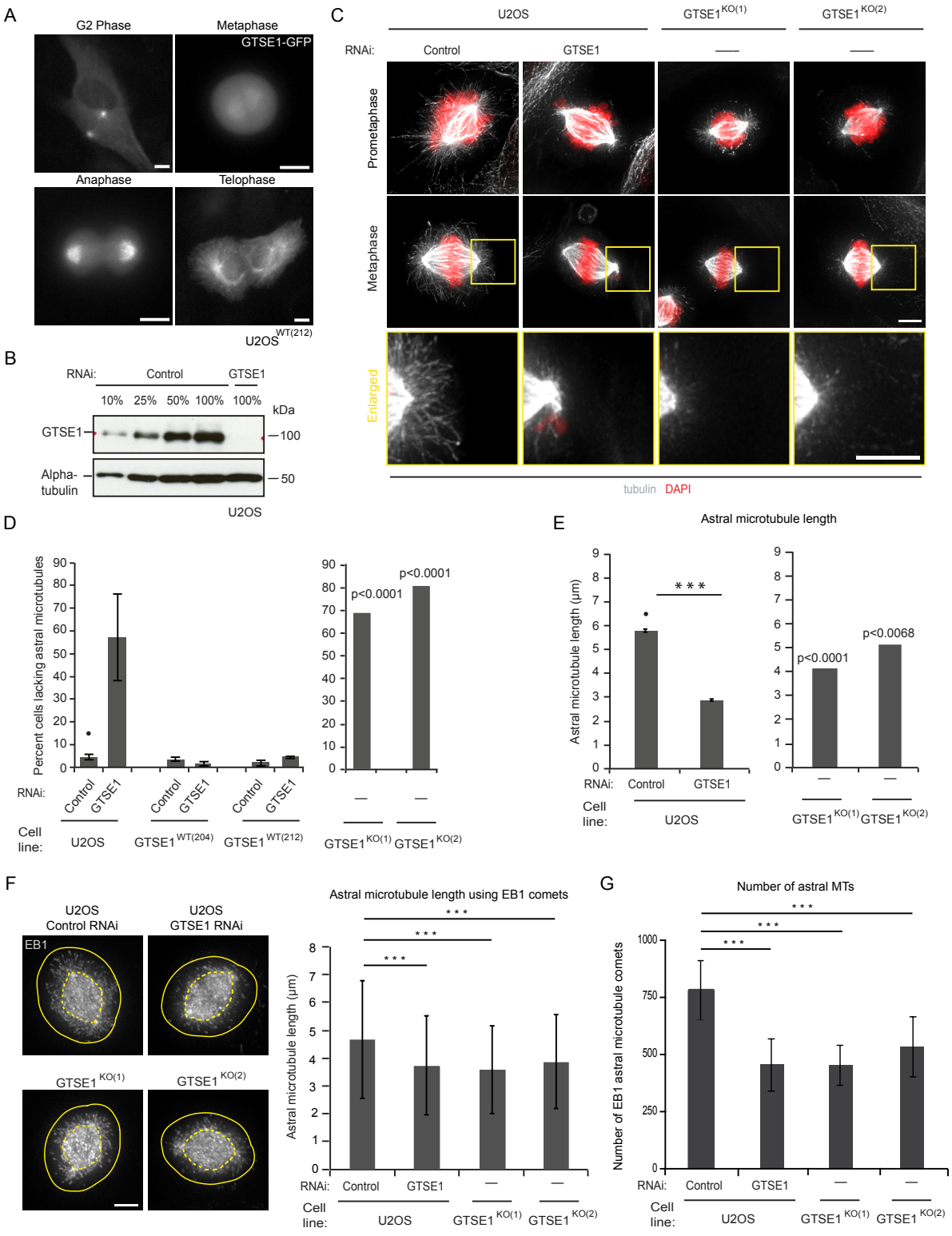

Figure 8. GTSE1 stabilizes astral MTs during mitosis

A. Representative live cell images showing localization of GTSE1-GFP during G2-phase, metaphase,

anaphase and telophase in U2OS$^{WT(212)}$ (Scale bar represents 10 μm). **B.** Western blot of U2OS cells lysate (indicated with the dilution) either treated with control RNAi or GTSE1 RNAi and probed for GTSE1 and α-tubulin displaying >90% reduction in GTSE1 levels. **C.** Representative immunofluorescence images of prometaphase and metaphase U2OS cells after GTSE1 RNAi and GTSE1 knockout clones (GTSE1$^{KO(1)}$ and GTSE1$^{KO(2)}$) showing MTs (α-tubulin) and DNA (DAPI). Enlarged inset shows short astral MTs in U2OS cells after GTSE1 RNAi and in U2OS GTSE1 knockout clones. **D.** Quantification of percentage of cells showing short astral MTs. Left bar graph shows percent cells lacking astral MTs after control and GTSE1 RNAi in U2OS cells and two U2OS clones stably expressing siRNA resistant version of GTSE1 (n > 150 cells over 3 experiments per condition). The right bar graph shows percentage of GTSE1 knockout cells (GTSE1$^{KO(1)}$ and GTSE1$^{KO(2)}$) lacking astral MTs {n > 100 cells; p-values were obtained from a chi-squared test comparing to the U2OS control condition (marked with •)}. **E.** Quantification of average astral MT length. The length of 10 longest astral MTs was measured using α-tubulin immunofluorescence. Left bar graph shows average astral MT length after control and GTSE1 RNAi in U2OS cells (10 astral MTs were measured per cell. n = 10 cells per experiment per condition; 3 experiments). The right bar graph shows average astral MT length in GTSE1 knockout cells (GTSE1$^{KO(1)}$ and GTSE1$^{KO(2)}$) (10 astral MTs were measured per cell. n = 10 cells per experiment per condition.) **F.** Immunofluorescence images of U2OS cells after control and GTSE1 RNAi and GTSE1 knockout clones (GTSE1$^{KO(1)}$ and GTSE1$^{KO(2)}$) stained with EB1, showing reduced EB1 comets following GTSE1 RNAi and in GTSE1 knockout clones. Bar graph shows quantification of astral MT length measured using EB1 plus tip position relative to the centrosome (n > 5800 astrals from a single experiment; error bars represent standard deviation; p-values were obtained using a Kruskal-Wallis test followed by Conover-Iman test); (Analysis was performed by Dr. Rondelet; Bendre et al., 2016). **G.** Graph shows number of astral MTs that was determined by quantifying EB1 comets in U2OS cells following GTSE1 and control RNAi and in U2OS GTSE1 knockout cells (GTSE1$^{KO(1)}$ and GTSE1$^{KO(2)}$) (n ≥ 13 cells per condition from a single experiment; error bars represent standard deviation; p-values were obtained using an Anova and a Tukey's test); (Analysis was performed by Dr. Rondelet; Bendre et al., 2016). All scale bars represent 5 μm unless stated otherwise and all error bars when not specified represent standard error of the mean. p≤0.05*, p≤0.01**, p≤0.001***

To confirm that the phenotypes seen after GTSE1 siRNA were specific to GTSE1 depletion, we depleted endogenous GTSE1 in two clonal U2OS cell lines (GTSE1$^{WT(204)}$ and GTSE1$^{WT(212)}$) stably expressing a GTSE1-GFP siRNA resistant BAC transgene (Scolz et al., 2012; Bird et al., 2011). siRNA resistant GTSE1-GFP localized normally to the mitotic spindle and spindle poles (Figure 8A), and reducing endogenous GTSE1 levels in these

U2OS clones did not affect astral MT stability, confirming specificity of GTSE1 siRNA (Figure 8D) (Analysis was performed by Dr. Bird; Bendre et al., 2016).

We further verified the effect of GTSE1 depletion on astral MT stability, by knocking out genomic copies of GTSE1 from U2OS cells using CRISPR/Cas9 gene editing (Cong et al., 2013; Ran et al., 2013). We could isolate two viable U2OS clonal cell lines where GTSE1 was efficiently knocked out ($GTSE1^{KO(1)}$ and $GTSE1^{KO(2)}$) (Generated by Dr. Rondelet and Nadine Schmidt). Analysis of GTSE1 knockout clones using α-tubulin and EB1 immunofluorescence also displayed a dramatic reduction in astral MT stability (Figure 8C-G).

The effect of GTSE1 depletion on astral MT stability was also studied in three different cell lines. Reducing levels of GTSE1 by RNAi in Hela Kyoto, HCT116 and MCF-7 cell lines led to a >80% decrease in GTSE1 levels after 48 h (Figure 9B, D and F). Depletion of GTSE1 in Hela Kyoto and HCT116 adversely affected astral MT stability during prometaphase and metaphase (Figure 9A and 9C). The effect on astral MT stability after GTSE1 depletion was more pronounced in Hela Kyoto cells as compared to HCT116 cells. However, depletion of GTSE1 had no effect on astral MT stability in MCF-7 cell line (Figure 9E). Interestingly, depletion of GTSE1 in Hela Kyoto cells led to an increase in number of cells with multipolar spindles (data not shown).

It has been shown in several studies that astral MTs are required for orientating the mitotic spindle parallel to the substratum, which is important for defining the axis for cell division (Pearson and Bloom, 2004; di Pietro et al., 2016). As depletion of GTSE1 leads to a loss of astral MTs, we measured the angle made by the metaphase spindle relative the substratum (Figure 9G). In line with the astral phenotype, 31% of U2OS cells showed mis-orientation of the spindle after depletion of GTSE1 as compared to only 9% after control RNAi (Figure 9G). Thus, GTSE1 is required for astral MT stability and proper spindle orientation.

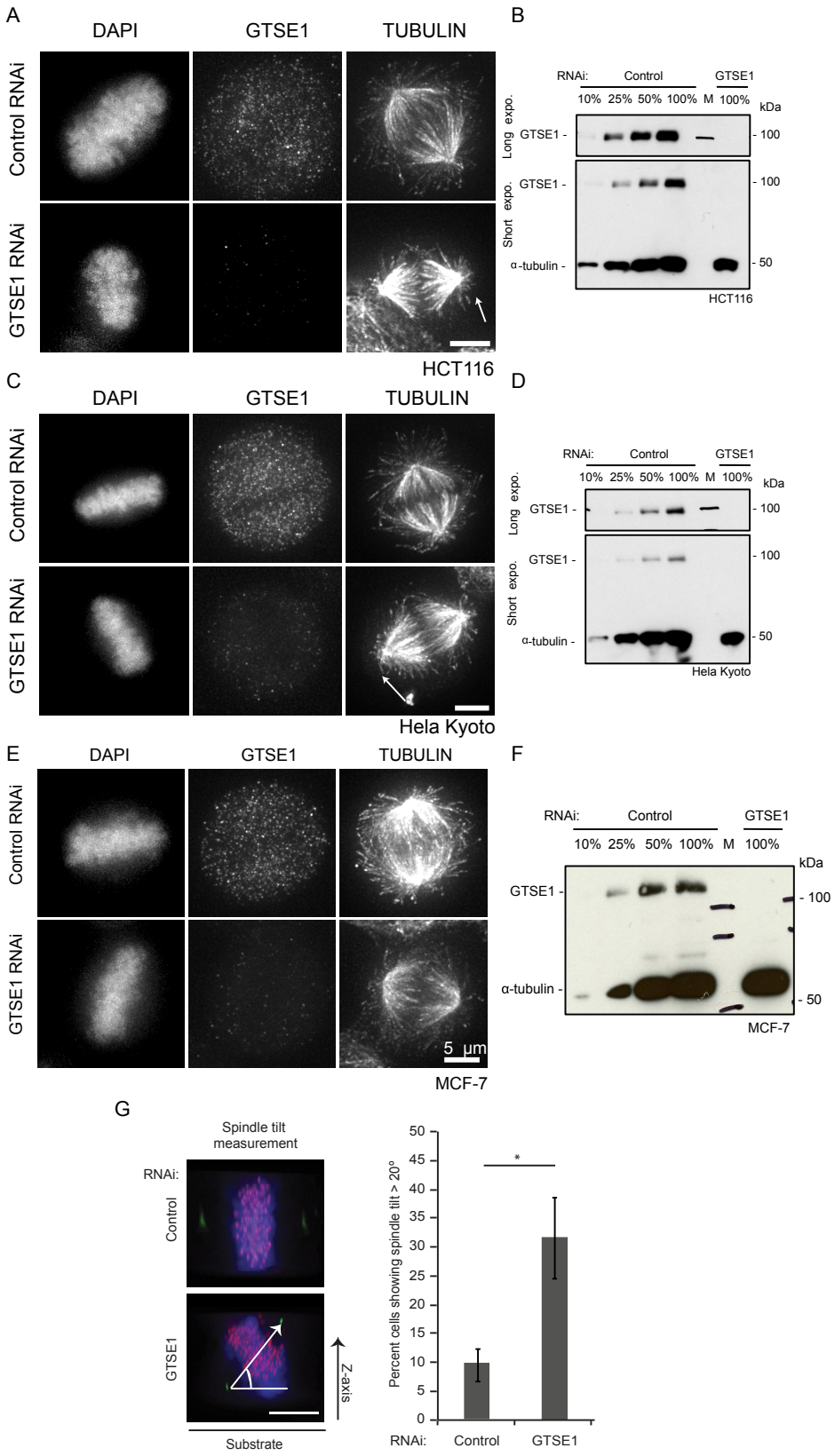

Figure 9. GTSE1 stabilizes astral MTs in Hela Kyoto and HCT116 and is required for spindle orientation

A. Representative immunofluorescence images depicting shorter astral MTs in HCT116 cells after

GTSE1 RNAi as compared to control RNAi. Cells were probed for α-tubulin (MTs), GTSE1 and DAPI (DNA). White arrows show reduced astral MTs. **B.** Western blot of HCT116 cell lysates after control and GTSE1 RNAi. Dilutions of control lysates were used to determine efficiency of GTSE1 depletion. **C.** Immunofluorescence images of Hela Kyoto cells showing short astral MTs after GTSE1 RNAi. Cells were stained with α-tubulin (MTs), GTSE1 and DAPI (DNA). White arrows show reduced astral MTs. **D.** Western blot of Hela Kyoto cell lysate after control and GTSE1 RNAi showing >90% depletion of GTSE1. **E.** Immunofluorescence images of MCF-7 cells stained for MTs (α-tubulin), GTSE1 and DNA (DAPI) showing no effect on astral MT stability after GTSE1 RNAi. **F.** Western blot of MCF-7 cell lysate showing efficient (>90%) depletion of GTSE1 as compared to control RNAi. **G.** Analysis of spindle orientation. Immunofluorescence images of U2OS cells viewed sideways showing normal spindle orientation in control cells and tilted spindles after GTSE1 RNAi. Cells were stained with anti-CREST (KTs), Cep135 (centrosomal marker) and DAPI (DNA). The spindle tilt was measured by calculating the angle made by the centrosomes with the substratum. Bar graph displays percentage of U2OS cells with mis-oriented spindles (>20° angle with the substratum) following control or GTSE1 RNAi (n > 140 cells over 3 experiments per condition). All scale bars represent 5 μm and all error bars when not specified represent standard error of the mean. $p \leq 0.05$*, $p \leq 0.01$**, $p \leq 0.001$***

3.2 GTSE1 is required for efficient chromosome alignment

In addition to astral MT phenotype, depletion of GTSE1 in U2OS cells using RNAi affected chromosome alignment and mitotic progression. After GTSE1 depletion, 50% of U2OS cells showed a few chromosomes that were not aligned at the metaphase plate (Figure 10A and 10B). Defects in chromosome alignment were efficiently rescued in two U2OS clonal cell lines stably expressing BAC based siRNA-resistant GTSE1-GFP transgene, after depletion of endogenous GTSE1, confirming specificity of siRNA (Figure 10B); (Analysis was performed by Dr. Bird; Bendre et al., 2016). We next examined chromosome alignment in U2OS GTSE1 knockout clones ($GTSE1^{KO(1)}$ and $GTSE1^{KO(2)}$) and saw a subtle yet significant increase in cells with misaligned chromosomes (Figure 10B). It was evident that even in absence of GTSE1 these clones survived and aligned chromosomes efficiently, indicating that these GTSE1 knockout clones might have evolved through selection of some (epi)genetic adaptation. GTSE1 knockout clones could have adapted by reducing the spindle size, as this might allow the cell to efficiently align chromosomes at the metaphase plate as the distance these chromosomes have to travel from the spindle pole to the spindle equator will be shorter. Therefore, we quantified spindle length using Cep135 immunofluorescence and did not observe a significant change after depletion of GTSE1 and in GTSE1 knockout

clones (Figure 10C). Furthermore, the levels of other proteins like Ch-Tog, TACC3, p-TACC3 and Aurora B that have been identified to play an important role in regulating MT dynamics during mitosis remained unaltered in GTSE1 knockout clones (Figure 10D-F) (Analysed by Dr. Rondelet).

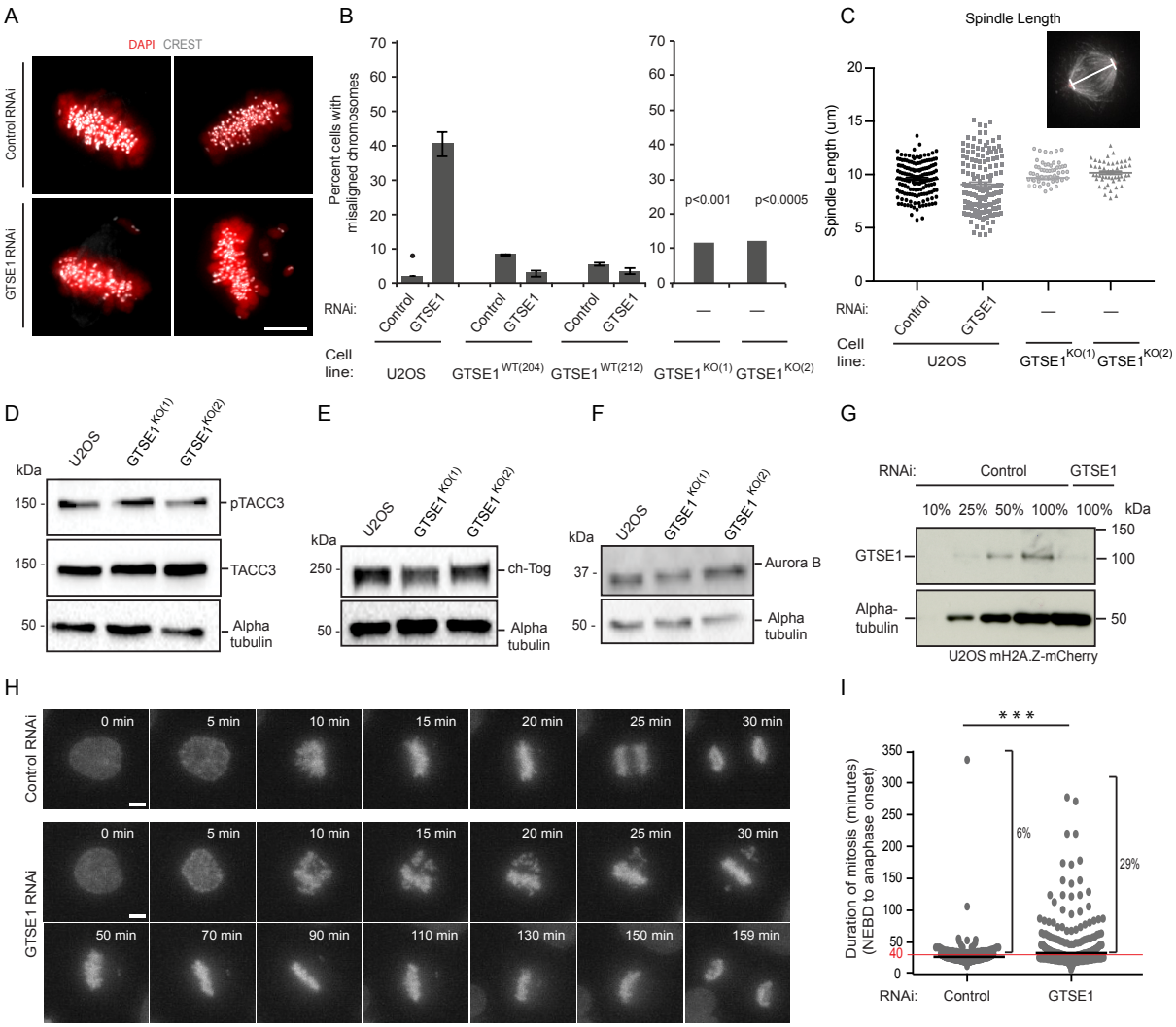

Figure 10. GTSE1 is required for proper chromosome alignment

A. Representative immunofluorescence images of U2OS cells showing misaligned chromosomes during metaphase after GTSE1 RNAi. The cells were probed with anti-CREST (KTs) and DAPI (DNA). **B.** Quantification of mis-aligned chromosomes. Left bar graph displays percentage of cells with misaligned chromosomes after GTSE1 RNAi in U2OS cells and two U2OS clonal lines stably expressing siRNA resistant GTSE1 (n > 150 cells over 3 experiments per condition). The bar graph on the right shows percentage of U2OS GTSE1 knockout clones ($GTSE1^{KO(1)}$ and $GTSE1^{KO(2)}$) with mis-aligned chromosomes {p-values were obtained from a chi-squared test comparing to the U2OS control condition (marked with •); n > 100 cells}. **C.** Quantification of spindle length in U2OS cells following control and GTSE1 RNAi (n≥145 cells per condition over 4 independent experiment) and

U2OS GTSE1 knockout cells lines (GTSE1$^{KO(1)}$ and GTSE1$^{KO(2)}$) (n≥50 cells each). **D-F.** Western blots showing pTACC3, TACC3, Ch-Tog and Aurora B protein levels in mitotic U2OS GTSE1 knockout clones (GTSE1$^{KO(1)}$ and GTSE1$^{KO(2)}$). Tubulin levels were used as a loading control. (WB were done by Dr. Rondelet; Bendre et al., 2016) **G.** Western blot of U2OS mH2A.Z-mCherry cell lysate displaying efficient depletion (>90%) of GTSE1 using RNAi. **H.** Still frames from live cell time-lapse movies showing time required for alignment of chromosomes at the metaphase plate after control RNAi (upper single row) and GTSE1 RNAi (bottom two rows). **I.** Chart shows average duration of mitosis (NEBD to anaphase onset) after GTSE1 RNAi and control RNAi (control RNAi: 28.4 ± 20.5 min, n=269; GTSE1 RNAi: 42.5 ± 36.3 min, n = 295). Black bars represent the average and the red line represents the 90th percentile of control cells. The graph shows a higher percentage of GTSE1 depleted cells (29.2 %) with mitotic duration longer than 40 minutes as compared to 5.9% of control depleted cells. All scale bars represent 5 μm and all error bars when not specified represent standard error of the mean. p≤0.05*, p≤0.01**, p≤0.001***

In order to study the fate of misaligned chromosomes, and to check if depletion of GTSE1 impaired the SAC function, mitotic progression of GTSE1-depleted cells was studied by live cell imaging. U2OS cell line stably expressing a BAC based m-Cherry tagged histone variant H2A.Z was used for this assay. Western blot analysis following GTSE1 RNAi in U2OS H2A.Z-mCherry displayed a >80% reduction in GTSE1 levels as compared to control cells (Figure 10G). U2OS H2A.Z-mCherry cells treated with control and GTSE1 RNAi were imaged for 8 hours with images taken after every minute. Only 5.9% of cells treated with control RNAi took longer than 40 min to align their chromosomes, in contrast to 29.5% of cells treated with GTSE1 RNAi (Figure 10H and I). These results indicate that GTSE1-depleted cells took longer to align their chromosomes at the metaphase plate and did not enter anaphase with misaligned chromosome, confirming presence of an active SAC after GTSE1 depletion. This suggests that GTSE1 is required for proper chromosome congression and alignment during metaphase.

We also tested the effect of GTSE1 depletion on chromosome alignment in Hela Kyoto, HCT116 and MCF-7 cell lines. Loss of GTSE1 led to an increase in the number of Hela Kyoto and HCT116 cells showing a few misaligned chromosomes. However, the phenotype was more pronounced in Hela Kyoto cells as compared to HCT116 cells (data not shown). Surprisingly, loss of GTSE1 in MCF-7 cells did not affect metaphase chromosome alignment.

3.3 GTSE1 stabilizes KT MTs and KT-MT attachment

GTSE1 is required for proper chromosome alignment and timely onset of anaphase. As GTSE1 is required for astral MT stability, we wondered whether GTSE1 might also affect KT MT stability, thereby increasing chromosome mis-alignment. To test this hypothesis, we decided to investigate K-fiber stability and KT-MT attachment stability during metaphase. First we tested if MTs in the inner spindle were affected after GTSE1 depletion. Therefore, we measured the inner spindle intensity using α-tubulin immunofluorescence after control and GTSE1 RNAi and observed a significant reduction in the inner spindle α-tubulin intensity in GTSE1-depleted cells (Figure 11A). This suggested that in addition to astral MTs, GTSE1 might stabilize KT and/or interpolar MTs as well. Then we determined if GTSE1 localized specifically to K-fibers in cold-treated U2OS cells expressing GTSE1-GFP. Cold treatment leads to depolymerization of non-KT MTs, leaving behind cold-stable KT MTs. Immunofluorescence analysis of cold-treated cells using antibodies against GFP, α-tubulin and a KT marker (CREST) showed GTSE1 clearly localizing to cold-stable K-fibers (Figure 11B); (Analysis was performed by Dr. Rondelet; Bendre et al., 2016).

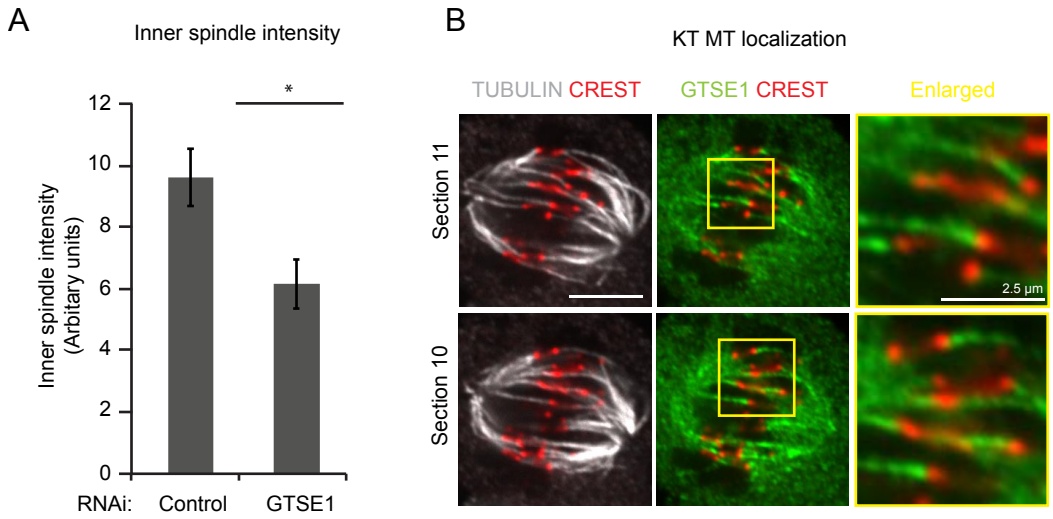

Figure 11. GTSE1 stabilizes spindle MTs and localizes to K-fibers

A. Quantification of "inner spindle α-tubulin" intensity of fixed U2OS cells following control and GTSE1 RNAi (n ≥ 19 per experiment per condition; 3 experiments). **B.** Representative immunofluorescence images of cold-treated U2OS$^{WT(303)}$ cells showing K-fiber localization of GTSE1-GFP. The cells were stained for MTs (α-tubulin), KTs (CREST) and GTSE1 (GFP); (Localization of GTSE1-GFP to K-fibers was done by Dr. Rondelet). All scale bars represent 5 µm and all error bars when not specified represent standard error of the mean. p≤0.05 *, p≤0.01**,

$p \leq 0.001$ ***

As GTSE1 localized to K-fibers, we next tested the effect of GTSE1 on K-fiber stability and KT-MT attachment stability by three different approaches. First, we analyzed if GTSE1 was stabilizing KT MTs by quantifying the number of cells with stable KT MT population after cold-treatment. U2OS cells either treated with control or GTSE1 RNAi were arrested in G2/M transition using a Cdk1 inhibitor and then released in normal media for 1 h. After 1 h, these cells were cold-treated for 17 min and immediately fixed and stained using α-tubulin and CREST antibodies. It was evident that cells depleted of GTSE1 showed a significant reduction in the cold-stable KT MT population as compared to control treated cells (Figure 12A and 12B).

Stable KT MTs and stable KT-MT attachments are highly interdependent. Reducing GTSE1 levels showed less stable KT MTs, implying reduced KT-MT attachment stability. Mad1 is a component of the SAC, (Howell et al., 2004), which is recruited to KTs with improper KT-MT attachments during metaphase. Thus, we looked at Mad1 accumulation at KTs after depletion of GTSE1 as readout for KT-MT attachment defects. Indeed, U2OS metaphase cells depleted of GTSE1, displayed an increased accumulation of Mad1 at KTs of aligned chromosomes as compared to control cells, signifying a defect in KT-MT attachments (Figure 12C and D). Defective KT-MT attachments can have an impact on the inter-KT tension, which can be independently measured by determining the distance between two sister KTs. The inter-KT distance between two sister chromatids was measured using CREST immunofluorescence and a very subtle yet significant reduction in the inter-KT distance was observed in GTSE1-depleted cells (Figure 12E and 12F). However as shown in Figure 12E, the relative distribution of the inter-KT distance was skewed towards lower values after GTSE1 RNAi, indicating a decrease in the inter-KT tension.

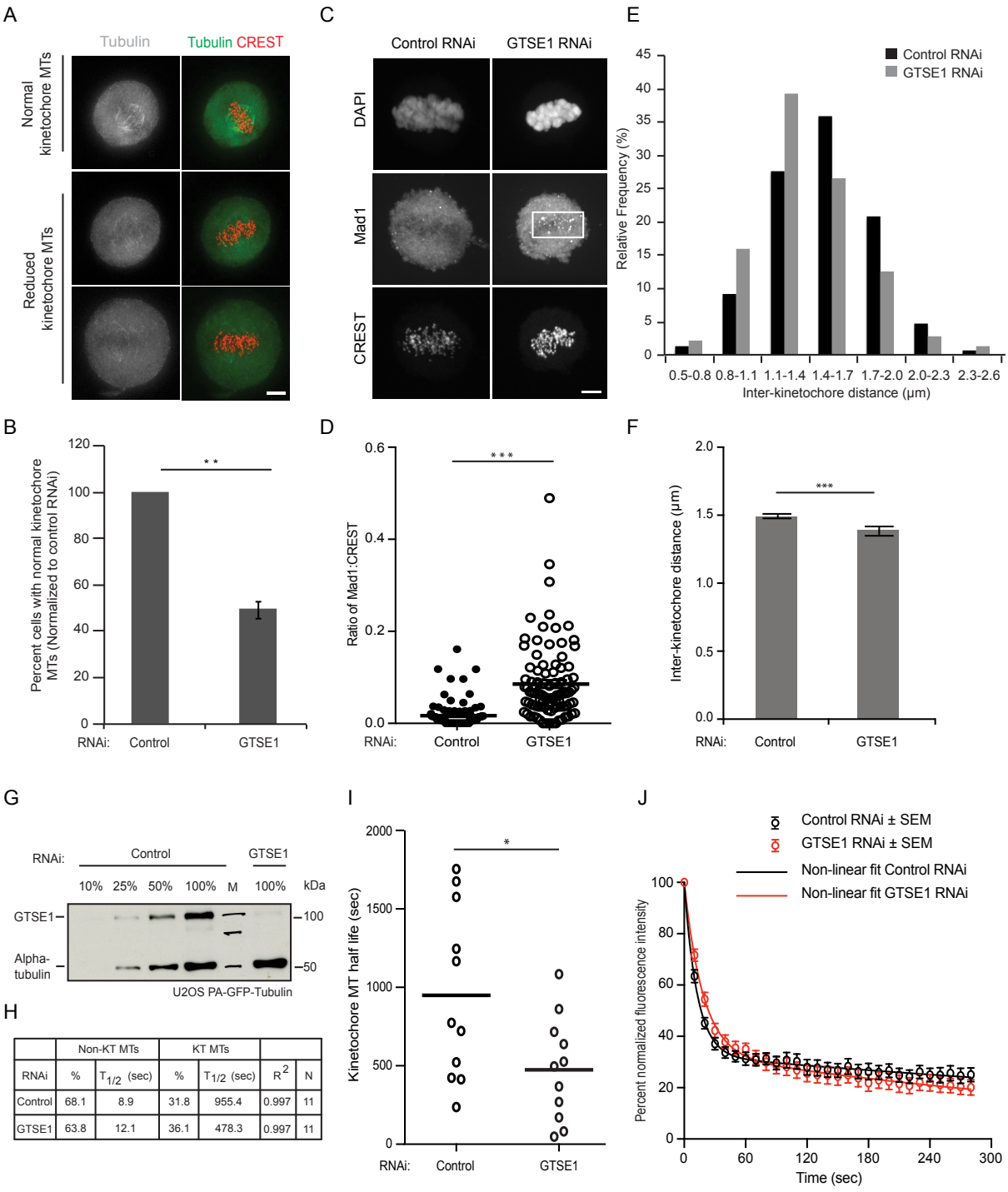

	Non-KT MTs		KT MTs			
RNAi	%	$T_{1/2}$ (sec)	%	$T_{1/2}$ (sec)	R^2	N
Control	68.1	8.9	31.8	955.4	0.997	11
GTSE1	63.8	12.1	36.1	478.3	0.997	11

Figure 12. GTSE1 stabilizes KT MTs and KT-MT attachment

A-B. Analysis of K-fiber stability. Immunofluorescence images of U2OS cells treated with cold temperature for 17 min, showing cold-stable KT MTs (normal kinetochore MTs) and destabilized K-fibers (reduced kinetochore MTs). The cells were probed with anti-α-tubulin (MTs), and anti-CREST (KTs). The bar chart shows quantification of percent cells with normal KT MTs in U2OS cells upon depletion of GTSE1. All values were normalized to control values (n > 100 cells per experiment; 3 experiments per condition) **C-D.** Mad1 accumulation at KTs after GTSE1 depletion. Representative

images display accumulation of Mad1 at KTs in GTSE1-depleted cells (white box). U2OS cells were blocked using Cdk1 inhibitor (RO-3306) and released in normal media for 1 h to enrich the total number of cells in metaphase. Cells were then fixed and stained with Mad1, CREST (KTs) and DAPI (DNA). Bar graph shows the ratio of Mad1 positive KTs in U2OS cells after control and GTSE1 RNAi (n > 90 cells from three independent experiments). **E.** Analysis of inter-KT distance. Histogram shows relative distribution of inter-KT distances in control and GTSE1-depleted U2OS cells. The inter-KT distance was measured using CREST signal. The relative distribution of inter-KT distance was skewed towards lower values after GTSE1 RNAi, suggesting decreased inter-KT tension. **F.** Bar chart shows the average inter-KT distance in U2OS cells following control and GTSE1 RNAi (n=445 sister-KT pairs over 3 independent experiments). **G.** Western blot of U2OS cells expressing photoactivable (PA)-GFP, probed with anti-GTSE1 and anti-α-tubulin showing efficient depletion of GTSE1 after RNAi. **H-J.** Fluorescence dissipation after photoactivation experiments to determine the KT-MT half life (t1/2) after GTSE1 RNAi using U2OS cells expressing PA-GFP-tubulin. Table showing the values for percentage of non-KT and KT MT, half lives (t1/2) for non-KT and KT MTs, coefficient of regression (predicts how closely the data fits to the regression curve) and the number of cells analyzed. Scattered plot shows KT MT half-life in control or GTSE1-depleted U2OS cells expressing photoactivable (PA) GFP-tubulin. Each circle represents the KT MT half-life of a single cell; bars represent the average. Graph showing average normalized fluorescence intensity at each time-point following photoactivation of PA-GFP-tubulin in U2OS metaphase spindles treated with control or GTSE1 RNAi. Solid lines represent the double exponential fit for control and GTSE1 RNAi. Error bars represent standard error of the mean. n = 11 cells over 3 experiments per condition. All scale bars represent 5 μm and all error bars when not specified represent standard error of the mean. $p \leq 0.05$ *, $p \leq 0.01$**, $p \leq 0.001$ ***

We further confirmed this defect in KT MT stability and KT-MT attachment stability by using fluorescence dissipation after photoactivation (FDAPA) assay. U2OS cells stably expressing photoactivatable (PA)-GFP-tubulin were used to measure the loss of fluorescence after photoactivation (Bakhoum et al., 2009a). Depletion of GTSE1 using RNAi produced a >90% reduction in GTSE1 protein levels in U2OS-PA-GFP-tubulin cell line (Figure 12G). PA-GFP-tubulin in a small area around the KT-MT attachment region on the metaphase spindle was activated and fluorescence intensity of the half spindle containing the activated area was measured at each time point (every 10 sec for 5 min). The background was subtracted by measuring fluorescence intensity of the other non-activated half spindle. Loss of fluorescence after photobleaching was controlled by measuring fluorescence intensities within an activated region on taxol stabilized spindles. Fluorescence values after background

subtraction and correction for photobleaching were normalized and fitted to a double exponential decay curve. The half-lives (t1/2) of a fast component, which corresponds to non-KT MTs and a slow component that corresponds to KT fibers, was calculated. U2OS cells treated with control RNAi showed a KT-MT t1/2 of 955.4 sec, whereas, the KT-MT t1/2 was dramatically reduced to 478.3 sec after GTSE1 RNAi (Figure 12H-J). Surprisingly, the t1/2 of non-KT MTs was increased following GTSE1 RNAi (Figure 12H). Non-KT MTs can be easily destabilized and indeed we observed a lesser percentage of non-KT MT following GTSE1 RNAi (Figure 12H). Therefore we speculated that we might be mostly measuring the turnover of stable KT MT, which caused a subtle yet significant increase in the non-KT MT half-life following GTSE1 RNAi. These results suggest that GTSE1 is required for KT MT stability, which is important for maintaining stable KT-MT attachments that control proper alignment of chromosomes at the metaphase plate.

3.4 Mitotic defects following GTSE1 depletion are dependent on depolymerase activity of MCAK

GTSE1 plays a significant role during mitosis by regulating the overall MT stability and chromosome alignment. We next wanted to understand the molecular mechanism by which GTSE1 influences mitosis. GTSE1 binds directly to the MT lattice and displays plus tip tracking activity during interphase. However, as the cell enters mitosis GTSE1 becomes highly phosphorylated by Cdk1 and Aurora A, and does not bind directly to MTs nor shows plus tip accumulation but is seen associated with the mitotic spindle and spindle poles (Scolz et al., 2012 and our unpublished data). This implies that GTSE1 is recruited to the spindle by other protein interactors. Clearly, the role of GTSE1 in stabilizing MTs should be indirect as it does not directly bind MTs. Previous studies have shown that GTSE1 interacts with the TACC3-Ch-Tog-Clathrin complex (Hubner et al., 2010). This complex is known to stabilize the K-fibers by cross-linking KT MTs by forming inter-MT bridges (Kinoshita, 2005; Lin et al., 2010; Booth et al., 2011; Cheeseman et al., 2013; Nixon et al., 2015). Depletion of TACC3 or clathrin affects MT stability and leads to the loss of GTSE1 from the spindle and spindle poles, implicating that GTSE1 is recruited to the spindle via the TACC3-Ch-Tog-Clathrin complex (Hubner et al., 2010). Therefore, we tested whether the reverse was true i.e. if depleting GTSE1 affected the localization of TACC3 to the spindle. TACC3 localization to the spindle was determined by normalizing TACC3 intensity with α-tubulin intensity in U2OS GTSE1 knockout cells and in U2OS cells after control and GTSE1 RNAi using immunofluorescence of TACC3 and α-tubulin. Consistent with previous reports, depletion of

GTSE1 either using RNAi or in U2OS GTSE1 knockout cells did not significantly affect the levels of TACC3 on the spindle (Figure 13A and 13B), suggesting that some other protein interactor was influencing GTSE1's mitotic function (Hubner et al., 2010).

Previous studies in which GTSE1 was affinity purified followed by mass spectrometric analysis revealed that GTSE1 interacts with MCAK/Kif2C, a microtubule depolymerase (Hubner et al., 2010). MCAK belongs to the kinesin-13 family of depolymerases and localizes to the centromeres, centrosome, midbody and MT tips during mitosis (Figure 6A; Wordeman and Mitchison, 1995). Interestingly, phenotypes observed after depletion of GTSE1 i.e. loss of astral MTs, multipolar spindles and chromosome misalignments are typical to those seen after excess activity of MCAK. This promoted us to hypothesize that normally in cells, GTSE1 might attenuate MCAK's depolymerase activity during mitosis. Therefore upon depleting GTSE1, MCAK possibly becomes over active (Maney et al., 1998; Moore and Wordeman, 2004; Zhang et al., 2011).

If the mitotic defects seen after loss of GTSE1 were through increased depolymerase activity of MCAK, then we speculated that depleting MCAK along with GTSE1 might restore the mitotic phenotypes. To test this, we depleted GTSE1 and MCAK individually and together using RNAi in U2OS cells and observed a >90% depletion of the respective proteins when tested with western blot (Figure 8B, 13C, D). As observed earlier, cells without GTSE1 displayed spindles with dramatically shorter astral MTs and misaligned chromosomes (Figure 13E). Depletion of MCAK alone led to the appearance of characteristic "hairy" spindles, due to increased spindle and astral MT density and length, which is in line with previous reports (Rankin and Wordeman, 2010; Rizk et al., 2009) (Figure 13E). Remarkably, depletion of MCAK along with GTSE1 in U2OS cells dramatically increased the number of cells displaying spindles with long and abundant astral MTs, implying a role of MCAK in affecting astral MT stability in absence of GTSE1 (Figure 13E and 13F). We also quantified the astral MT length after codepletion of GTSE1 and MCAK, which was restored to 6.2 μm in contrast to 2.8 μm after GTSE1 RNAi (Figure 13G). As astral MTs are essential for proper spindle orientation, we checked if co-depletion of GTSE1 and MCAK could rescue the spindle orientation defect. Indeed in line with the astral phenotype, codepletion of GTSE1 and MCAK restored this defect as only 9% of cells showed spindle misorientation as compared to 31% after GTSE1 RNAi (Figure 13H). We could confirm that this was not

specific only to astral MTs, as the defect in the inner spindle intensity was partially rescued after co-depletion of GTSE1 and MCAK (Figure 13I).

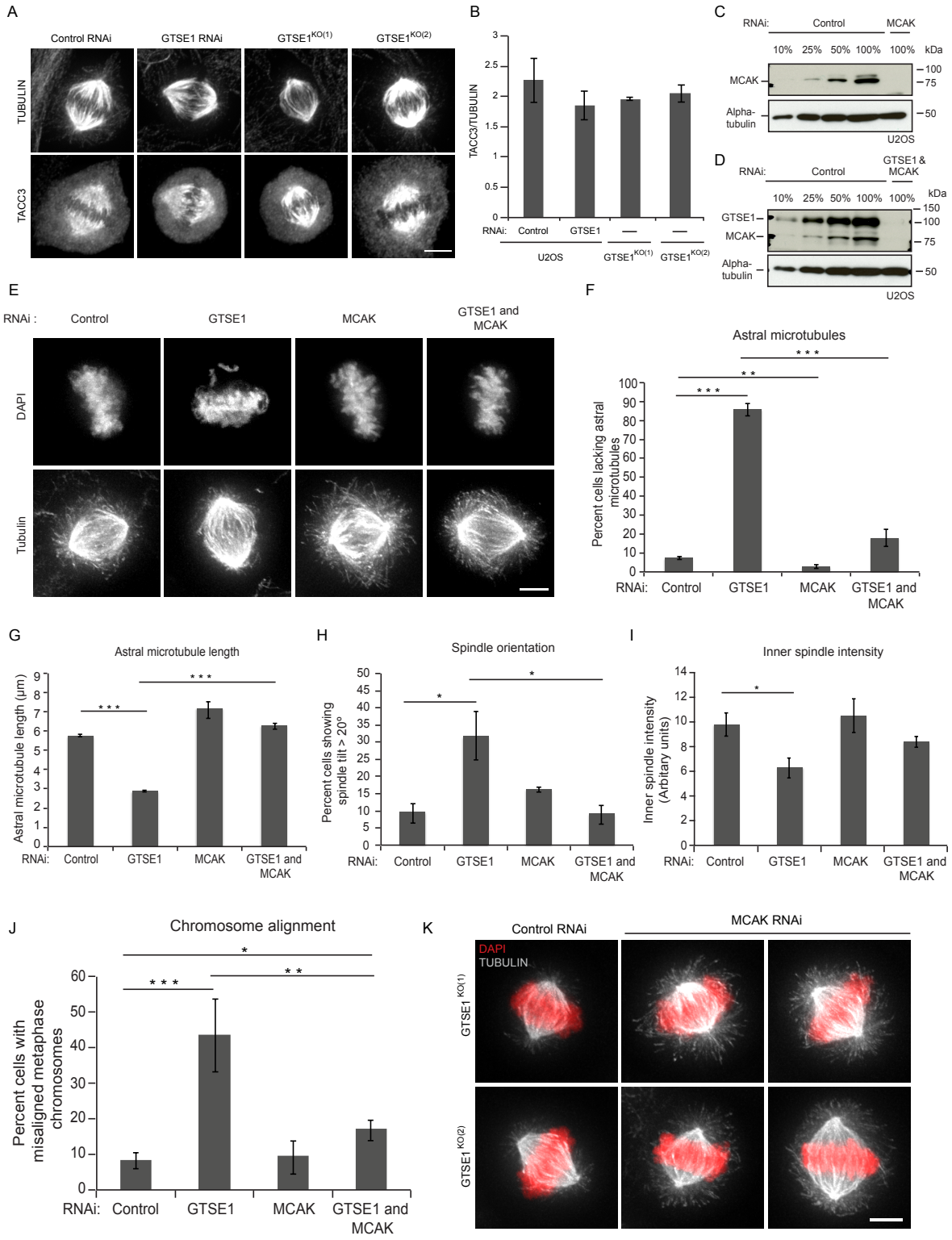

Figure 13. Mitotic defects following GTSE1 depletion are dependent on depolymerase activity of MCAK

A. TACC3 localization after loss of GTSE1. Representative fluorescence micrographs of U2OS cells following control and GTSE1 RNAi and U2OS GTSE1 knockout clones ($GTSE1^{KO(1)}$ and $GTSE1^{KO(2)}$) stained for MTs (α-tubulin) and TACC3. **B.** Bar chart showing recruitment of TACC3 on spindles in U2OS cells following control and GTSE1 RNAi ($n \geq 50$ cells per condition over 3 independent experiments) and U2OS GTSE1 knockout clones ($GTSE1^{KO(1)}$ and $GTSE1^{KO(2)}$) ($n \geq 50$ cells each over 2 independent experiments). The recruitment of TACC3 to the spindle was determined by normalizing TACC3 fluorescence intensity values to α-tubulin intensities (Analysis was performed by Dr. Rondelet). **C-D.** Western blots of U2OS whole-cell lysates probed with anti-MCAK independently and together with anti-GTSE1. α-tubulin was used as a loading control. U2OS cells were subjected to MCAK depletion or co-depletion of MCAK and GTSE1 for 48 h. Indicated dilution of control cell lysates were used for determining the efficacy of depletion. **E.** Phenotype analysis following co-depletion of GTSE1 and MCAK. Representative immunofluorescence images of U2OS cells stained with anti-α-tubulin (MTs) and DAPI (DNA) after depletion of endogenous GTSE1, MCAK and co-depletion of GTSE1 and MCAK using RNAi. Control cells were treated with scrambled RNAi. **F-I.** Quantification of percentage of cells lacking astral MTs ($n > 100$ cells per experiment; 3 experiments per condition), average astral MT length (100 astrals/condition/experiment, 3 independent experiments), spindle orientation ($n>140$ cells, 3 independent experiments), inner spindle α-tubulin intensity (>19 cells for each condition per experiment; 3 independent experiments) after control, GTSE1, MCAK and co-depletion of GTSE1 and MCAK in U2OS cells after immunofluorescence as shown in E. **J.** Quantification of percent cells with misaligned chromosomes during metaphase after treatment with control, GTSE1, MCAK and GTSE1 and MCAK RNAi in U2OS cells. ($n>100$ cells per experiment, data is from 3 independent experiments). **K.** Representative fluorescence micrographs of U2OS GTSE1 knockout clones ($GTSE1^{KO(1)}$ and $GTSE1^{KO(2)}$) stained for α-tubulin and DAPI (DNA) showing restoration of astral phenotype upon MCAK depletion. All scale bars represent 5 μm and all error bars when not specified represent standard error of the mean. $p\leq0.05$ *, $p\leq0.01$**, $p\leq0.001$ ***

MCAK localizes to KTs during prometaphase and metaphase and plays a crucial role in establishing proper KT-MT attachments. Over-expression of MCAK has been shown to produce more dynamic KT-MT attachments leading to problems in chromosome alignment (Zhang et al., 2011). We reasoned that hyperactive MCAK following loss of GTSE1 might destabilize KT MTs and impede chromosome alignment during metaphase. Therefore, we looked at chromosome alignment following co-depletion of GTSE1 and MCAK and saw a significant reduction in the percentage of cell with misaligned chromosomes, corroborating MCAK's involvement in causing misaligned chromosomes in the absence of GTSE1 (Figure

13J). Interestingly, reducing levels of MCAK in U2OS GTSE1 knockout clones also restored the observed mitotic defects (Figure 13K).

These results suggest that the mitotic defects observed after loss of GTSE1 are due to increased depolymerase activity of MCAK during mitosis and these defects can be ameliorated by decreasing the levels of MCAK by RNAi. Thus, GTSE1 negatively regulates MCAK's depolymerase activity during mitosis to ensure MT stability for establishment of proper KT-MT attachments.

3.5 GTSE1 specifically affects MCAK's depolymerase activity and spindle localization during metaphase

Previous studies where GTSE1-GFP was immunoprecipitated followed by mass spectrometric analysis showed consistent enrichment of another kinesin-13 family member, Kif2A in addition to MCAK (Hubner et al., 2010). Therefore, we wanted to investigate if GTSE1 was specifically antagonizing MCAK's depolymerase activity or whether it also attenuated Kif2A's depolymerase activity. To study this, Kif2A was depleted individually or along with GTSE1 using RNAi in U2OS cells, which led to a >60% reduction of Kif2A protein levels (Figure 14B). Surprisingly, co-depletion of Kif2A and GTSE1 did not restore the GTSE1 depletion associated defects in astral MT stability or chromosome alignment, implying that GTSE1 specifically attenuated MCAK's depolymerase activity during prometaphase and metaphase (Figure 14A).

As GTSE1 specifically inhibits MCAK's depolymerase activity, we wanted to determine if loss of GTSE1 had an effect on the stability and localization of MCAK. The expression levels of MCAK remained unchanged following GTSE1 RNAi (Figure 14D). To have a closer look at MCAK's spindle localization, GTSE1 was depleted in U2OS cells and Hela Kyoto cells stably expressing BAC based MCAK-GFP. MCAK's spindle association was analyzed by normalizing MCAK's intensity to α-tubulin intensity at the inner spindle using immunofluorescence analysis. In both cell lines, MCAK localization to the inner spindle was significantly higher after loss of GTSE1 as compared to control cells (Figure 14C, 14E and 14F). Thus, GTSE1 specifically affects MCAK's localization and activity during mitosis.

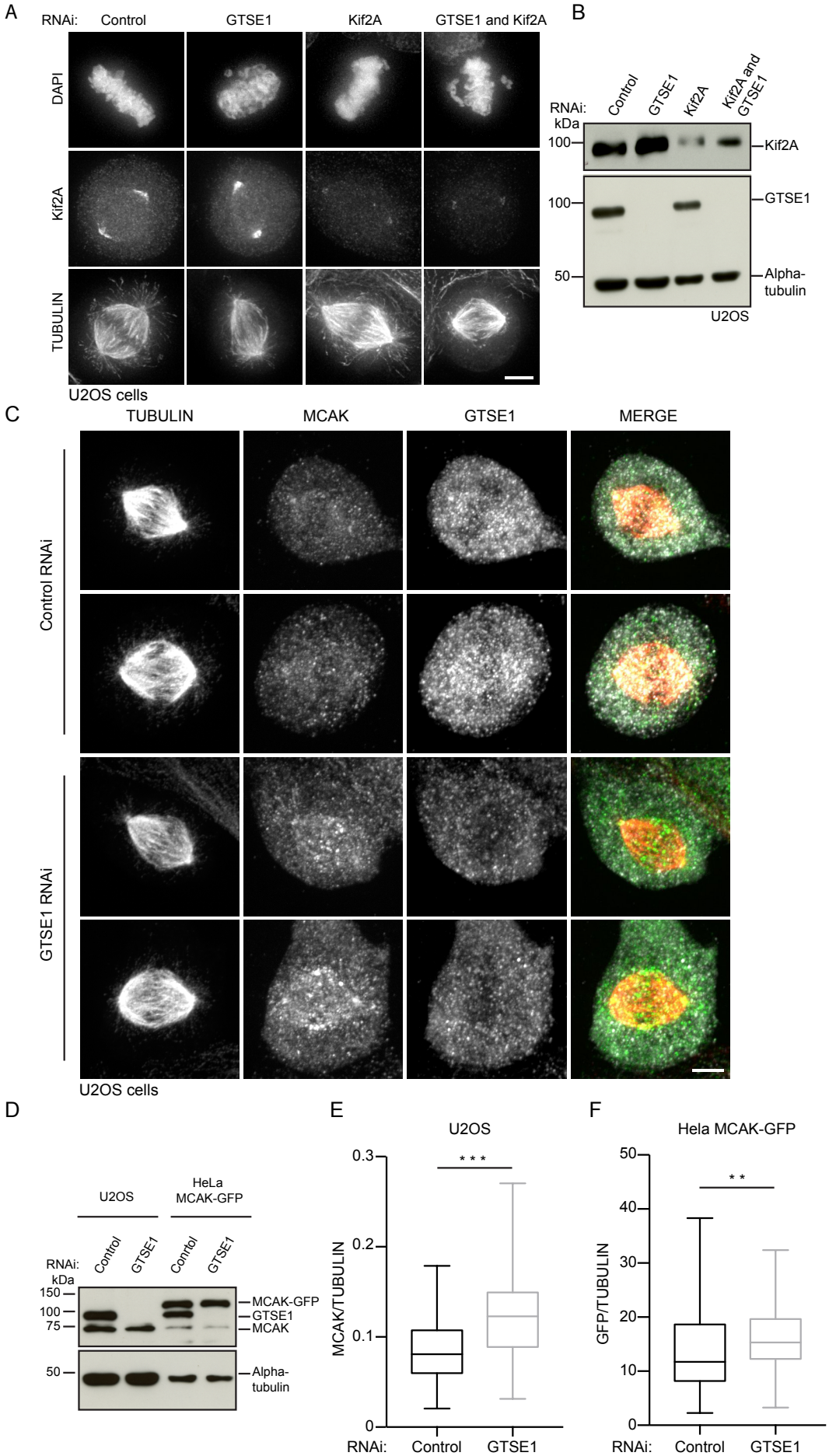
A
RNAi: Control
GTSE1
Kif2A
GTSE1 and Kif2A
DAPI
Kif2A
TUBULIN
U2OS cells
B
RNAi:
Control
GTSE1
Kif2A
Kif2A and GTSE1
kDa
100
Kif2A
100
GTSE1
50
Alpha-tubulin
U2OS
C
TUBULIN
MCAK
GTSE1
MERGE
Control RNAi
GTSE1 RNAi
U2OS cells
D
U2OS
HeLa MCAK-GFP
RNAi:
Control
GTSE1
Control
GTSE1
kDa
150
100
75
MCAK-GFP
GTSE1
MCAK
50
Alpha-tubulin
E
U2OS
***
MCAK/TUBULIN
0.3
0.2
0.1
0
RNAi: Control GTSE1
F
Hela MCAK-GFP
**
GFP/TUBULIN
50
40
30
20
10
0
RNAi: Control GTSE1

Figure 14. GTSE1 specifically affects MCAK's depolymerase activity and spindle localization during metaphase

A. Phenotype analysis after Kif2A and GTSE1 RNAi. Representative fluorescence micrographs of fixed U2OS cells probed for anti-α-tubulin (MTs), Kif2A and DAPI (DNA) after depletion of endogenous GTSE1, Kif2A and co-depletion of GTSE1 and Kif2A using RNAi. **B.** Western blot of U2OS cell lysates following control, GTSE1, Kif2A and co-depletion of Kif2A and GTSE1 probed with anti-α-tubulin (MTs), anti-Kif2A and anti-GTSE1. **C.** Spindle localization of MCAK following GTSE1 depletion. Immunofluorescence images of U2OS cells showing increased MCAK spindle localization upon GTSE1 RNAi. U2OS cells were fixed and stained with anti-MCAK, anti-α-tubulin and anti-GTSE1 antibodies, 48 h post control and GTSE1 RNAi. **D.** Western blots of U2OS cells and Hela Kyoto cells stably expressing MCAK-GFP probed with anti-MCAK, anti-GTSE1 and anti-α-tubulin antibody. The cells were subjected to GTSE1 depletion for 48 h and showed no difference in the expression levels of MCAK upon control or GTSE1 RNAi. **E-F.** Box plot showing quantification of MCAK recruitment at the inner spindle after control and GTSE1 RNAi in U2OS (E) and Hela Kyoto MCAK-GFP cells (F). MCAK intensity at the inner spindle was normalized to α-tubulin intensities ($n \geq 105$ U2OS metaphase cells over 3 independent experiments; p-values were obtained using Mann-Whitney U test; $n \geq 89$ Hela Kyoto MCAK-GFP cells over 3 independent experiments; p-values were obtained using Mann-Whitney U test). All scale bars represent 5 micrometers. All error bars represent standard error of the mean. $p \leq 0.05$ *, $p \leq 0.01$ **, $p \leq 0.001$ ***

3.6 GTSE1 interacts with MCAK in cells

During mitosis, GTSE1 affects MCAK's subcellular localization and efficiently antagonizes MCAK's depolymerase activity. We next wanted to determine if GTSE1 interacted with MCAK in cells. In order to test this, U2OS wild type cells and U2OS cells expressing BAC based NFLAP-GTSE1 were arrested in mitosis using nocodazole and protein extracts were prepared for co-immunoprecipitation (co-IP) assay. Endogenous GTSE1 was immunoprecipitated from U2OS wild type cells using anti-GTSE1 antibody and GFP-tagged GTSE1 was immunoprecipitated from U2OS NFLAP-GTSE1 cell line using anti-GFP antibody. Control IP was performed using anti-GFP antibody for wild type cells and 9E10 anti-myc antibody for tagged cells. Input samples and co-IP extracts were then analyzed by western blot. As shown in Figure 15A and 15B, both endogenous and GFP-tagged GTSE1 bind and pull down MCAK. As expected, in the control IP no protein band is visible confirming specificity of the antibody (Figure 15A and 15B). Next we wanted to assess if this interaction was mitosis specific. This was evaluated by blocking U2OS cells stably expressing BAC based GTSE1-LAP ($GTSE1^{WT(212)}$) in G2/S phase transition by single

thymidine block or in mitosis by using a nocodazole arrest. Protein extracts were immunoprecipitated using anti-GFP antibody and 9E10 anti-myc was used as a negative control. As shown in Figure 15C, GTSE1 efficiently binds to MCAK during mitosis but not during G2/S phase. This data raises the possibility that the interaction between GTSE1 and MCAK is phosphorylation dependent, as GTSE1 gets hyperphosphorylated during mitosis (Scolz et a., 2012 and our unpublished data).

We next wanted to narrow down the region in GTSE1 that is required for interaction with MCAK. To determine this, GFP-GTSE1 FL, GFP-GTSE1 1-460, GFP-GTSE1 1-338, GFP-GTSE1 1-246, GFP-GTSE1 1-187 and GFP-GTSE1 380-739 (Cloned by Yu-Chih Lin) were transiently transfected with MCAK-FL-myc in HEK293T cells (Figure 15D). Co-IPs were performed 24 h after transfection where GFP-GTSE1 FL and fragments were immunoprecipitated using anti-GFP antibody. As seen in Figure 15D, MCAK-FL-myc showed an interaction with FL GTSE1, GTSE1 1-460, GTSE1 1-338 and GTSE1 1-187 but not with GTSE1 380-739, suggesting that the interaction was via the N-terminus of GTSE1 (Figure 15D). Interestingly, MCAK did not Co-IP with GTSE1 1-246, which might be because we accidentally cleaved the fragment in such a way that an important motif or a structure, which is essential for binding to MCAK was lost (Figure 15D).

Similarly, in order to understand how MCAK interacts with GTSE1, we cloned the following MCAK fragments: myc-tagged N-terminal domain (1-181), N-terminal plus neck region (1-231), motor domain (232-583), neck plus motor domain (182-583) and C-terminal domain (584-725) of MCAK (Figure 15E). It has been well established that the N and C-terminal domains are required for dimerization and cellular localization of MCAK, whereas, the neck plus motor domain alone is sufficient for MT depolymerization (Tanenbaum et al, 2011; Maney et al., 2001). In order to narrow down the smallest interaction domain in MCAK, we transiently transfected the above mentioned myc-tagged MCAK fragments in HCT116 GTSE1-GFP overexpressing clone 30 and performed co-IPs 24 h after transfection using anti-GFP antibody. As shown in Figure 15E, the N-terminus of MCAK (1-181) was consistently co-immunoprecipitated with GTSE1-GFP FL. We could detect a very weak interaction of GTSE1 FL with MCAK FL and MCAK motor domain (232-583) (Figure 15E). These results indicate that the N-terminal domains of both GTSE1 and MCAK proteins mediate their interaction. However, as multiple regions in both proteins were pulled down, it

is plausible that the mode of interaction is complicated and involves interactions between multiple domains.

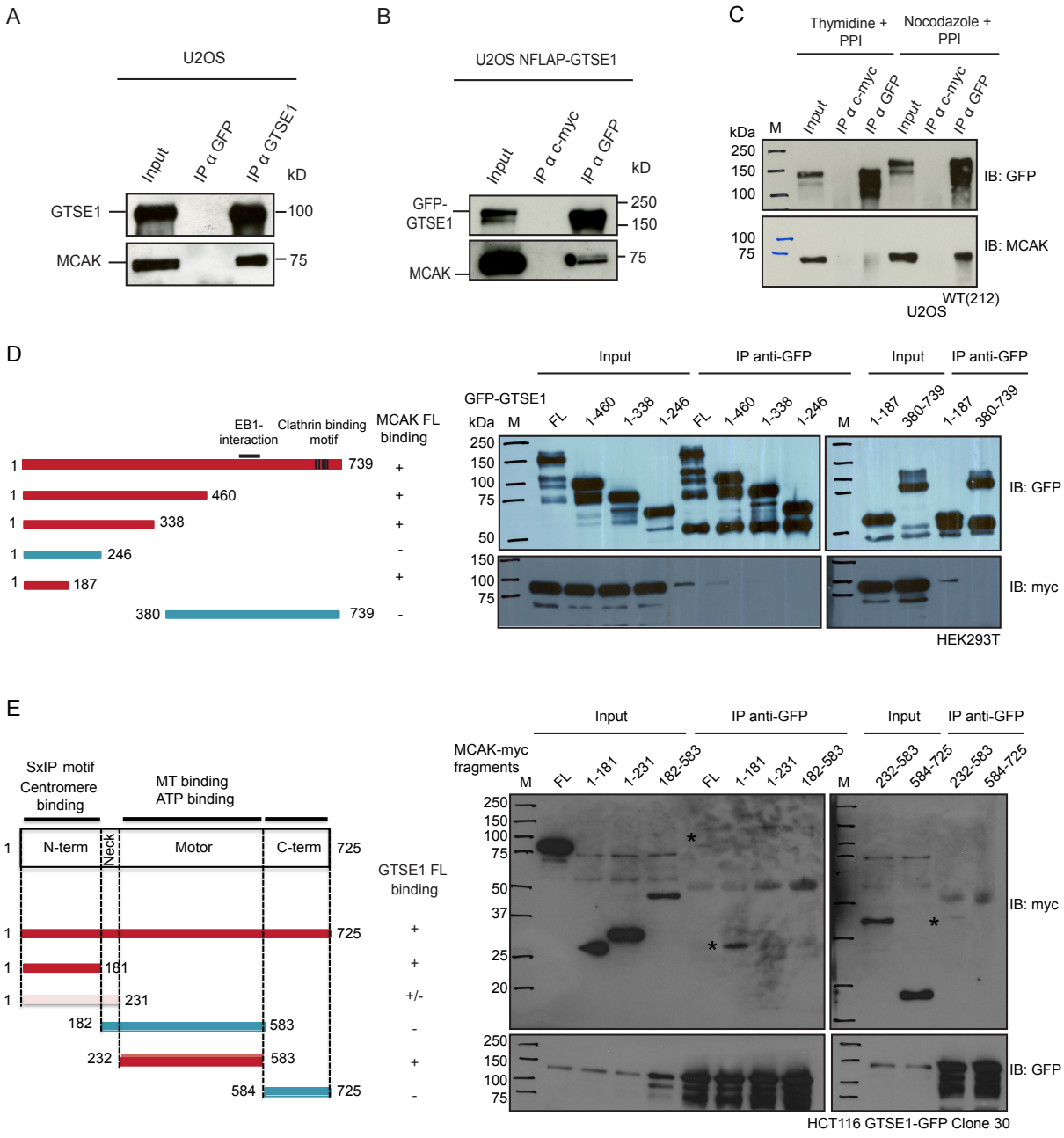

Figure 15. GTSE1 interacts with MCAK *in vivo*

A-B. Western blots of cell extracts immunoprecipitated to detect interaction between GTSE1 and MCAK. U2OS wild-type cells and U2OS cells stably expressing BAC based NFLAP-GTSE1 were arrested in mitosis with nocodazole, and protein extracts were immunoprecipitated with either anti-GFP antibody or 9E10 anti-myc antibody as a control antibody and anti-GTSE1 antibody or anti-GFP antibody. Input and immunoprecipitated fractions were run by SDS-PAGE, Western blotted and probed with either anti-GFP or anti–GTSE1 antibody and anti-MCAK antibody. As seen in A and B,

GTSE1 and GTSE1-GFP can efficiently pull down endogenous MCAK. **C.** Western blots of cell extracts immunoprecipitated to check if interaction between GTSE1 with MCAK was mitosis specific. U2OS cells stably expressing GTSE1-LAP ($U2OS^{WT(212)}$) were either arrested in mitosis with nocodazole or in G2/S phase transition using a single thymidine block. Co-IPs were done in presence of phosphatase inhibitor (PPI) to prevent loss of any phosphorylations. Protein extracts were immunoprecipitated using either 9E10 anti-myc antibody as control antibody or anti-GFP antibody. Input and immunoprecipitated fractions were processed for SDS-PAGE followed by Western blot and probed with anti-GFP and anti-MCAK antibody. GTSE1-GFP could efficiently pull down endogenous MCAK during mitosis. **D.** Western blot analysis of HEK293T asynchronous cell lysates following co-IP using anti-GFP antibody. HEK293T cells were transiently co-transfected with myc-tagged MCAK FL and following GTSE1 fragments; GFP-GTSE1 FL, GFP-GTSE1 1-460, GFP-GTSE1 1-338, GFP-GTSE1 1-246, GFP-GTSE1 1-187 and GFP-GTSE1 380-739 (Cloned by Yu-Chih Lin). The blot was probed with anti-GFP and anti-myc antibodies. As seen GFP-GTSE1 FL, GFP-GTSE1 1-460, GFP-GTSE1 1-338, GFP-and GFP-GTSE1 1-187 could pull down myc tagged MCAK FL. **E.** Western blot analysis of asynchronous HCT116 stable clone 30 overexpressing GTSE1-GFP after IP using anti-GFP antibody. HCT116 GTSE1-GFP clone 30 was transiently transfected with the following MCAK fragments; myc-tagged N-terminal MCAK (1-181), N-terminus plus neck (1-231), motor domain (232-583), motor plus neck domain (182-583) and C-terminus (584-725) of MCAK. The blot was probed with anti-GFP and anti-myc antibody. Endogenous GTSE1-GFP could pull down the MCAK FL, N-terminal domain (1-181) and motor domain (232-583) of MCAK (black asterisk). M stands for molecular weight standards (kDa).

3.7 Aurora A phosphorylated GTSE1 directly interacts with MCAK

Next we wanted to test the possibility of a direct interaction between GTSE1 and MCAK. To confirm their interaction *in vitro*, we bacterially purified GST-tagged GTSE1 N-terminal (1-460 aa) and C-terminal (463-739 aa) fragments (Cloned by Yu-Chih Lin). *In vitro,* GST pull-down was performed by immobilizing GST-GTSE1 fragments on GSH beads and incubating them with His-MCAK FL protein purified from insect cells (produced by Gary Brouhard). GST alone was used as a negative control. As shown in Figure 16A, we could specifically pull down His-MCAK FL with the N-terminal fragment of GTSE1 confirming that they interact directly, independent of phosphorylation. To test the interaction between full-length proteins, GST-GTSE1 and His-MCAK were purified from insect cells. Interestingly, a direct interaction between GST-GTSE1 FL and His-MCAK FL could not be detected. As GTSE1 strongly interacts with MCAK during mitosis, and GTSE1 is hyper-phosphorylated during mitosis (Figure 15C), we wondered if the interaction between GST-GTSE1 FL and His-

MCAK FL was phosphorylation dependent. To test this, GST pull-downs were performed using GST-GTSE1 FL phosphorylated using either Cdk1 or Aurora A, and untreated MCAK. GST was used as a negative control. The kinases were inactivated using appropriate inhibitors before mixing the two proteins to prevent phosphorylation of MCAK. Phosphorylation of GTSE1 by Aurora A and Cdk1 was confirmed by staining with ProQ Diamond stain and equal loading was confirmed by CBB staining (Figure 16B). Remarkably, as seen in Figure 16C, only GST-GTSE1 when phosphorylated by Aurora A could efficiently pull down MCAK, suggesting that GTSE1 phosphorylation by Aurora A enhances its interaction with MCAK. This data is in accordance with our previous results, further implying that during mitosis, Aurora A phosphorylation, at least partly, regulates GTSE1-MCAK interaction for maintaining proper MT dynamics.

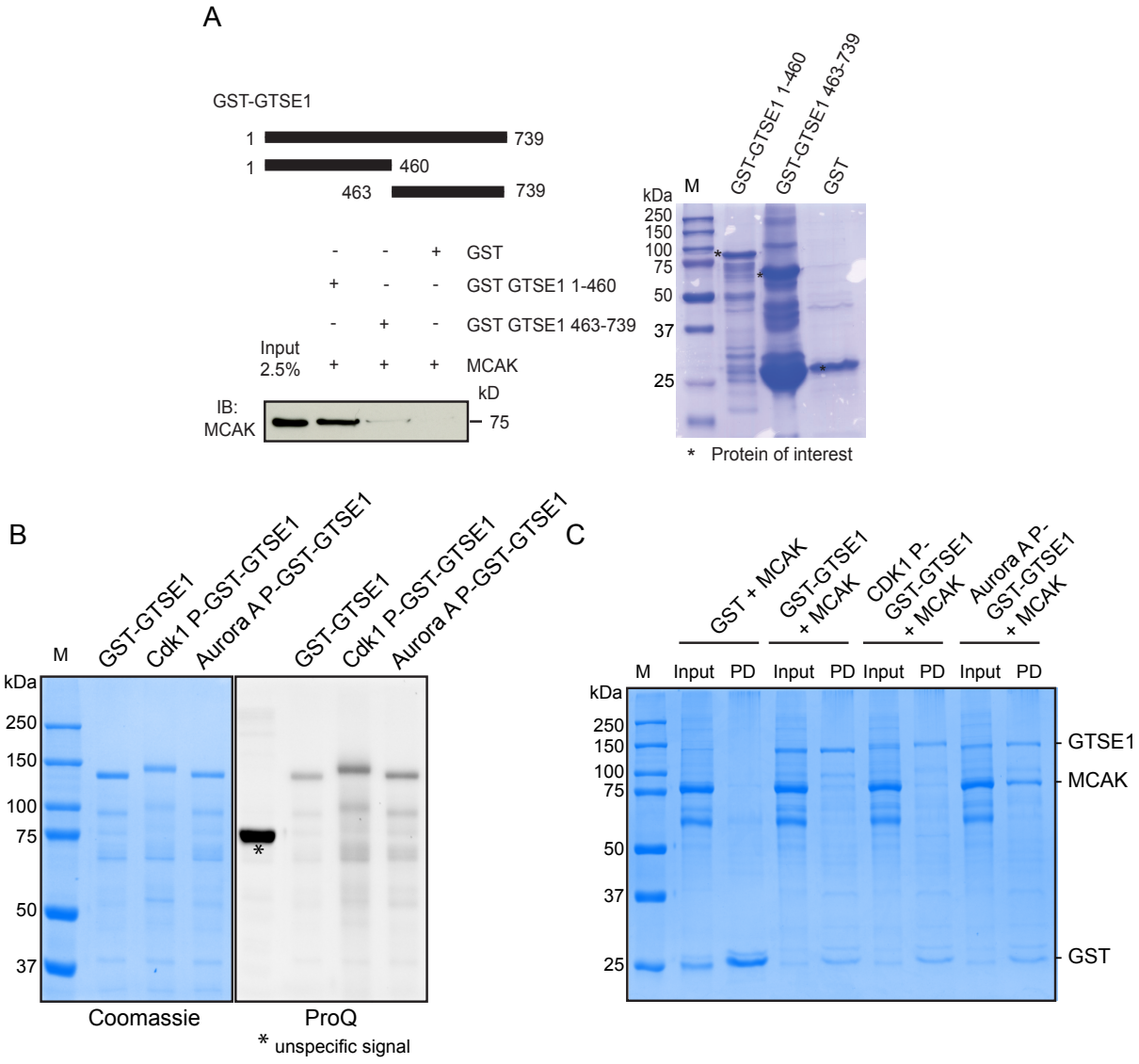

Figure 16. GTSE1 directly interacts with His-MCAK FL

A. Western blot to detect His-MCAK FL after *in vitro* GST pull-down using GST-tagged N-terminus (1-460), C-terminus (463-739) and GST alone. The blot was probed with anti-MCAK antibody. The Coomassie stained gel shows loading control and purity of bacterially purified proteins. N-terminus of GTSE1 can efficiently pull down His-MCAK FL. **B**. Coomassie stained gel showing equal loading of proteins. The same gel was stained before with ProQ phospho-specific stain to confirm phosphorylation of proteins by respective kinases. **C.** *In vitro* GST pull-down showing interaction between Aurora A phosphorylated GST-GTSE1 FL and His-MCAK FL. GST-GTSE1 FL purified from insect cells was phosphorylated using 1:100 Cdk1 or Aurora A at 4 °C overnight followed by inactivation of kinases using either 5 μM RO-3306 (Cdk1 inhibitor) or 500 nM MLN8054 (Aurora A inhibitor) for 10 min on ice. Pull-downs were performed by incubating either phosphorylated or non-phosphorylated GST-GTSE1 FL with His-MCAK FL for 1 h on ice. Inputs and pull-downs were processed by SDS-PAGE and gels were stained with CBB. As seen, His-MCAK FL was efficiently pulled down with Aurora A phosphorylated GST-GTSE1 FL. M: Molecular weight standards.

Next, we confirmed the dependency of Aurora A phosphorylation on direct interaction between GTSE1 and MCAK by SEC. As shown in Figure 17A-E, a clear binding between Aurora A phosphorylated GTSE1 FL and His-MCAK FL is evident in contrast to untreated GTSE1 FL. Similarly, the N-terminal fragment of GTSE1 (1-460 aa) also shows a strong interaction with His-MCAK FL when phosphorylated by Aurora A (Figure 18A-E). In contrast to our pull-down results, we did not observe any consistent interaction between the non-phosphorylated N-terminus (1-460) of GTSE1 and His-MCAK FL by SEC. The C-terminal fragment does not bind to His-MCAK FL irrespective of phosphorylation by Aurora A (Figure 19A-E). This data confirms that MCAK binds directly to the N-terminal fragment of GTSE1 and Aurora A phosphorylation further enhances this interaction.

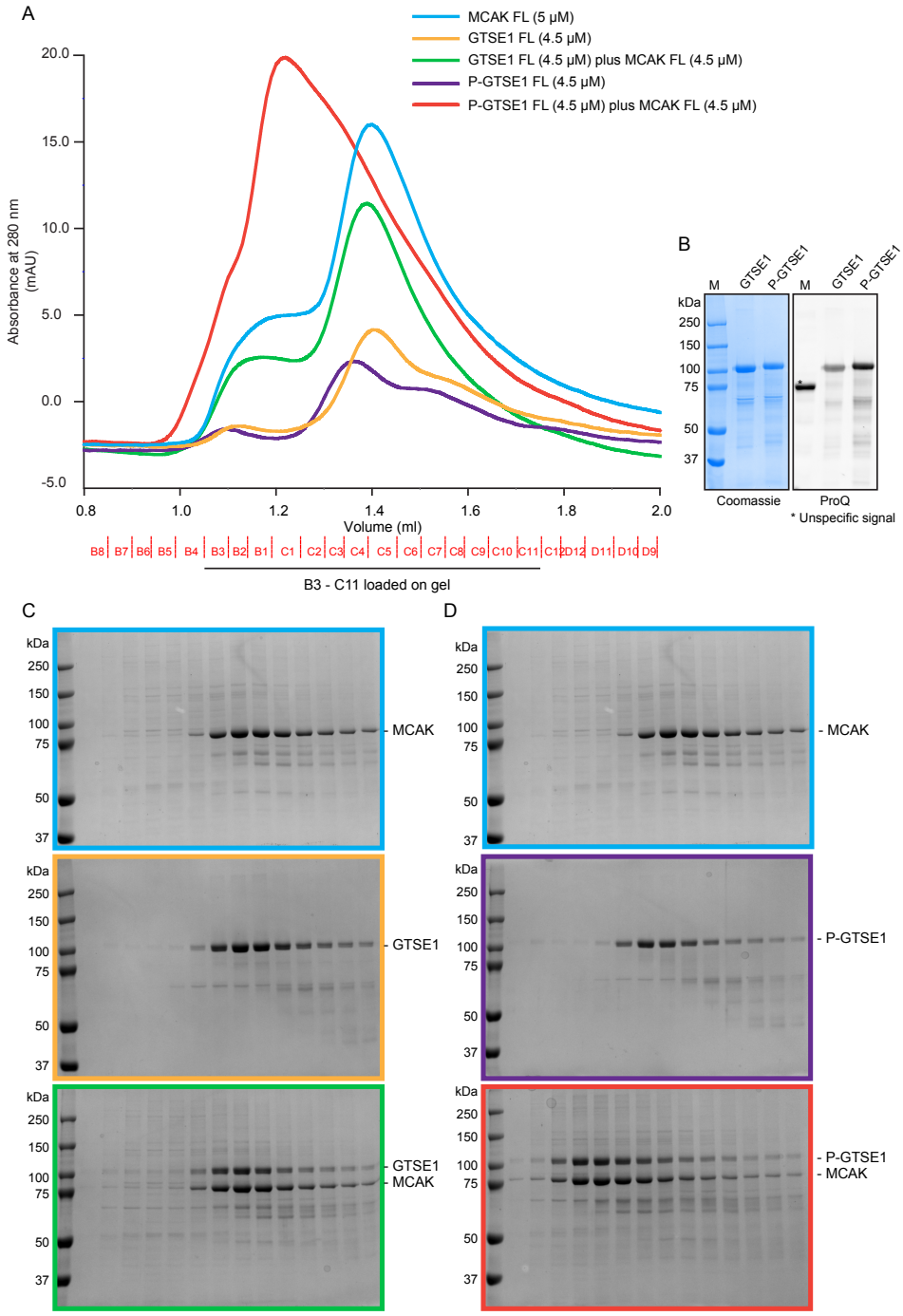

Figure 17. Size Exclusion Chromatography (SEC) showing direct interaction between P-GTSE1 FL and His-MCAK FL

SEC profiles and SDS-PAGE analysis of GTSE1 FL and His-MCAK FL complex **A.** Chart shows SEC elution profiles for His-MCAK FL (blue), GTSE1 FL (orange), Aurora A phosphorylated GTSE1 (P-GTSE1; violet), GTSE1 FL with His-MCAK FL (green), P-GTSE1 FL with His-MCAK FL (red). **B**. SDS-PAGE analysis of un-phosphorylated and GTSE1 FL phosphorylation by Aurora A. Equimolar protein amounts were used and the efficiency of phosphorylation was determined by ProQ Diamond staining. **C.** SDS-Page analysis showing no major shift in molecular weight (green curve in

chromatograph) in presence of GTSE1 FL and His-MCAK FL indicating no interaction between these two proteins. **D.** SDS-Page analysis showing a dramatic shift in molecular weight (red curve in chromatograph) in presence of Aurora A phosphorylated P-GTSE1 FL and His-MCAK FL indicating a strong interaction between these two proteins. M: Molecular weight standards. mAu: milli arbitrary units

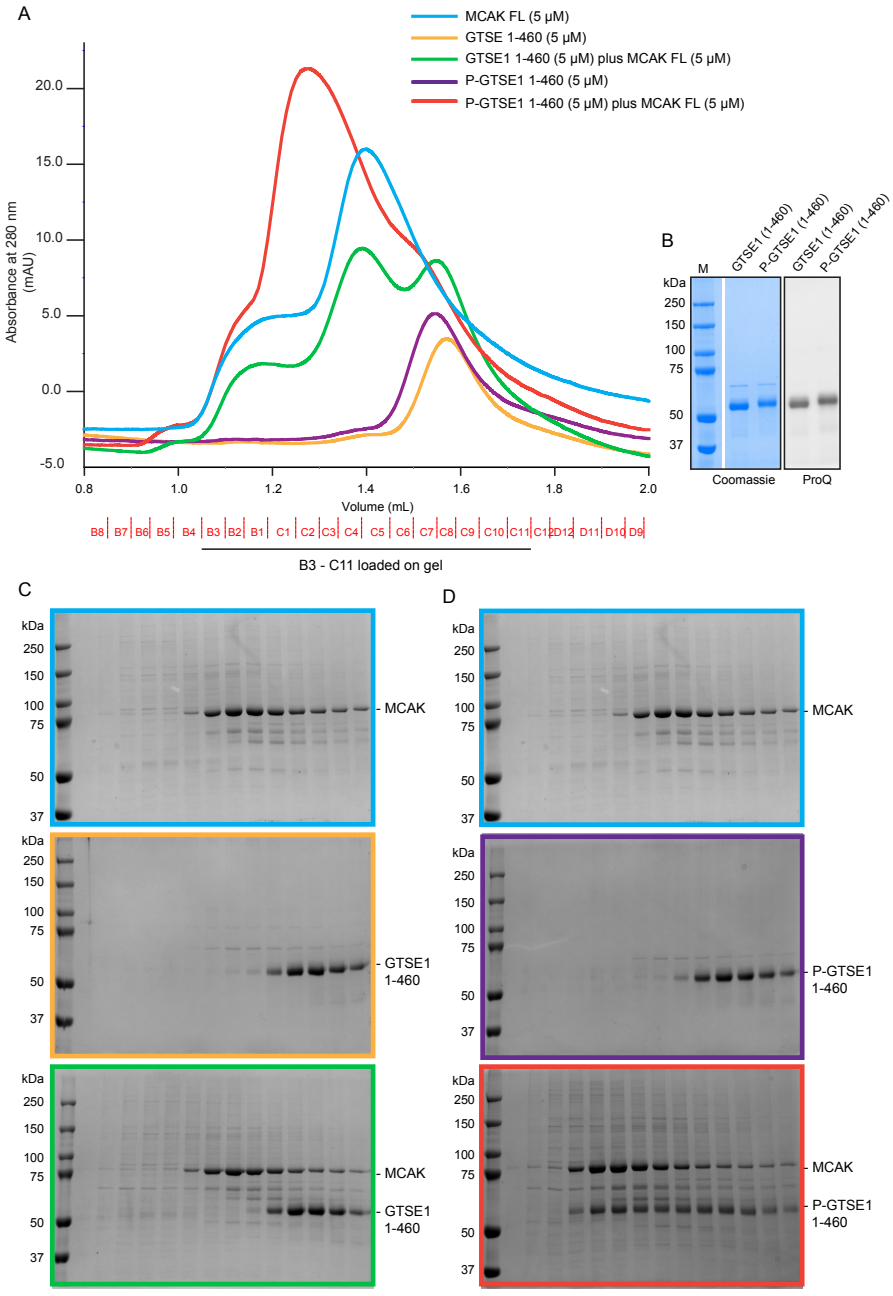

Figure 18. Size Exclusion Chromatography (SEC) showing direct interaction between P-GTSE1 1-460 and His-MCAK FL

SEC profiles and SDS-PAGE analysis of GTSE1 1-460 and His-MCAK FL complex **A.** Chart shows SEC elution profiles for His-MCAK FL (blue), GTSE1 1-460 (orange), Aurora A phosphorylated GTSE1 1-460 (P-GTSE1 1-460; violet), GTSE1 1-460 with His-MCAK FL (green),

P-GTSE1 1-460 with His-MCAK FL (red). **B**. SDS-PAGE analysis of un-phosphorylated and GTSE1 1-460 phosphorylation by Aurora A. Equimolar protein amounts were used and the efficiency of phosphorylation was determined by ProQ Diamond staining. **C.** SDS-Page analysis showing no major shift in molecular weight (green curve in chromatograph) in presence of GTSE1 1-460 and His-MCAK FL indicating no interaction between these two proteins. **D.** SDS-Page analysis showing a dramatic shift in molecular weight (red curve in chromatograph) in presence of Aurora A phosphorylated P-GTSE1 1-460 and His-MCAK FL indicating a strong interaction between these two proteins. M: Molecular weight standards. mAu: milli arbitrary units

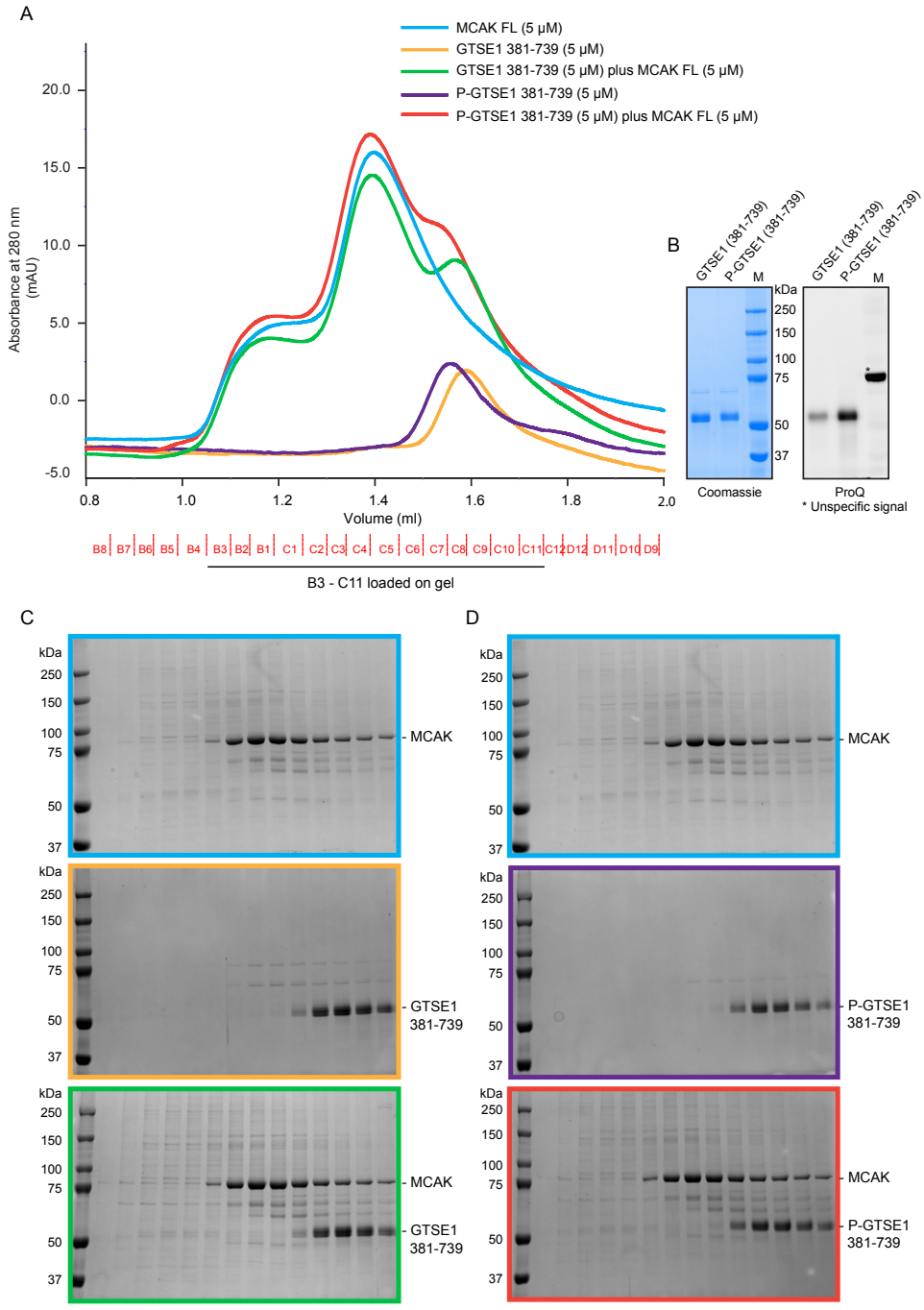

Figure 19. Size Exclusion Chromatography (SEC) showing absence of direct interaction between P-GTSE1 381-739 and His-MCAK FL

SEC profiles and SDS-PAGE analysis of GTSE1 381-739 and His-MCAK FL complex **A.** Chart shows SEC elution profiles for His-MCAK FL (blue), GTSE1 381-739 (orange), Aurora A phosphorylated GTSE1 381-739 (P-GTSE1 381-739; violet), GTSE1 381-739 with His-MCAK FL (green), P-GTSE1 381-739with His-MCAK FL (red). **B**. SDS-PAGE analysis of un-phosphorylated and GTSE1 381-739 phosphorylation by Aurora A. Equimolar protein amounts were used and the efficiency of phosphorylation was determined by ProQ Diamond staining. **C.** SDS-Page analysis showing no major shift in molecular weight (green curve) in presence of GTSE1 381-739 and His-MCAK FL indicating no interaction between these two proteins. **D.** SDS-Page analysis showing no shift in molecular weight (red curve) in presence of Aurora A phosphorylated P-GTSE1 381-739 and His-MCAK FL indicating no interaction between these two proteins. M: Molecular weight standards. mAu: milli arbitrary units

3.8 GTSE1 inhibits MCAK's depolymerase activity *in vitro*

In **section 3.4,** we showed that GTSE1 inhibits MCAK's depolymerase activity *in vivo*, therefore, we now wanted to examine GTSE1's ability to antagonize MCAK's depolymerase activity *in vitro*. We tested this via two different assays. First, we performed a sedimentation assay where taxol stabilized MTs were incubated for 30 min at room temperature along with MCAK and ATP (1.5 μM) to depolymerize MTs. This reaction mixture was centrifuged at 90,000 rpm for 10 min at 25°C. Ultra-centrifugation causes MTs to sediment in the pellet fraction whereas the tubulin dimers stay in the supernatant. The supernatant and pellet were then processed for SDS-PAGE and stained with CBB to analyze the extent of MT depolymerization. We optimized the concentration of MCAK and tubulin and then maintained them at constant values of 200 nM for MCAK and 1.66 μM for tubulin and titrated GTSE1. Remarkably, at a concentration of 2000 nM and 1000 nM (i.e. 10:1 and 5:1 GTSE1: MCAK), GTSE1 completely inhibits MCAK's depolymerase activity as most of the tubulin stays in the pellet fraction (Figure 20A and 20B). An inverse correlation can be seen between the extent of depolymerization and the amount of GTSE1. Reducing the amounts of GTSE1 causes an increase in amounts of tubulin observed in the supernatant (Figure 20B). At 1:1 stoichiometry GTSE1 partially inhibits MCAK's depolymerase activity. This data indicates that GTSE1 can efficiently inhibit MCAK's depolymerase activity *in vitro*.

In a second assay that was performed in collaboration with Gary Brouhard and Conrad Hall

(Bendre et al., 2016), we tested the effect of GTSE1 on MCAK's depolymerization rates on GMPCPP MTs using Total Internal Reflection Fluorescence microscopy (TIRF) (Helenius et al., 2006). Depolymerization of TAMRA-labeled GMPCPP MTs occurred from both the ends in presence of 50 nM MCAK alone (Figure 20C). Addition of equimolar (50 nM) or excess (250 nM) GTSE1 completely inhibited MCAK's capability to depolymerize MTs (Figure 20C), which is in compliance with our sedimentation assay results.

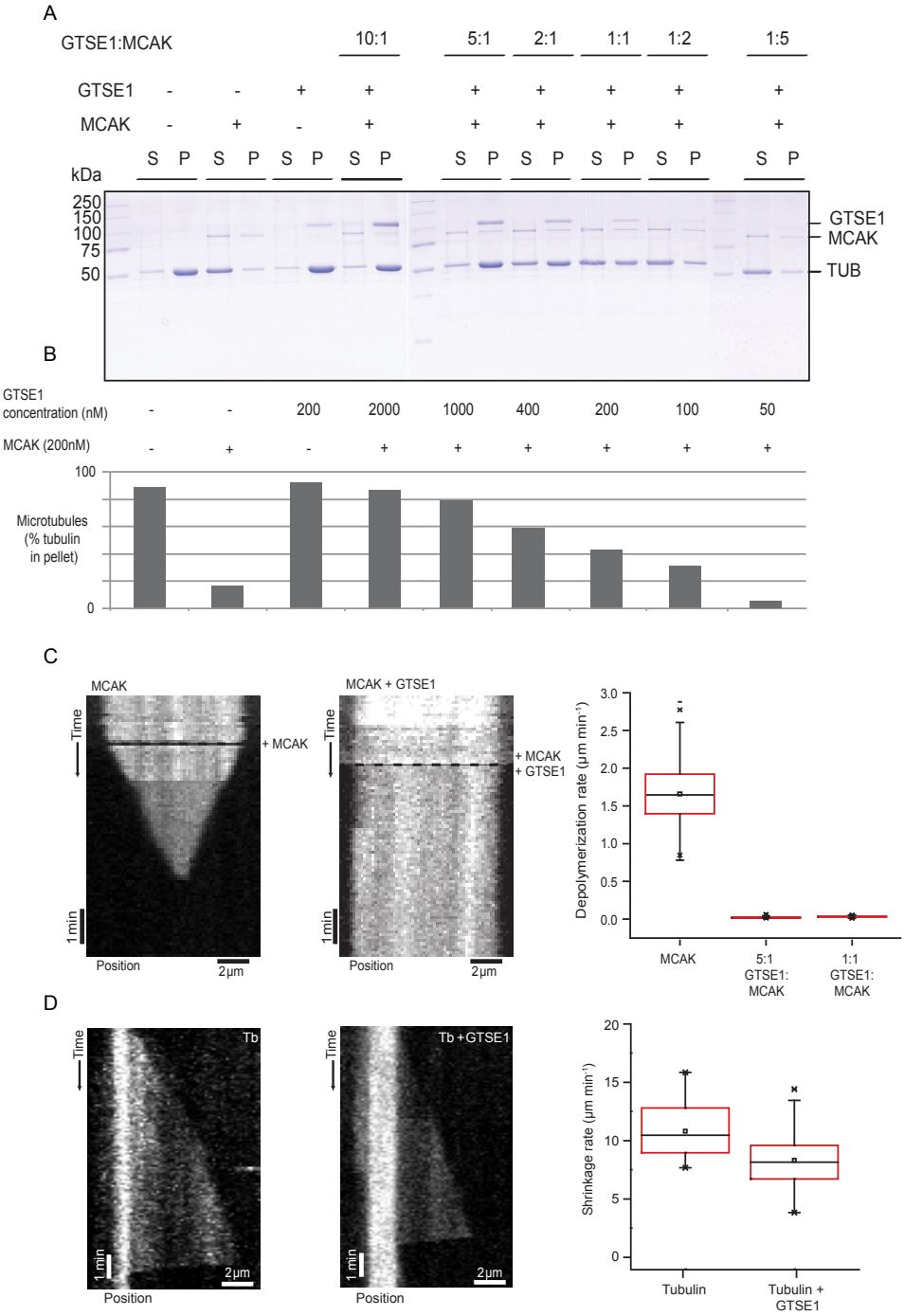

Figure 20. GTSE1 inhibits MCAK's depolymerase activity *in vitro*

A. Sedimentation assay to study the effect of GTSE1 on MCAK's depolymerase activity. Taxol stabilized MTs (1.66 μM) were incubated with MCAK (200 nM), ATP (1.5 μM) and with different concentrations of GTSE1, 2000 nM (10:1, GTSE1: MCAK), 1000 nM (5:1), 400 nM (2:1), 200 nM (1:1), 100 nM (1:2), 40 nM (1:5). The reaction was incubated for 30 min at room temperature followed by centrifugation at 90,000 rpm for 10 min at 25°C. The supernatant and pellet were processed for SDS-PAGE and stained with CBB to analyze the extent of depolymerization. As seen at 10:1, 5:1 (GTSE1: MCAK) stoichiometry GTSE1 completely inhibits MCAK depolymerase activity. **B.** Graph showing quantification of the Coomassie gel in A displaying the percentage of MTs in the pellet in presence of MCAK and different concentrations of GTSE1. **C.** Kymograph displaying a GMPCPP stabilized MT undergoing depolymerization in presence of 50 nM MCAK. The black dashed line represents the time at which MCAK was added. Second kymograph depicts a GMPCPP stabilized MT maintaining constant length in the presence of 50 nM MCAK plus 250 nM GTSE1. The black dashed line represents the start of the experiment when MCAK and GTSE1 were added. The box plot shows depolymerization rates of GMPCPP stabilized MTs in the presence of 50 nM MCAK alone, 50 nM MCAK with a 5 fold excess of GTSE1, and 50 nM MCAK with an equimolar amount of GTSE1. **D.** Kymographs of MT growth and catastrophe in the presence of 20 μM tubulin alone or 20 μM tubulin with 250 nM GTSE1 from a GMPCPP MT seeds. Box-plot shows the shrinkage rate following catastrophe of 20 μM tubulin alone and 20 μM tubulin with 250 nM GTSE1. TRIF assay and kymographs were performed by Conrad Hall; Bendre et al., 2016.

In our *in vitro* assays, it is possible that GTSE1 intrinsically stabilizes MTs as a result of which MCAK cannot depolymerize MTs. To test this, we looked at MT shrinkage rates after catastrophes in presence of 250 nM GTSE1 alone and observed a small but significant reduction in the MT shrinkage rate (Figure 20D). These results indicate that GTSE1 does have a minor impact on MT stability, however, this effect of GTSE1 alone on MT stability is very subtle and cannot explain the complete inhibition of MT destabilization by MCAK.
These results confirm that GTSE1 inhibits MCAK's depolymerase activity *in vitro.*

3.9 Depleting GTSE1 reduces chromosome mis-segregation frequency in CIN cancer cell lines

The precise regulation of MCAK activity is required to determine levels of CIN in cells. Some cancer cell lines show intrinsically hyper-stable KT-MT attachments, which are prone to persistent erroneous KT-MT attachments that elevates the number of lagging chromosomes during anaphase. Lagging chromosomes are generally a result of persistent merotely and are considered to be an indirect readout for chromosome mis-segregation and CIN. Interestingly, it has been shown that artificially increasing MCAK activity in cancer cell

lines exhibiting high CIN renders the KT-MT attachments more dynamic. This facilitates error correction, further decreasing the frequency of lagging chromosomes and suppressing CIN (Bakhoum et al., 2009a; Bakhoum et al., 2009b). As depletion of GTSE1 mimics the phenotypes observed after MCAK overexpression we decided to study the effect of GTSE1 on anaphase chromosome segregation defects in CIN cell lines. Intriguingly, the percentage of cells showing anaphase defects decreased significantly, after depletion of GTSE1 in U2OS and Hela Kyoto cell lines. (Figure 21A-C). Remarkably, the frequency of anaphase defects was even further reduced in GTSE1 knockout clones (Figure 21C). Interestingly, loss of MCAK and co-depletion of MCAK and GTSE1 led to an increase in the percentage of cells showing anaphase chromosome segregation defects. This is in line with our previous results, where we observed reduced MT stability and KT-MT attachment stability following GTSE1 depletion, which is suggestive of increased MCAK activity (Maney et al., 1998; Kline-Smith et al., 2004; Thompson and Compton, 2011) (Figure 21A and 21C). This indicates that the decrease in anaphase defects after GTSE1 depletion is indeed due to increased MCAK activity, as there is no reduction in anaphase defects after depleting GTSE1 along with MCAK. Importantly, depletion of GTSE1 specifically affected the frequency of lagging chromosomes but did not influence chromatid bridges or acentric chromosome fragments in U2OS and Hela Kyoto cells that arise due to pre-mitotic replicative stress (Burrell et al., 2013) (Figure 22A-C). Thus, GTSE1 regulates KT-MT attachment stability by antagonizing MCAK depolymerase activity, which is crucial for efficient chromosome segregation.

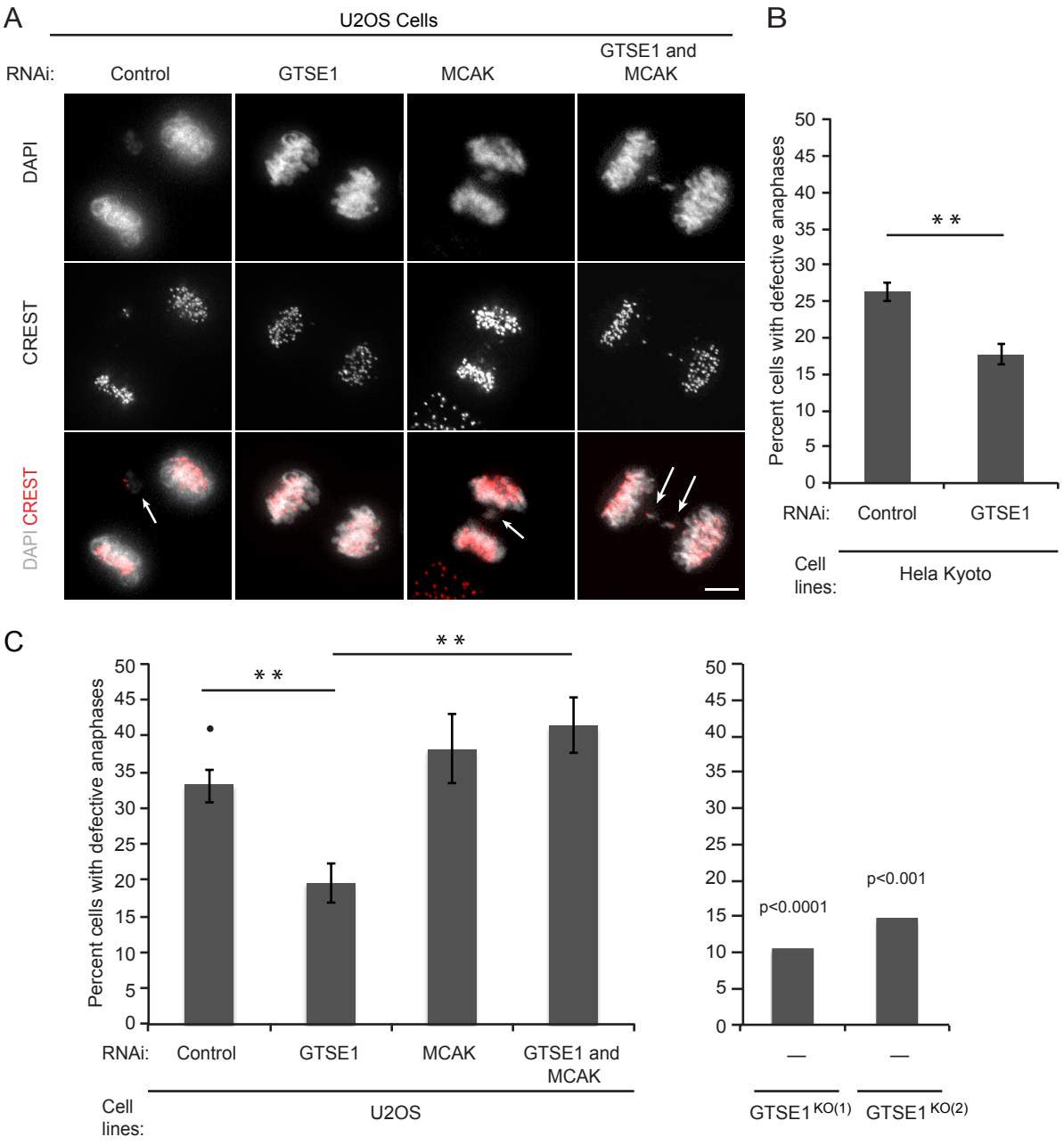

Figure 21. Depleting GTSE1 reduces chromosome mis-segregation frequency in CIN cancer cell lines

A. Representative immunofluorescence images of U2OS cells showing lagging chromosomes (white arrows) that are stained with DAPI (DNA), anti-CREST (KTs) after depletion of endogenous GTSE1, MCAK, co-depletion of GTSE1 and MCAK and control RNAi. **B.** Quantification of percentage of cells showing anaphase defects after control and GTSE1 RNAi in Hela Kyoto cells (n > 390 per condition over 3 experiments). **C.** Left bar graph depicts quantification of percentage of cells showing anaphase defects after control, GTSE1, MCAK RNAi and co-depletion of GTSE1 and MCAK in U2OS cells (n > 65 per experiment; 3 experiments per condition). Right chart shows quantification of percentage of cells showing anaphase defects in U2OS GTSE1 knockout clones (GTSE1$^{KO(1)}$ and

GTSE1$^{KO(2)}$) (p-values were obtained from a chi squared test comparing to the U2OS control condition (marked with •); n > 100 cells). All scale bars represent 5 micrometers. All error bars represent standard error of the mean. p≤0.05 *, p≤0.01 **, p≤0.001 ***

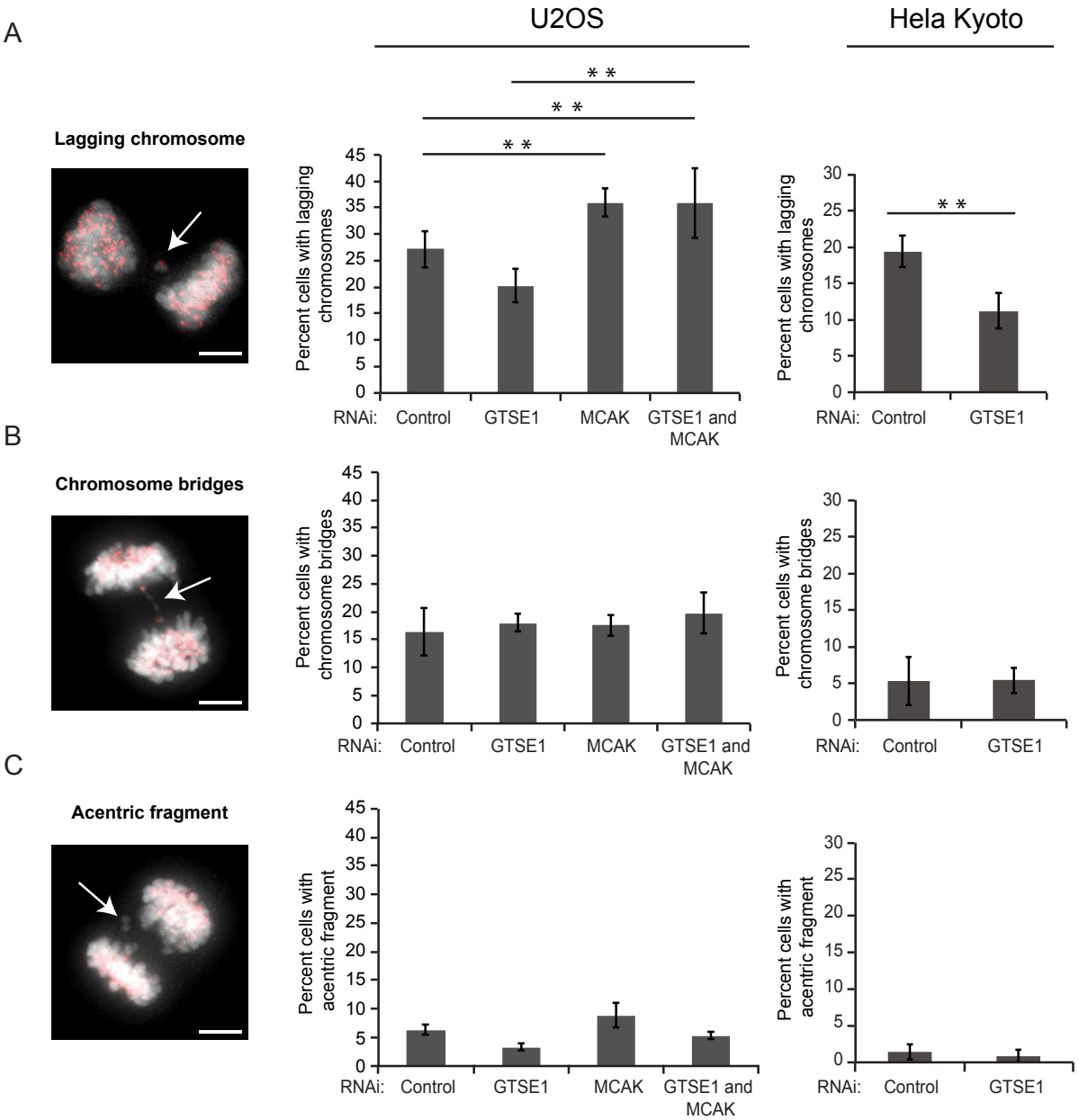

Figure 22. Quantification of anaphase defects (lagging chromosomes, chromosome bridges, acentric chromosomal fragments)

A. Representative immunofluorescence image of an anaphase cell showing lagging chromosome (white arrow). Left chart depicts quantification of percent cells showing lagging chromosomes after control, GTSE1, MCAK RNAi and co-depletion of GTSE1 and MCAK in U2OS cells. Right chart displays quantification of percentage of cells showing lagging chromosomes after control and GTSE1

RNAi in Hela Kyoto cells. **B.** Representative immunofluorescence image of an anaphase cell showing chromosome bridge (white arrow). Left chart shows quantification of chromosome bridges in U2OS cells, whereas, right chart shows the same in Hela Kyoto cells. **C.** Representative immunofluorescence image of an anaphase cell showing acentric chromosome fragment (white arrow). Quantification of percentage of cells showing acentric fragments in U2OS cells (left chart) and Hela Kyoto cells (right chart). All immunofluorescence images show DNA (DAPI) and KTs (CREST). (n > 220 U2OS cells with defective anaphases over 3 independent experiments; n > 390 Hela Kyoto cells with defective anaphases over 3 independent experiments). All scale bars represent 5 micrometers. All error bars represent standard error of the mean. $p \leq 0.05$ *, $p \leq 0.01$ **, $p \leq 0.001$ ***

3.10 Overexpression of GTSE1 induces segregation defects in HCT116 cells.

Several cancer cell lines like U2OS show high CIN as a consequence of hyperstable KT-MT attachments (Bakhoum et al., 2009a, Bakhoum et al., 2009b). GTSE1 has been reported to be up regulated in solid tumors and cancer cell lines (Scolz et al., 2012). Therefore, we wanted to examine whether overexpression of GTSE1 in a chromosomally stable diploid cell line can induce CIN. To analyze this, we generated stable clones overexpressing GTSE1-GFP in nearly diploid, low CIN HCT116 cell line. We isolated and used two clones, one expressing 3-fold higher and the second expressing 10-fold higher amounts of GTSE1 than control cells (Figure 23A). These clones were maintained for approximately 60 generations by cultivating them under anti-biotic selection. We wanted to ensure that overexpression of GTSE1 does not affect GTSE1's spindle localization and alter spindle morphology. HCT116 clones overexpressing GTSE1-GFP showed normal spindle morphology and chromosome alignment (Figure 23B). As shown in Figure 23C, GTSE1-GFP normally localized to cold-stable K-fibers in both GTSE1-GFP overexpressing clones. As GTSE1 is recruited to K-fibers via the TACC3-Ch-Tog-Clathrin complex, it was important to analyze if GTSE1 overexpression affected the spindle localization and protein levels of this complex. To study this, we looked at TACC3 levels by western blot and measured the spindle intensity of TACC3 in control and GTSE1-GFP overexpressing clones and normalized it to tubulin levels. As shown in Figure 23A and 23D-G, GTSE1-GFP overexpressing clones displayed a 30% increase in tubulin intensity without having a dramatic influence on TACC3 spindle association and TACC3 protein levels.

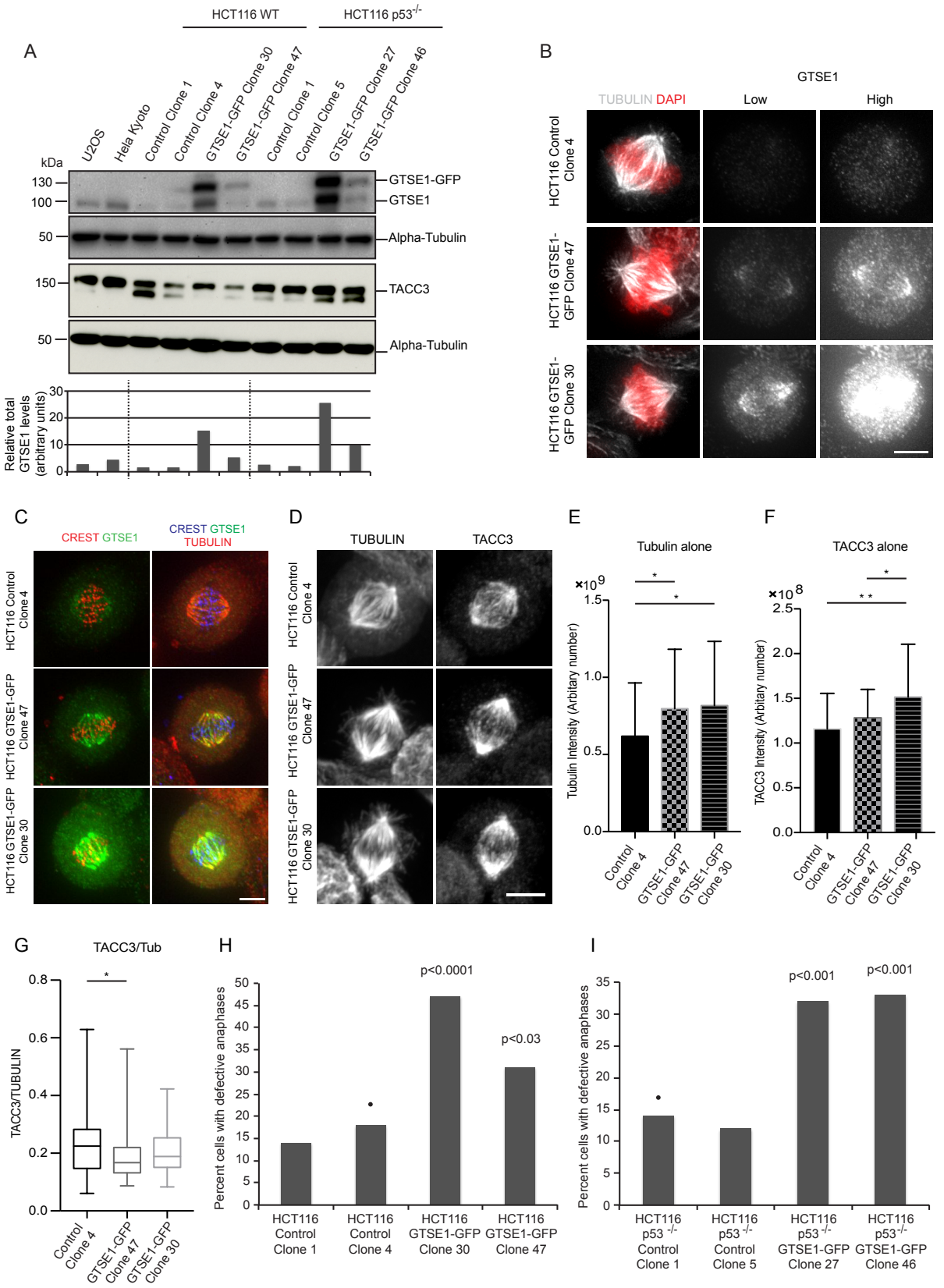

Figure 23. Overexpression of GTSE1 induces segregation defects in HCT116 cells without affecting spindle morphology

A. Western blot of cell lysates from U2OS cells, Hela Kyoto cells, HCT116 and HCT116 p53$^{-/-}$

control and GTSE1-GFP overexpressing clones for comparing relative expression levels of GTSE1 and TACC3. The blot was probed with anti-GTSE1, anti-α-tubulin, and anti-TACC3. Band intensities were determined using Image J and the values were normalized with tubulin band intensities. Relative abundance of proteins is plotted in the small graph below the blot. **B.** Representative fluorescence micrographs of HCT116 control clone 4, GTSE1-GFP overexpressing clone 47 and clone 30 showing normal spindle morphology during metaphase. The cells were fixed and probed with ani-GTSE1, anti-α-tubulin (MTs) and DAPI (DNA). **C.** Representative immunofluorescence images of cold-treated HCT116 control clone 4, GTSE1-GFP overexpressing clone 47 and clone 30 showing K-fiber localization of GTSE1-GFP. The cells were stained for MTs (α-tubulin), KTs (CREST) and GTSE1 (GFP). **D.** TACC3 localization after GTSE1-GFP overexpression. Representative fluorescence micrographs of HCT116 control clone 4, GTSE1-GFP overexpressing clone 47 and clone 30 stained for α-tubulin and TACC3. **E-G.** Bar chart to shows α-tubulin inner spindle intensity (E), TACC3 inner spindle intensity (F) ratio of TACC3/α-tubulin intensity on inner spindles of HCT116 clones as shown in D ($n \geq 52$ cells per condition for 1 experiment; p-values were obtained using an Anova and Tukey's test; error bars represent standard deviation). **H.** Quantification of percentage of cells showing anaphase defects in HCT116 control clone 1, clone 4, GTSE1-GFP overexpressing clone 47 and clone 30 ($n \geq 99$; p-values were obtained from chi-squared tests comparing control clones designated with •). **I.** Chart shows quantification of anaphase defects in HCT116 $p53^{-/-}$ control clone 1, clone 5, GTSE1-GFP overexpressing clone 27 and clone 46 ($n \geq 104$; p-values were obtained from chi-squared tests comparing control clones designated with •). All scale bars represent 5 μm and all error bars when not specified represent standard error of the mean. $p \leq 0.05$ *, $p \leq 0.01$**, $p \leq 0.001$ ***

Next we quantified the frequency of anaphase segregation defects following GTSE1-GFP overexpression and observed a significant increase in HCT116 cells overexpressing GTSE1-GFP as compared to mock-treated control cells (Figure 23H). Most diploid cells are intolerant to chromosome mis-segregation and CIN, as chromosome mis-segregation leads to cellular growth retardation or death via the p53 apoptotic pathway (Thompson and Compton, 2010; Thompson and Compton, 2008). As p53 apoptotic pathway eliminates cells with aneuploidy genomes, we also produced stable HCT116 p53-/- clones overexpressing GTSE1-GFP to study CIN over several generations. We isolated two clones, one overexpressing 8-fold higher and a second one expressing 3-fold higher amounts of GTSE1 as compared to control clones (Figure 23A). As shown in Figure 23I, GTSE1-GFP overexpressing HCT116 p53-/- clones showed increased anaphase segregation defects as compared to mock-treated clones. This suggests that overexpression of GTSE1 increases anaphase defects, which might induce CIN.

3.11 Overexpression of GTSE1 induces CIN in HCT116 cells.

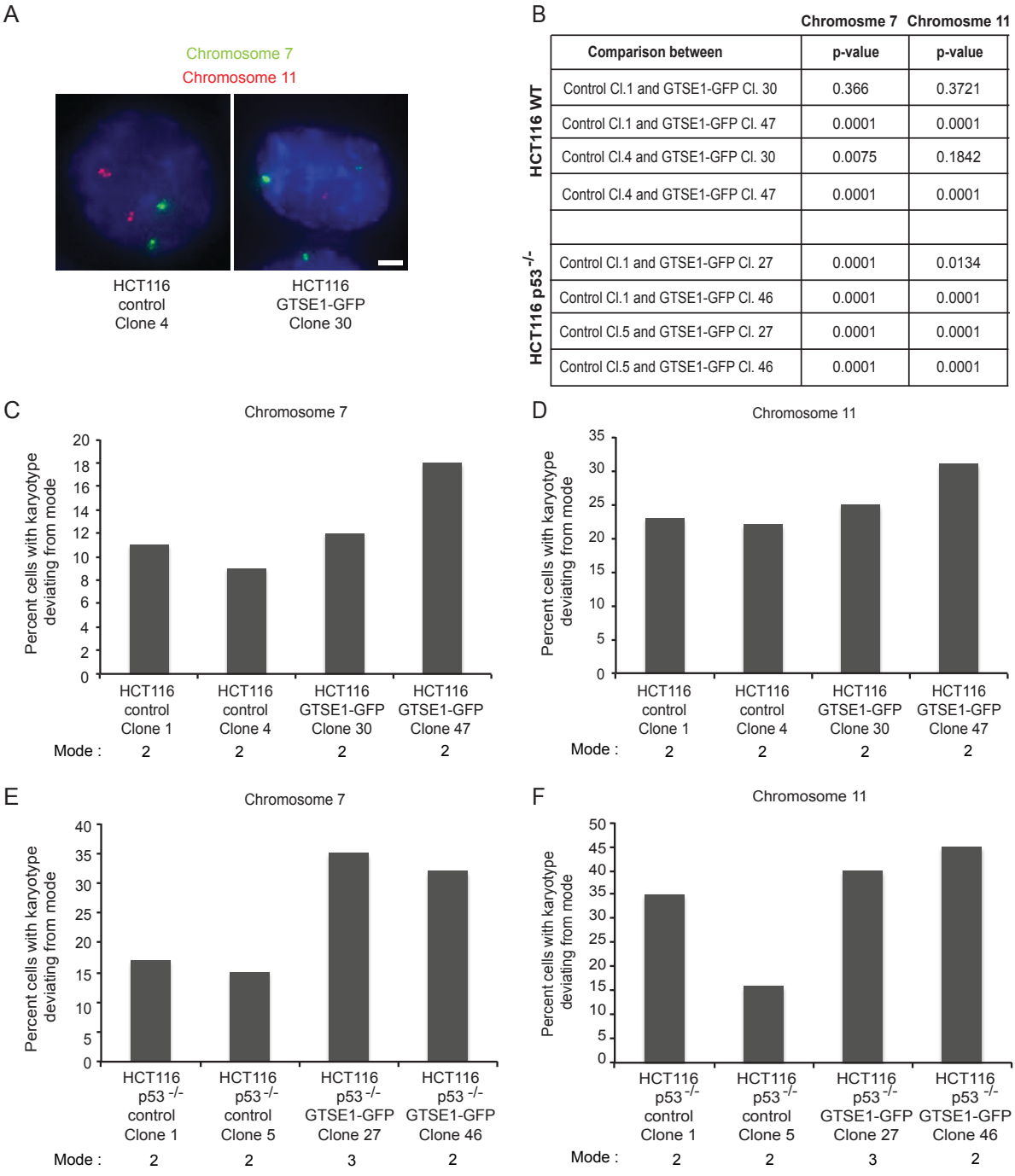

Figure 24. Overexpression of GTSE1 induces CIN in HCT116 cells

A. Images showing normal chromosome segregation in HCT116 control clone 1 (cells show 2 green spots – chromosome 7, 2 red spots – chromosome 11) and mis-segregation in HCT116 GTSE1-GFP overexpressing clone 30 (once cell shows 2 green spots – chromosome 7, 1 red spot – chromosome 11 and the other cell shows 2 green and red spots for chromosome 7 and 11, respectively). **B.** Table shows p values from comparing the statistically significant deviances from the modal number of chromosomes in control versus GTSE1-GFP overexpressing HCT116 and HCT116 p53$^{-/-}$ cells. P-

values were calculated using a chi-squared analysis comparing the indicated clonal cell lines. **C-D.** Graphical representation of percentage of HCT116 cells showing deviation of karyotype from modal of 2 for chromosome 7 and 11, respectively. HCT116 cells overexpressing GTSE1-GFP show higher mis-segregation rates as compared to HCT116 control cells after cultivation for ~ 63 generations (n > 980 cells per clone). **E-F.** Bar chart displays percent HCT116 $p53^{-/-}$ showing deviating of karyotype from modal (modal number shown below the graph) for chromosome 7 and 11, respectively. HCT116 p53-/- cells overexpressing GTSE1- GFP show higher mis-segregation rates as compared to HCT116 p53-/- control cells after cultivation for ~ 63 generations (n>1000 cells per clone).

Overexpression of GTSE1 increased the frequency of anaphase defects in HCT116 clones. We next wanted to test if long-term overexpression of GTSE1 might induce CIN in diploid HCT116 clones by using Fluorescence *in situ* Hybridization (FISH) analysis. Two HCT116 mock-transfected and two GTSE-GFP overexpressing clones were grown for ~ 63 generations and then processed for FISH with chromosome-specific α-satellite DNA probes for chromosomes 7 and 11 (Figure 24A). We counted >900 cells per clone and identified the modal number for each of these chromosomes and quantified the fraction of cells in the population deviating from that modal. As shown in Figure 24B-D, HCT116 clones over-expressing GTSE1-GFP showed a higher deviation from modal as compared to control clones. Similarly, two HCT116 p53-/- mock-transfected and two GTSE-GFP overexpressing clones were analyzed by FISH and the overexpressing clones showed even a higher deviation from the disomic state as compared to mock-transfected control clones (Figure 24B, 24E and 24F). This data demonstrates that overexpressing GTSE1 for several generations induces CIN plausibly by hyper-stabilizing KT-MT attachments as a result of reduced MCAK activity that leads to persistent merotely in chromosomally stable HCT116 cell line.

4. Discussion

The precise regulation of MAPs during mitosis is crucial for fine-tuning MT dynamics required for proper chromosome alignment and accurate segregation. Here we show a novel mechanism wherein GTSE1 tunes MT dynamics during mitosis by inhibiting MCAK's depolymerase activity. Loss of GTSE1 has a negative impact on the global MT stability, which compromises the ability of cells to properly orient their spindles and align chromosomes. In contrast, depletion of GTSE1 in highly CIN U2OS and Hela cell lines reduces the frequency of lagging chromosomes owing to reduced KT-MT attachment stability. These phenotypes observed upon loss of GTSE1 can be attributed to the enhanced depolymerase activity of MCAK. GTSE1 interacts directly with MCAK and attenuates its depolymerase activity *in vivo* and *in vitro*. Interestingly, overexpressing GTSE1 in diploid cancer cell lines induces aneuploidy by increasing the frequency of chromosome mis-segregation events. GTSE1 is frequently found overexpressed in solid tumors and cancers, and this study sheds light on the potential molecular mechanism by which GTSE1 might induce aneuploidy.

4.1 GTSE1 stabilizes astral MTs

GTSE1 localizes to spindle MTs and spindle poles during mitosis, where it stabilizes astral MTs by protecting them from the potent depolymerase activity of MCAK. Cells depleted of GTSE1 display short astral MTs, implying a defect in MT elongation (Figure 8). Reports suggest that the native environment in the vicinity of centrosomes regulates MT-nucleation and growth, and this is reliant on the concentration of MAPs at the spindle poles (Wieczorek et al., 2015). Interestingly, MCAK's localization to the spindle was increased following loss of GTSE1 (Figure 14 C-F). Therefore, it is plausible that the balance between polymerizing, stabilizing and depolymerizing MAPs at the centrosomes is disturbed post GTSE1 depletion. Increase in depolymerase activity of MCAK at centrosomes might impede astral MT elongation. Thus, at centrosomes, GTSE1 might counteract MCAK's depolymerase activity creating an environment favorable for astral MT growth and elongation. We could test this by recruiting RNAi resistant GTSE1 specifically to centrosomes and depleting endogenous GTSE1 by RNAi. We could also look at astral MT lengths and MCAK localization in cells overexpressing GTSE1. We could isolate centrosomes from mammalian cells and study astral MT dynamics *in vitro* in presence of purified GTSE1 and MCAK.

In addition, the effect of GTSE1 depletion on astral MT stability was analyzed in three different cancer cell lines. Hela and HCT116 cells displayed shorter astral MTs after GTSE1 depletion, whereas, astral MTs in MCF-7 cells were unaffected (Figure 9). We also studied the effect of GTSE1 depletion in mouse embryonic stem (mES) cells and observed an increase in the number of cells lacking astral MTs (data not shown; performed by Lisa Mazul). Generally, cancer cell lines display a heterogeneous karyotype, which might lead to a variation in GTSE1 and MCAK expression levels. This deviation in expression levels could explain the disparity in the astral MT stability phenotype observed in different cell lines. Therefore, it would be interesting to check and correlate the relative protein amounts of MCAK and some upstream and downstream effectors in different cancerous and non-cancerous cell lines. Moreover, apart from loss in astral MT stability, Hela and mES cells exhibited a radical increase in the number of cells with multipolar spindles. It has been shown previously that overexpression of MCAK destabilizes MTs and leads to multipolar spindles (Zhang et al., 2011; Holmfeldt et al., 2004). Perturbing levels of MT destabilizing and stabilizing proteins like MCAK and Ch-Tog creates an imbalance of forces at the centrosomes instigating centrosome fragmentation and multipolar spindle formation, which might be relevant in the context of GTSE1 depletion (DeLuca et al., 2008; Holmfeldt et al., 2004).

4.2 GTSE1 stabilizes K-fibers and regulates chromosome alignment

During mitosis, GTSE1 becomes hyperphosphorylated and does not bind directly to MTs but instead is recruited to the spindle and spindle poles via the TACC3-Ch-Tog-Clathrin complex (Hubner et al., 2010). Phosphorylation of TACC3 by Aurora A is crucial for formation of the TACC3-Ch-Tog-Clathrin complex (Hood et al., 2013; Cheeseman et al., 2011). It has been reported that the TACC3-Ch-Tog-Clathrin complex stabilizes K-fibers by cross-linking KT MTs through formation of a “mesh” of inter-MT bridges (Nixon et al., 2015; Cheeseman et al., 2013; Hood et al., 2013; Booth et al., 2011). GTSE1 binds to clathrin via five putative clathrin binding sites in the C-terminus and has been proposed to be a part of this mesh (Nixon et al., 2015 and our unpublished data). Interestingly, inhibition of Aurora A, clathrin or TACC3 displaces GTSE1 from the spindle (Hubner et al., 2010). Furthermore, depletion of TACC3 or clathrin in cells produces spindles with destabilized astral MTs as well as KT MTs and misaligned chromosomes (Kinoshita et al., 2005; O'Brien et al., 2005; Peset et al., 2005; Royle et al., 2005). These phenotypes observed after loss of TACC3 or clathrin are strikingly similar to the phenotypes seen after GTSE1 depletion, leading us to postulate that

the phenotypes observed after loss of TACC3 or clathrin could be attributed to displacement of GTSE1 from the spindle. It is evident from our results that GTSE1 it is the most downstream of all the components of the TACC3-Ch-Tog-Clathrin complex as we do not observe any change in the expression level or spindle localization of TACC3 and clathrin following GTSE1 depletion (Figure 13 A and B; Hubner et al., 2010; our unpublished data).

Our data suggests that the defect observed in alignment of chromosomes following GTSE1 RNAi was dependent on MCAK's depolymerase activity, as co-depleting MCAK and GTSE1 restored the chromosome alignment phenotype. MCAK accumulates strongly at KTs, centrosomes and weakly on the mitotic spindle (Wordeman and Mitchison, 1995). Previous reports show that overexpression of MCAK leads to chromosome misalignment due to improper MT dynamics and imbalance of forces (Shao et al., 2015; Zhang et al., 2011). We reasoned that loss of GTSE1 leads to hyperactivity of MCAK, which increases MT turnover at KTs, reducing the stability of KT-MT attachments, causing an increase in misaligned chromosomes (Figure 10-12). FDAPA experiments showed increased KT MTs turnover following GTSE1 depletion (Figure 12H-J). However, depleting GTSE1 led to a subtle yet significant decrease in the non-KT MT turnover (Figure 12H). Interestingly, we also observed a small reduction in the percentage of non-KT MTs in GTSE1-depleted cells (Figure 12H). It has been shown that a small fraction of MCAK associates with the non-KT MT plus ends and MCAK-depleted cells display stabilization of non-KT MTs (Tanenbaum et al., 2011c; Kollu et al., 2009). We postulate that loss of GTSE1 may cause a MCAK-dependent reduction in the proportion of non-KT MTs. As a result of which, we might be predominantly measuring the half-life of KT MTs leading to higher non-KT MT half-life values. This observation needs to be further investigated and can be tested by performing FDAPA assays in cells overexpressing MCAK. It would also be interesting to look at non-KT MTs following co-depletion of GTSE1 and another protein like Nuf2 that is crucial for maintaining stable KT MTs (Cai et al., 2009; DeLuca et al., 2005). Loss of Nuf2 disrupts K-fibers and co-depletion of GTSE1 along with Nuf2 might radically destabilize the non-KT MTs in addition to the K-fibers due to enhanced activity of MCAK (Cai et al., 2009; DeLuca et al., 2005).

In addition to the loss of K-fiber stability, we observed Mad1 recruitment to a subset of metaphase aligned KT and a net reduction in KT tension following GTSE1 RNAi (Figure 12).

However, the observed decrease in the inter-KT distance following GTSE1 depletion was very minimal. We speculate that GTSE1 might reduce K-fiber stability by affecting the number of MTs/fiber as it acts through the TACC3-Ch-Tog-Clathrin complex and it has been shown previously that clathrin depletion reduces the K-fiber stability whereas, temporal inactivation of TACC3 during metaphase decreases the inter-KT tension (Cheeseman et al., 2013; Booth et al., 2011). It would be interesting to study metaphase K-fiber stability after transient inactivation of GTSE1 during metaphase in order to eliminate accumulation of defects that might have been generated following GTSE1 RNAi during early phases of the cell cycle. Additionally, we would like to confirm the localization of key KT proteins required for KT-MT attachment stability following GTSE1 depletion.

Thus, we hypothesize that GTSE1 might stabilize K-fibers by modulating MT growth and dynamics by inhibiting MCAK's depolymerase activity and thus facilitating K-fiber stability by formation of inter-KT bridges. It is important to note that co-depletion of TACC3 and MCAK restored phenotypes observed after TACC3 depletion in *Xenopus* egg extracts and vertebrate cells further strengthening our hypothesis (Kinoshita et al., 2005; our unpublished data).

Our data implies that GTSE1 stabilizes KT MTs required for proper chromosome alignment by inhibiting MCAK's depolymerase activity. However, the underlying molecular mechanism that affects chromosome alignment after GTSE1 depletion is still unclear. We observed that cells depleted of GTSE1 took longer to align their chromosomes at the metaphase plate, however cells entered anaphase only after all chromosomes were properly aligned (Figure 10H and 10I). We speculate that the short astral MTs as a result of increased MCAK activity might be compromised in efficient capture of peripheral chromosomes post NEBD (Braise et al., 2014). Due to this, a few chromosomes are initially 'stuck' at the spindle poles and are eventually transported to the spindle equator by kinesin motors (Reviewed in Maiato et al., 2017). In addition to shorter astral MTs, another reason for misalignment of chromosomes could be that kinesin motors are less efficient in a GTSE1 RNAi background, owing to abnormal non-KT and KT MT dynamics due to hyperactivity of MCAK. These motor proteins are highly sensitive to changes in MT dynamics and use differences in post translation modifications of stable and dynamic MTs as a navigation system (Reviewed in Maiato et al., 2017). Therefore, it would be interesting to test for an

alteration in tubulin post-translational modifications following GTSE1 RNAi by western blot and immunofluorescence analysis.

Knockout of GTSE1 in U2OS cells affected astral MT stability but hardly had any effect on alignment of chromosomes. These cells had somehow 'adapted' to endure the loss of GTSE1 and we speculated that these cells might have 'adapted' by reducing the cell or spindle size. Reducing cell size will lead to shorter spindles, which might increase the efficiency of capturing peripheral chromosomes (Good et al., 2013). However, the spindle length of U2OS GTSE1 knockout cells was surprisingly similar to U2OS control cells (Figure 10C). We also looked at the expression levels of MCAK, TACC3, p-TACC3, Aurora B and Ch-Tog in U2OS GTSE1 knockout and control cells and did not observe any significant difference (Figure 10D-F). We were surprised that GTSE1 knocked out U2OS cells were viable but it is important to note that despite our best efforts we could isolate only two complete GTSE1 knockout clones. We presume that these GTES1 knockout clones might have "adapted" and are propagating by activating another pathway, which enables proper chromosome alignment in absence of GTSE1.

4.3 GTSE1 directly interacts with MCAK

Previous studies to investigate the GTSE1 interactome by mass spectrometric analysis showed consistent enrichment of MCAK over several experiments (Hubner et al., 2010). Using *in vivo* co-IPs, we could show that GTSE1 FL interacts with MCAK FL during mitosis and this interaction is dependent on phosphorylation (Figure 15A-C).

In order to narrow down the MCAK interaction domain in GTSE1, we performed *in vivo* co-IP assays. We observed an interaction between MCAK FL and GTSE1 FL and the following N-terminal fragments of GTSE1: GTSE1 1-460, GTSE1 1-338 and GTSE1 1-187 (Figure 15D). Notably, we did not detect an interaction between MCAK and GTSE1 1-246 and the C-terminus of GTSE1 (380-739) (Figure 15D). Intriguingly, the GTSE1 1-246 fragment ends right before a putative Aurora A phosphorylation site. This serine residue (S247) was found to be phosphorylated during G2 phase and mitosis (our unpublished data). S247 might be important for this interaction and GTSE1 1-246 lacking this S247 could not bind to MCAK. Nevertheless, we saw an interaction between GTSE1 1-187 and MCAK, implying that either MCAK binds to GTSE1 at multiple sites or the real binding interface is between GTSE1 1-187. GTSE1 1-246 might form some intra-molecular secondary structures that concealed the

MCAK binding domain or this fragment was titrated away through interaction with other proteins, thus preventing its interaction with MCAK. We plan to perform *in vitro* pull-down experiments using purified GTSE1 fragments in order to delineate the interaction domain in GTSE1.

Similarly, we performed co-IP experiments using MCAK fragments in order to define the GTSE1 interaction domain in MCAK. We consistently observed a very weak interaction of GTSE1 FL with MCAK FL and the motor domain (232-583) and a strong interaction with N-terminal domain (1-181) of MCAK (Figure 15E). The N-terminal domain (1-181) is essential for KT binding, +TIP tracking, and regulating MT dynamics for assembling a bipolar spindle (Honnappa et al., 2009; Ems Mc-Clung et al., 2007). This stretch of protein is highly phosphorylated by Aurora B and controls MCAK's subcellular localization (Zhang et al., 2007; Lan et al., 2004). Interestingly, the N-terminus and the C-terminus together influence MCAK's depolymerase activity and bipolar spindle assembly (Ems Mc-Clung et al., 2007). It is plausible that in addition to there being multiple MCAK binding sites on GTSE1, GTSE1 also harbours multiple binding sites on MCAK, as we detected an interaction of GTSE1 with the N-terminal and motor domain. Conversely, GTSE1 could bind to an interface that is formed through an interaction between the N-terminus and motor domain of MCAK. As this interaction between GTSE1 and MCAK appears to be stronger in mitosis as compared to interphase (Figure 15C; Figure 16C), and as this interaction seems to be mediated, in part, due to mitosis specific Aurora A phosphorylation of GTSE1, an open question is, if this interaction is enhanced by mitosis-specific phosphorylation of MCAK as well. Furthermore, the smallest region of MCAK required for binding to GTSE1 remains to be determined and will be assessed using purified proteins by *in vitro* pull-down assays.

Likewise, *in vitro* pull-down assays using proteins purified from insect cells showed a direct interaction between Aurora A phosphorylated GST-GTSE1 FL, untagged GTSE1 FL, GTSE1 1-460 and His-MCAK FL (Figure 16-19). The interaction between the FL GTSE1 and His-MCAK was dependent on Aurora A phosphorylation (Figure 16B, C; Figure 17). We saw a phosphorylation independent weak interaction between the N-terminus of GTSE1 (1-460) and MCAK in pull-downs; however, it is plausible this interaction is very weak, therefore, it is difficult to consistently detect it by SEC (Figure 16A; Figure 18). However, GTSE1 1-460 phosphorylated by Aurora A showed a strong interaction with MCAK (Figure 18).

Irrespective of phosphorylation by Aurora A, the C-terminus of GTSE1 (381-739) did not show an interaction with MCAK (Figure 19). Mass spectrometric analysis of GTSE1 during different phases of the cell cycle showed that Aurora A phosphorylates GTSE1 at several sites during mitosis and G2 phase (our unpublished data). The N-terminus of GTSE1 is especially, heavily phosphorylated by Aurora A *in vitro* at several canonical and non-canonical Aurora A phosphorylation sites, which further strengthens our results (our unpublished data).

GTSE1 is an intrinsically disordered protein and we speculate that GTSE1 might display intra-molecular interactions as it shows local patches of positively and negatively charged amino acids. It has been shown in previous studies that phosphorylation of intrinsically disordered proteins can stabilize or destabilize its native structure and radically influence its cellular function (Bah and Forman-Kay, 2016). As GTSE1 is highly phosphorylated during mitosis, we think that phosphorylation might impart a global negative charge on GTSE1, inhibiting long-range and short-range intra-molecular contacts. It is also plausible that in addition to destabilizing intra-molecular interactions, phosphorylation of GTSE1 elicits stabilization of a new secondary structure that leads to formation of a novel MCAK binding motif. Previous reports indicate the importance of phosphorylation-dependent interactions and the evolution of structural motifs that interact specifically with phosphorylated amino acid residues (Bah and Forman-Kay, 2016; Jin and Pawson, 2012). This might explain the requirement of phosphorylation on FL GTSE1 for binding directly to MCAK. On the other hand, the MCAK binding site must be exposed in non-phosphorylated GTSE1 1-460 allowing a weak interaction with MCAK, which gets further strengthened upon phosphorylation. Our findings indicate that MCAK directly interacts with the N-terminal domain of GTSE1 and this interaction is dependent on Aurora A phosphorylation. We could test the above stated hypothesis by first checking for intra-molecular GTSE1 interaction pre- and post-Aurora A phosphorylation by preforming *in vitro* pull-downs using GTSE1 fragments. Secondly, we could try to determine the structure of GTSE1 before and after phosphorylation by Aurora A using NMR (Eliezer, 2006; Goda et al., 2015).

4.4 Potential mechanisms: How GTSE1 inhibits MCAK's depolymerase activity

Our *in vitro* and *in vivo* studies demonstrate that GTSE1 inhibits MCAK's depolymerase activity. Furthermore, we were able to demonstrate a direct interaction between GTSE1 FL and MCAK FL in an Aurora A phosphorylation dependent manner. However, our TIRF and

sedimentation assays illustrate an inhibition of MCAK's depolymerase activity by GTSE1 where both proteins were purified from insect cells and were not pre-phosphorylated by any kinase. This raises the question – how does GTSE1 inhibit MCAK's depolymerase activity if their interaction is phosphorylation dependent? We observed that GTSE1 directly binds to MTs and partly stabilizes them (Figure 20D and our unpublished data). Thus, it is possible that in our TIRF and sedimentation assays, GTSE1 might be directly binding to GMPCPP or taxol stabilized MTs thus, preventing binding of MCAK to MTs as well as depolymerization of MTs. We predict that GTSE1 might have a higher affinity for GTP bound tubulin as we observed a strong binding of GTSE1 to GMPCPP seeds as compared to dynamic MTs in a previous assay (our unpublished data). Furthermore, we have evidence that there is less MCAK bound to MTs in the presence of GTSE1 in our *in vitro* TIRF and sedimentation assays (our unpublished data). GMPCPP and taxol stabilized MTs do not represent a physiological state in cells, therefore it is important to study the antagonistic relationship between GTSE1 and MCAK *in vitro* using dynamic MTs. Additionally as GTSE1 has higher affinity for stable MTs, it would be fascinating to check if amounts of GTSE1 recruited to MTs is increased in cells treated with taxol.

It is important to note that in our *in vitro* TIRF and sedimentation assays, GTSE1 might bind directly to MTs. However in cells during mitosis, GTSE1 does not show direct interaction with MTs but is recruited to spindle MTs via the TACC3-Ch-Tog-Clathrin complex (Scolz et al., 2012; Hubner et al., 2010 and our unpublished data). Preliminary *in vitro* and *in vivo* analyses demonstrate that hyper-phosphorylation of GTSE1 by Aurora A and Cdk1 in mitosis impairs GTSE1's binding to MTs (Scolz et al., 2012 and our unpublished data). We have also shown that GTSE1, when phosphorylated by Aurora A, binds directly to MCAK *in vitro*. Mass spectrometric analysis of GTSE1 immunoprecipitated from cells also revealed a number of phosphosites on GTSE1 corresponding to Cdk1 and Aurora A canonical and non-canonical sites (our unpublished data). Therefore, a reasonable assumption would be that Aurora A phosphorylated GTSE1 binds to and inhibits MCAK's depolymerase activity in cells as well. A possible conjecture could be that GTSE1 maintains its function of inhibiting MCAK during interphase and mitosis; during interphase, minimally phosphorylated GTSE1 binds directly to MTs and MT plus ends where it might inhibit MCAK's depolymerizing activity (Figure 25), however, as the cell enters into mitosis, hyper-phosphorylation of GTSE1 by Aurora A prevents its MT binding but enhances its binding to MCAK. GTSE1

localizes to spindle MTs and spindle poles through binding to TACC3-Ch-Tog-Clathrin complex and stabilizes MTs by directly interacting with MCAK and inhibiting its depolymerase activity thus, further facilitating formation of inter-KT MT bridges (Figure 25). Why cells have devised such a complex mode of inhibition of MCAK's depolymerase activity by GTSE1 across the cell cycle remains an open question. During mitosis, GTSE1 relocates from MT plus ends and MT lattice to spindle MTs through binding to TACC-Ch-Tog-Clathrin complex where it might play a crucial role in locally fine-tuning MT dynamics by inhibiting MCAK's depolymerase activity.

In cells, MCAK is a potent MT depolymerase and is precisely regulated in time and cellular space to maintain proper MT dynamics during mitosis. Several mechanisms involving phosphorylation of MCAK and intra-molecular interactions have been proposed to control and regulate MCAK's depolymerase cycle and activity (Braun et al., 2014; Domnitz et al., 2012; Rankin and Wordeman, 2010; Kline-Smith et al., 2004; Lan et al., 2004; Walczak et al., 2002; Maney et al., 1998). MCAK is a cell cycle regulated protein and is known to be phosphorylated by several mitotic kinases in the cell. Phosphorylation by Aurora A, Aurora B, and Cdk1 have been shown to inhibit MCAK's depolymerase activity, whereas, phosphorylation by Plk1 enhances it (Ritter et al., 2015b; Sanhaji et al., 2014; Shao et al., 2015; Zhang et al., 2011; Sanhaji et al., 2010; Zhang et al., 2008; Zhang et al., 2007; Ohi et al., 2004). Recently, it has been proposed that phosphorylation of MCAK by Aurora B in the neck domain triggers a conformational change that reduces MCAK's depolymerase activity *in vitro* (Zong et al., 2016; Talapatra et al., 2015; Ems-McClung et al., 2013). In solution and at MT ends, MCAK exists in a "closed" conformation where one of its C-terminal tails interacts with the interface between two motor domains (Talapatra et al., 2015; Ems-McClung et al., 2013). MCAK in its closed conformation is a potent MT depolymerase. Phosphorylation by Aurora B or interaction with the MT lattice elicits a release of the C-terminal tail and "opens" MCAK thus, diminishing its depolymerase activity (Talapatra et al., 2015; Ems-McClung et al., 2013). This transition between "closed" and "open" state is emerging as an important point for regulation of MCAK's depolymerase activity. It is fascinating to deliberate about this conformational change in the context of GTSE1 (Figure 25), as it opens up an avenue to test if and how GTSE1 affects this conformational change of MCAK. Förster Resonance energy transfer (FRET)-biosensors of MCAK (received from Claire Walczak, Ems-McClung Et al., 2013) will be used in combination with Fluorescence

Lifetime Imaging Microscopy (FLIM) to assess if GTSE1 binding stimulates a similar conformational change in MCAK.

Moreover, the depolymerase activity of MCAK is under the control of phosphorylation by different mitotic kinases (Ritter et al., 2015b; Sanhaji et al., 2014; Shao et al., 2015; Zhang et al., 2011; Sanhaji et al., 2010; Zhang et al., 2008; Zhang et al., 2007; Ohi et al., 2004). Our findings also show that Aurora A phosphorylated GTSE1 directly binds to MCAK. Another possible mode of inhibition is that GTSE1 antagonizes MCAK's depolymerase activity by directly binding to MCAK and stimulating a change in conformation such that the phosphosites become more accessible to mitotic kinases. Therefore, these kinases can easily phosphorylate MCAK and this inhibits its depolymerase activity. We can test this hypothesis by checking the phosphorylation status of MCAK in cells and *in vitro,* in the absence and presence of GTSE1. Furthermore, we could test this by performing *in vitro* TIRF and sedimentation assays using purified GTSE1 and MCAK proteins. If Aurora A phosphorylated GTSE1 already inhibits the depolymerase activity of non-phosphorylated MCAK, then it is likely that GTSE1 is antagonizing MCAK's activity via another mode of action.

Aurora A and Plk1 phosphorylate MCAK at S719, which modulates MCAK's conformation (Zong et al., 2016). In a recent report it has been shown that mutations (E715A/E716A or S719A) in the far C-terminus of MCAK, brings the C-terminus more closer to the N-terminus producing a more "closed" conformation (Zong et al., 2016). This conformation of MCAK leads to increased accumulation of MCAK at poles, negatively affecting MT growth and elongation at spindle poles (Zong et al., 2016). These mutations do not affect MCAK's depolymerase activity but lead to spindles with unfocused poles due to increased accumulation of MCAK at poles further causing abnormal MT dynamics. Interestingly, we observed an enrichment of MCAK on the mitotic spindle following depletion of GTSE1. Few spindles displayed detached poles after GTSE1 depletion, which could be attributed to increased activity of MCAK at poles. Thus, it is plausible that normally at poles Aurora A phosphorylated GTSE1 strongly binds to MCAK "opening" its conformation and inhibiting it's depolymerase activity.

Another interesting hypothesis is that a direct interaction between GTSE1 and MCAK alters MCAK's MT binding capacity. In a recent report, a kinesin binding protein (KBP) has been

discovered that interacts with the motor domain of a subset of kinesins and prevents their MT association (Kevenaar et al., 2016). It would be interesting to check whether GTSE1 physically sequesters MCAK away from the spindle and precludes its binding to MTs (Figure 25). These questions will be addressed by single molecule studies using fluorescently labeled proteins with a TIRF assay.

In order to answer how GTSE1 inhibits MCAK's depolymerase activity during mitosis, we plan to phosphorylate GTSE1 by Aurora A and perform sedimentation assays and TIRF analysis in presence and absence of MCAK. Furthermore, we want to narrow down the MCAK binding domain and the MT binding domain of GTSE1, and check if they are exclusive or if they overlap. In case they overlap, it would be fascinating to check if Aurora A mediates a GTSE1 phospho-switch that prevents GTSE1 from binding to MTs but enhances its binding to MCAK thus directly inhibiting its MT depolymerase activity during mitosis.

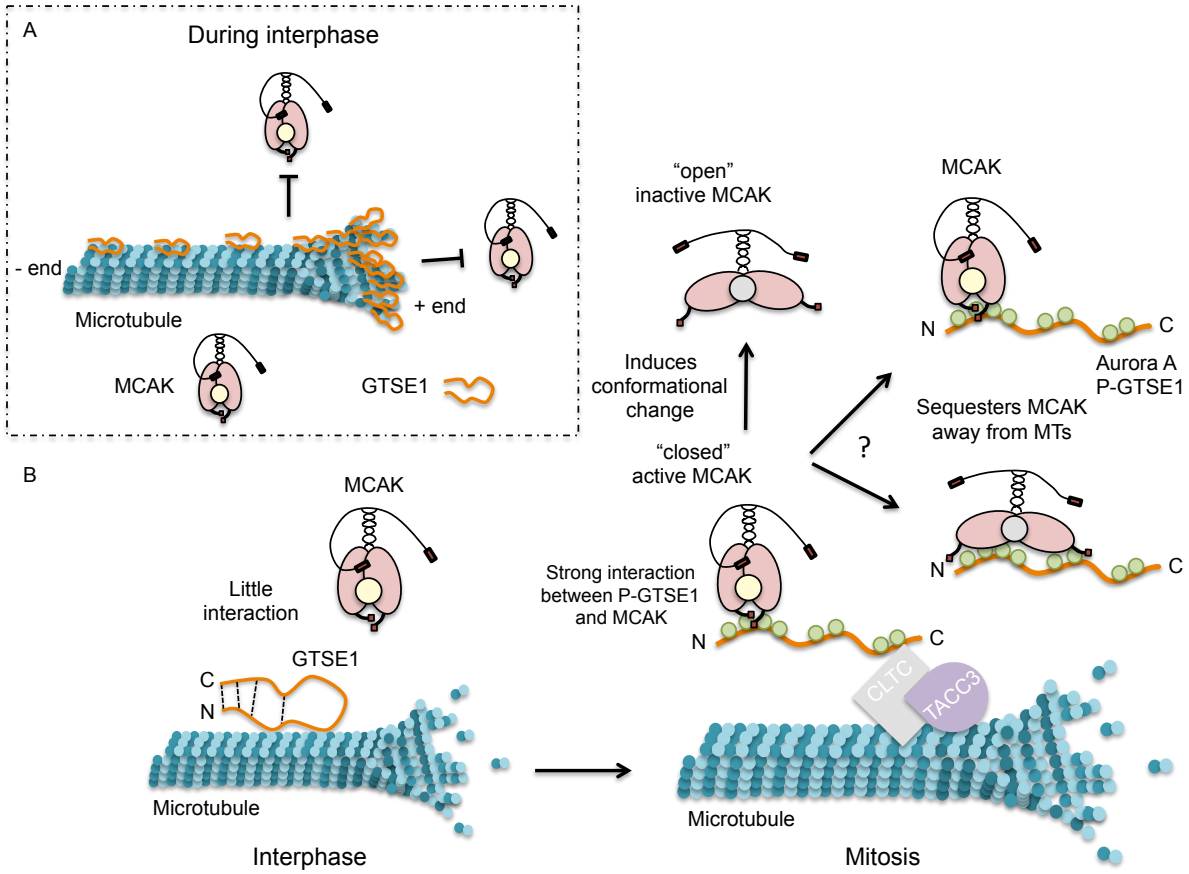

Figure 25. Hypothesis: How GTSE1 inhibits MCAK's depolymerase activity

A. Plausible mechanism by which GTSE1 inhibits MCAK's depolymerase activity during interphase.

According to our speculation, GTSE1 binds directly to MTs and hinders MCAK's 1D diffusion and binding to MTs lattice and plus ends, thus, reducing its potent depolymerase activity. **B.** Possible mechanism by which GTSE1 inhibits MCAK's depolymerase activity during mitosis. GTSE1 might show some long-range and short-range intra-molecular interactions during interphase. As the cell enters into mitosis, hyper-phosphorylation of GTSE1 by Aurora A might impart a global negative charge on GTSE1 preventing any intra-molecular interactions. Phosphorylation might facilitate new intra-molecular interactions leading to formation of a MCAK binding pocket. On the other hand, phosphorylation of GTSE1 might impede direct binding to MTs due to electrostatic repulsion but enhance indirect binding to MTs via interaction with the TACC3-Ch-Tog-Clathrin complex. GTSE1 might inhibit MCAK's depolymerase activity during mitosis by two possible mechanisms: first by directly binding to "closed active" MCAK and stimulating a change in its conformation to the "open" inactive form. Second could be by directly binding and sequestering either 'active closed' or 'inactive open' MCAK in the cytoplasm and preventing it from binding to MTs.

4.5 Does GTSE1 inhibit other kinesin-13 family members?

Kinesin-13 family consists of Kif2A, Kif2B and Kif2C/MCAK, which are potent MT depolymerases. Kinesin-13 family members share a highly conserved motor domain and diverse N-terminal domains. Interestingly, mass spectrometric analysis revealed an interaction of GTSE1 with Kif2A and Kif2C/MCAK. Kif2A localizes to spindle poles and is required for maintaining proper MT dynamics at spindle poles and for cytokinesis. Phenotypes observed after GTSE1 depletion during metaphase were not restored after co-depletion of Kif2A and GTSE1. Kif2A localizes to the spindle midzone during cytokinesis and controls MT length required for proper execution of cytokinesis (Uehara et al., 2013). Loss of GTSE1 in U2OS cells mimics the cytokinesis phenotypes seen after Kif2A RNAi. Therefore, it would be interesting to check if GTSE1 interacts with Kif2A, and recruits it to the spindle midzone, where it is required for proper execution of cytokinesis. It would be fascinating to perform *in vitro* assays to test the effect of GTSE1 on kinesin-13 family members.

4.6 Role of GTES1 in CIN

Several CIN cancer cell lines frequently mis-segregate chromosomes because of hyper-stable KT-MT attachments. These hyper-stable KT-MT attachments result in persistent merotely, where one of the sister KT attaches to MTs emanating from both spindle poles. Merotelic attachments escape SAC detection and cause chromosomes with merotelic attachments to lag behind at the spindle equator during anaphase while the remaining chromosomes are pulled

towards the pole (Gregan, et al., 2011; Thompson and Compton, 2011; Cimini and Degrassi, 2005; Cimini et al., 2001). Lagging chromosomes generally end up in the right daughter cells as micronuclei and are considered as an indirect readout for hyper-stable KT-MT attachments (Huang et al., 2012; Thompson and Compton, 2011). There is clear evidence that impaired regulation of KT-MT attachments during mitosis is the underlying cause of aneuploidy and CIN, however, the molecular mechanisms responsible for MT stabilization in cancer cells still remains elusive. Our data suggests that modulating levels of GTSE1 in cancer cell lines has an impact on chromosome segregation. Interestingly, expression level of GTSE1 highly correlates with MCAK level in different tissues and cell lines (http://coxpresdb.jp/data/gene/51512.shtml). It has been shown that artificially increasing MCAK's activity by overexpression in highly CIN cancer cell lines like U2OS and Hela, suppresses lagging chromosomes and CIN (Bakhoum et al., 2009a, Bakhoum et al., 2009b). However, MCAK levels are generally not found to be down regulated in cancer cell lines and tumors (Sanhaji et al., 2011; Bakhoum et al., 2009a). GTSE1 is found overexpressed in several cancer cell lines and solid tumors (Scolz et al., 2012). We propose that GTSE1 might drive CIN through hyper-stabilization of KT-MT attachments by inhibiting MCAK's depolymerase activity. It is also a possible conjecture that overexpression of GTSE1 affects the expression levels of other SAC proteins or other protein complexes involved in modulating MT dynamics as stimulation of CIN in cancer cells is most likely due to complex changes in the expression pattern of multiple genes rather than just one gene (Thiru et al., 2014).

In a recent large-scale genome sequencing study, it was reported that genes encoding mitotic-specific proteins did not frequently display mutations (Orr and Compton, 2013). Instead, proteins that belong to core oncogenic signaling pathways that control cell cycle and apoptosis were frequently found mutated (Orr and Compton, 2013). This study revealed a concrete connection between mitosis and oncogenic signaling pathways, implying that misregulation of oncogenic pathways leads to abnormal cell cycle regulation and faulty mitosis to generate CIN (Orr and Compton, 2013). Misregulation of the DNA damage pathway due to loss of p53 results in tolerance and propagation of aneuploid genomes and CIN (Thompson and Compton, 2010; Bunz et al., 2002). Interestingly, GTSE1 interacts with p53 and down-regulates p53 levels, further inhibiting the p53-dependent apoptotic response upon overexpression (Monte et al., 2004; Monte et al., 2003). Therefore, we speculate that

overexpression of GTSE1 could induce CIN by simultaneously down-regulating p53-dependent apoptotic pathways and increasing the occurrence of chromosome mis-segregation. p53 also functions as a transcriptional activator and reports suggests that p53 controls the expression of several mitosis specific genes like GTSE1, Aurora kinase A, Foxm1, Plk2 and Plk4 (Kurinna et al., 2013; Collavin et al., 2000; Utrera et al., 1998). Several gain of function mutations that stabilize p53 have been described to induce genome instability (Peng et al., 2001; Gualberto et al., 1998). Mutated p53 is found overexpressed in several cancers and solid tumors (Eliyahu et al., 1984; Jenkins et al., 1984; Parada et al., 1984). One of the possibilities could be that over-expression of p53 leads to up-regulation of Aurora A and GTSE1, which increases the incidence of chromosome mis-segregation and CIN.

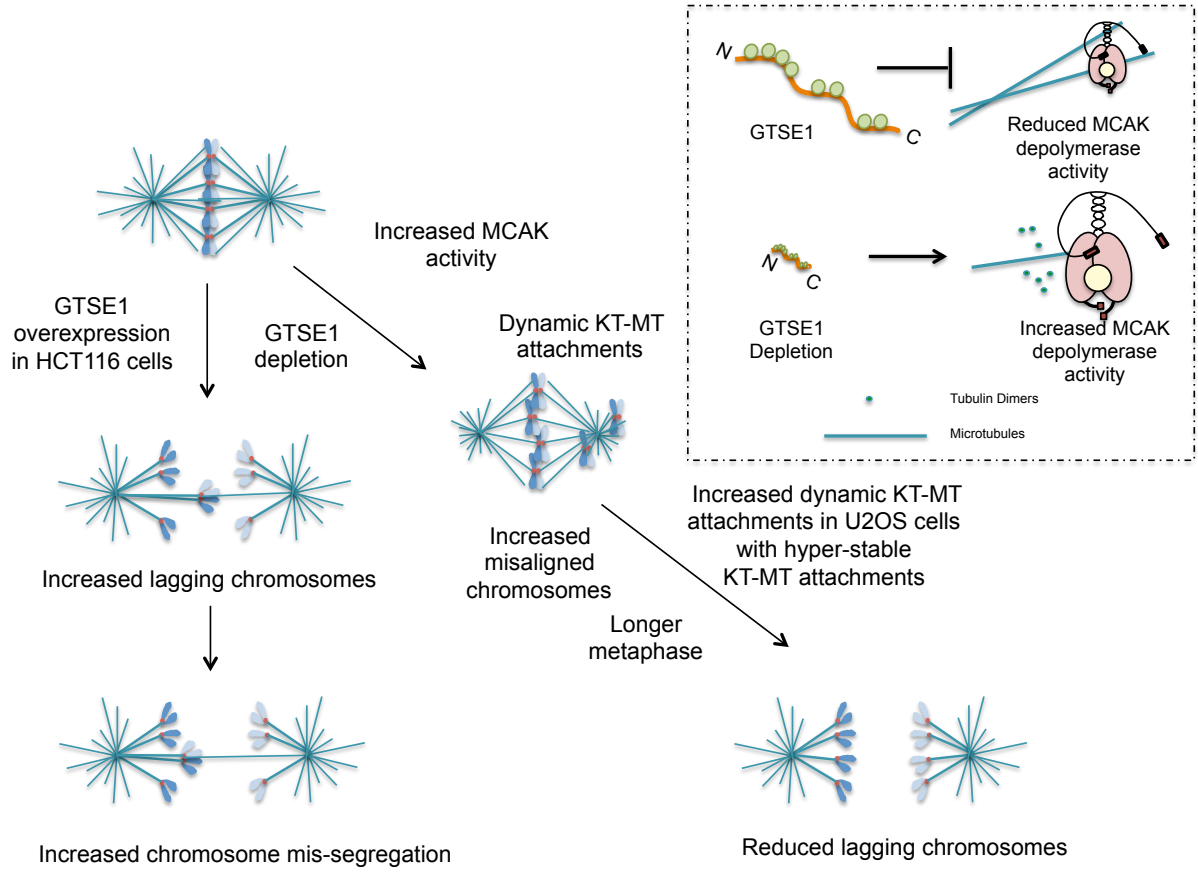

Figure 26. Role of GTSE1 in mitosis

GTSE1 plays a crucial role in maintaining MT stability, chromosome alignment and segregation during mitosis by antagonizing MCAK's depolymerase activity. In cells, GTSE1 inhibits MCAK's depolymerase activity and depletion of GTSE1 leads to hyper-activity of MCAK. Loss of GTSE1 in CIN U2OS cells, which overexpresses GTSE1, causes shorter astral MTs and misalignment of chromosomes. These cells take longer in metaphase but undergo anaphase onset only when all the

chromosomes are aligned. Hyper-activity of MCAK following loss of GTSE1 creates dynamic KT-MT attachments in the U2OS cells that normally have hyper-stable KT-MT attachments. This facilitates correction of KT-MT mal-attachments reducing the frequency of lagging chromosomes and chromosome mis-segregation. On the contrary, overexpression of GTSE1 in diploid HCT116 cells increases mis-segregation of chromosomes causing aneuploidy.

Aurora A is an oncogene found overexpressed in several cancers and drives tumorigenesis (D'Assoro et al., 2015; Carter et al., 2006). Our work predicts that GTSE1 might be a downstream effector in the Aurora A CIN-inducing pathway. It has recently been shown that Aurora A overexpression leads to an increase in the MT polymerization rates, which induces hyper-stabilization of KT MTs and CIN in colorectal cancer cells (Ertych et al., 2014). Aurora A phosphorylation is also required for formation and K-fiber localization of the TACC3-Ch-Tog–Clathrin complex. This complex forms a 'mesh' of inter-MT connections within KT MT bundles and is required for stabilizing KT MTs (Nixon et al., 2015; Hood et al., 2013; Booth et al., 2011). GTSE1 has been proposed to be a part of this complex (Nixon et al., 2015). As Aurora A phosphorylation is crucial for recruitment of this complex to the spindle, it would be interesting to test if more GTSE1 localizes to the spindle upon Aurora A overexpression. As GTSE1 acts downstream of Aurora A, we could test if overexpression of GTSE1 also increases the MT polymerization rates by inhibiting MCAK's depolymerase activity. We think that overexpression of Aurora A might recruit more GTSE1 along with TACC3-Ch-Tog-Clathrin complexes to the spindle thus, hyper stabilizing K-fibers via two pathways; first by physically linking and stabilizing K-fiber and second via direct inhibition of MCAK's depolymerase activity.

In this study, we could show that GTSE1 functions as a MT stabilizing protein during mitosis by inhibiting MCAK's depolymerase activity (Figure 26). GTSE1 is important for elongation of astral MTs from centrosomes and for stabilizing KT MTs. Through regulation of MT stability by inhibiting the depolymerase activity of MCAK, GTSE1 controls proper chromosome alignment at metaphase and accurate segregation of chromosomes during anaphase. Increasing GTSE1 protein levels in diploid cells affects MT stability, which results in mis-segregation of chromosome, further inducing CIN. Furthermore, we could show that GTSE1 antagonizes MCAK's depolymerase activity *in vitro,* and these proteins directly interact in a phospho-dependent manner in cells and *in vitro*. In the future, it would be important to elucidate the exact molecular mechanism by which GTSE1 directly antagonizes

MCAK's activity *in vitro*. Understanding the mode of action of these proteins during mitosis might showcase new molecular mechanisms that proteins use to fine-tune important biological processes like cell division.

5. Summary

Chromosome segregation and genome stability are dependent on cellular regulation of microtubule (MT) dynamics. The precise regulation of MT dynamics during mitosis is essential to facilitate both kinetochore-microtubule (KT-MT) attachments, required for proper alignment of chromosomes, and error correction of KT-MT mal-attachments, required for accurate segregation of chromosomes. Increased chromosome segregation errors and elevated chromosomal instability (CIN) has been reported in cancer cells with hyper-stable KT-MT dynamics. In this thesis, we show that GTSE1, a protein found overexpressed in several cancer cell lines and tumours, stabilizes MTs required for proper chromosome alignment and chromosome segregation. GTSE1 associates with centrosomes, spindle MTs, and reducing GTSE1 protein levels in cells leads to a loss of astral MTs and a decrease in KT MT stability, which causes defects in spindle orientation and chromosome alignment, respectively. GTSE1 maintains precise levels of MT stability required for proper spindle orientation and chromosome alignment by antagonizing the MT-destabilizing activity of the MT depolymerase MCAK. GTSE1 antagonizes MCAK's depolymerase activity *in vitro,* and these proteins directly interact in a phospho-dependent manner in cells and *in vitro.* We show that reducing the abnormally high levels of GTSE1 in the highly CIN U2OS and Hela Kyoto cancer cell lines reduces the frequency of chromosome mis-segregation events in a MCAK-dependent manner. Conversely, artificially elevating GTSE1 protein levels in chromosomally stable cell lines leads to an increase in chromosome mis-segregation and CIN. Thus, GTSE1 promotes genome stability by controlling the precise MT dynamics required for the efficient alignment and segregation of chromosomes through antagonizing MCAK's MT depolymerase activity.

6. Zusammenfassung

Die Trennung der Chromosomen und die Stabilität des Genoms hängen von der zellulären Regulation der Mikrotubuli-Dynamik ab. Die präzise Regulation der Mikrotubuli-Dynamik während der Zellteilung ist essentiell um die Anheftung der Mikrotubuli an die Kinetochore zu gewährleisten. Sie ist Voraussetzung für die richtige Anordnung der Chromosomen, für die Korrektur von fehlerhaften Kinetochor-Mikrotubuli-Verbindungen sowie Bedingung für die richtige Verteilung der Chromosomen. In Krebszellen mit hyperstabilen Kinetochor-Mikrotubuli-Dynamiken treten häufiger Fehler bei der Verteilung der Chromosomen und eine erhöhte chromosomale Instabilität (CIN) auf.

In dieser Arbeit wurde gezeigt, dass GTSE1, ein Protein, das in mehreren Krebszelllinien und Tumoren überexprimiert ist, Mikrotubuli stabiliert. Dies ist wiederum eine Voraussetzung für die richtige Anordnung und Verteilung der Chromosomen. GTSE1 bindet an Zentrosomen und Spindel-Mikrotubuli. Eine Reduktion des Proteinlevels von GTSE1 in Zellen führt zu einem Verlust der Astral-Mikrotubuli und einer verminderten Stabilität der Kinetochor-Mikrotubuli, wodurch Fehler bei der Orientierung der Spindel und der Anordnung der Chromosomen auftreten. GTSE1 hält die Stabilität der Mikrotubuli auf einem präzisen Level, indem es der Mikrotubuli-destabilisierenden Aktivität der Mikrotubuli-Depolymerase MCAK entgegenwirkt, als Voraussetzung für die richtige Orientierung der Spindel und die Anordnung der Chromosomen. Aufgereinigtes GTSE1 bindet *in vitro* direkt an MCAK und hemmt dessen Depolymeraseaktivität. Ferner wurde in dieser Arbeit gezeigt, dass eine Reduktion der ungewöhnlich hohen GTSE1 Levels in den Krebszelllinien U2OS und Hela Kyoto, die eine hohe chromosomale Instabilität zeigen, die Häufigkeit der Fehlverteilung von Chromosomen senkt und dass dies in Abhängigkeit von MCAK geschieht. Im Gegensatz dazu bewirkt die künstliche Erhöhung der GTSE1 Levels in chromosomal stabilen Zelllinien eine vermehrte Fehlverteilung von Chromosomen und chromosomale Instabilität. Folglich kontrolliert GTSE1 die präzise Mikrotubuli-Dynamik indem es der Mikrotubuli-Depolymeraseaktivität von MCAK entgegenwirkt und fördert somit die Stabilität des Genoms. Dies ist Voraussetzung für die erfolgreiche Anordnung und Verteilung der Chromosomen.

Bibliography

Akhmanova, A., & Steinmetz, M. O. (2015). Control of microtubule organization and dynamics: two ends in the limelight. *Nature reviews Molecular cell biology*. 16, 711–726.

Akhmanova, A., & Steinmetz, M. O. (2008). Tracking the ends: a dynamic protein network controls the fate of microtubule tips. *Nature reviews Molecular cell biology*, *9*(4), 309-322.

Alberts, B., Johnson, A., Lewis, J., Raff, M., Roberts, K., & Walter, P. (2002). Molecular biology of the cell. new york: Garland science; 2002. *Classic textbook now in its 5th Edition*.

Allen, C., & Borisy, G. G. (1974). Structural polarity and directional growth of microtubules of Chlamydomonas flagella. *Journal of molecular biology*, *90*(2), 381IN47387-386IN55402.

Amos, L. A., & Klug, A. (1974). Arrangement of subunits in flagellar microtubules. *Journal of cell science*, *14*(3), 523-549.

Andrews, P. D., Ovechkina, Y., Morrice, N., Wagenbach, M., Duncan, K., Wordeman, L., & Swedlow, J. R. (2004). Aurora B regulates MCAK at the mitotic centromere. *Developmental cell*, *6*(2), 253-268.

Asenjo, A. B., Chatterjee, C., Tan, D., DePaoli, V., Rice, W. J., Diaz-Avalos, R., Silvestry, M., & Sosa, H. (2013). Structural model for tubulin recognition and deformation by kinesin-13 microtubule depolymerases. *Cell reports*, *3*(3), 759-768.

Bah, A., & Forman-Kay, J. D. (2016). Modulation of intrinsically disordered protein function by post-translational modifications. *Journal of Biological Chemistry*, *291*(13), 6696-6705.

Bakhoum, S. F., Thompson, S. L., Manning, A. L., & Compton, D. A. (2009a). Genome stability is ensured by temporal control of kinetochore–microtubule dynamics. *Nature cell biology*, *11*(1), 27-35.

Bakhoum, S. F., Genovese, G., & Compton, D. A. (2009b). Deviant kinetochore microtubule dynamics underlie chromosomal instability. *Current Biology*, *19*(22), 1937-1942.

Barr, A. R., & Gergely, F. (2008). MCAK-independent functions of ch-Tog/XMAP215 in microtubule plus-end dynamics. *Molecular and cellular biology*, *28*(23), 7199-7211.

Basilico, F., Maffini, S., Weir, J. R., Prumbaum, D., Rojas, A. M., Zimniak, T., De Antoni, A., Jeganathan, S., Voss, B., Van Gerwen, S. Krenn, V. Massimiliano, L., Valencia, A., Vetter I. R., Herzog, F., Raunser, S., Pasqualato, S., & Andrea Musacchio (2014). The pseudo GTPase CENP-M drives human kinetochore assembly. *Elife*, *3*, e02978.

Bechstedt, S., & Brouhard, G. J. (2012). Doublecortin recognizes the 13-protofilament microtubule cooperatively and tracks microtubule ends. *Developmental cell*, *23*(1), 181-192.

Bendre, S., Rondelet, A., Hall, C., Schmidt, N., Lin, Y. C., Brouhard, G. J., & Bird, A. W. (2016). GTSE1 tunes microtubule stability for chromosome alignment and segregation by inhibiting the microtubule depolymerase MCAK. *The Journal of cell biology, 215(5)*, 631-647.

Bhat, K. M., & Setaluri, V. (2007). Microtubule-associated proteins as targets in cancer chemotherapy. *Clinical Cancer Research*, *13*(10), 2849-2854.

Bieling, P., Laan, L., Schek, H., Munteanu, E. L., Sandblad, L., Dogterom, M., Brunner, D., & Surrey, T. (2007). Reconstitution of a microtubule plus-end tracking system in vitro. *Nature*, *450*(7172), 1100-1105.

Bird, A. W., & Hyman, A. A. (2008). Building a spindle of the correct length in human cells requires the interaction between TPX2 and Aurora A. *The Journal of cell biology*, *182*(2), 289-300.

Bird, A.W., Erler, A., Fu, J., Hériché, J.K., Maresca, M., Zhang, Y., Hyman, A.A. and Stewart, A.F. (2011). High-efficiency counterselection recombineering for site-directed mutagenesis in bacterial artificial chromosomes. *Nature methods*, *9*(1), 103-109.

Booth, D. G., Hood, F. E., Prior, I. A., & Royle, S. J. (2011). A TACC3/ch-TOG/clathrin complex stabilises kinetochore fibres by inter-microtubule bridging. *The EMBO Journal*, *30*(5), 906-919.

Boveri, T. (1902). Über mehrpolige mitosen als mittel zur analyse des zellkerns. *Verh. Phys. Med. Ges. Würzburg,* 35, 67–90

Boveri, T. (1914) In Zur Frage der Entstehung Maligner Tumoren. (Gustav Fischer, Jena), 1–64.

Braise, M., Aguiar, P., Geley, S., & Maiato, H. (2014). Kinetochore motors drive congression of peripheral polar chromosomes by overcoming random arm-ejection forces. *Nature cell biology*, *16*(12), 1249-1256.

Braun, A., Dang, K., Buslig, F., Baird, M. A., Davidson, M. W., Waterman, C. M., & Myers, K. A. (2014). Rac1 and Aurora A regulate MCAK to polarize microtubule growth in migrating endothelial cells. *J Cell Biol*, *206*(1), 97-112.

Brinkman, E. K., Chen, T., Amendola, M., & van Steensel, B. (2014). Easy quantitative assessment of genome editing by sequence trace decomposition. *Nucleic acids research*, *42*(22), e168-e168.

Brooker, A. S., & Berkowitz, K. M. (2014). The roles of cohesins in mitosis, meiosis, and human health and disease. *Cell Cycle Control: Mechanisms and Protocols*, 229-266.

Brouhard, G. J., Stear, J. H., Noetzel, T. L., Al-Bassam, J., Kinoshita, K., Harrison, S. C., Howard, J. & Hyman, A. A. (2008). XMAP215 is a processive microtubule polymerase. *Cell*, *132*(1), 79-88.

Bunz, F., Fauth, C., Speicher, M.R., Dutriaux, A., Sedivy, J.M., Kinzler, K.W., Vogelstein, B. and Lengauer, C. (2002). Targeted inactivation of p53 in human cells does not result in aneuploidy. *Cancer research*, *62*(4), 1129-1133.

Burns, K. M., Wagenbach, M., Wordeman, L., & Schriemer, D. C. (2014). Nucleotide exchange in dimeric MCAK induces longitudinal and lateral stress at microtubule ends to support depolymerization. *Structure*, *22*(8), 1173-1183.

Burrell, R.A., McClelland, S.E., Endesfelder, D., Groth, P., Weller, M.C., Shaikh, N., Domingo, E., Kanu, N., Dewhurst, S.M., Gronroos, E. and Chew, S.K. (2013). Replication stress links structural and numerical cancer chromosomal instability. *Nature*, *494*(7438), 492-496.

Cai, S., O'Connell, C. B., Khodjakov, A., & Walczak, C. E. (2009). Chromosome Congression in the Absence of K-Fibres. *Nature Cell Biology*, *11*(7), 832–838. http://doi.org/10.1038/ncb1890

Carmena, M., & Earnshaw, W. C. (2003). The cellular geography of aurora kinases. *Nature reviews Molecular cell biology*, *4*(11), 842-854.

Carter, S. L., Eklund, A. C., Kohane, I. S., Harris, L. N., & Szallasi, Z. (2006). A signature of chromosomal instability inferred from gene expression profiles predicts clinical outcome in multiple human cancers. *Nature genetics*, *38*(9), 1043-1048.

Cassimeris, L., & Morabito, J. (2004). TOGp, the human homolog of XMAP215/Dis1, is required for centrosome integrity, spindle pole organization, and bipolar spindle assembly. *Molecular biology of the cell*, *15*(4), 1580-1590.

Cassimeris, L., Becker, B., & Carney, B. (2009). TOGp regulates microtubule assembly and density during mitosis and contributes to chromosome directional instability. *Cell motility and the cytoskeleton*, *66*(8), 535-545.

Castoldi, M., & Popov, A. V. (2003). Purification of brain tubulin through two cycles of polymerization–depolymerization in a high-molarity buffer. *Protein expression and purification*, *32*(1), 83-88.

Cheeseman, L. P., Booth, D. G., Hood, F. E., Prior, I. A., & Royle, S. J. (2011). Aurora A kinase activity is required for localization of TACC3/ch-TOG/clathrin inter-microtubule bridges. *Communicative & integrative biology*, *4*(4), 409-412.

Cheeseman, I. M., & Desai, A. (2008). Molecular architecture of the kinetochore–microtubule interface. *Nature reviews Molecular cell biology*, *9*(1), 33-46.

Cheeseman, L. P., Harry, E. F., McAinsh, A. D., Prior, I. A., & Royle, S. J. (2013). Specific removal of TACC3–ch-TOG–clathrin at metaphase deregulates kinetochore fiber tension. *J Cell Sci*, *126*(9), 2102-2113.

Cimini, D., Howell, B., Maddox, P., Khodjakov, A., Degrassi, F., & Salmon, E. D. (2001). Merotelic kinetochore orientation is a major mechanism of aneuploidy in mitotic mammalian tissue cells. *The Journal of cell biology*, *153*(3), 517-528.

Cimini, D., & Degrassi, F. (2005). Aneuploidy: a matter of bad connections. *Trends in cell biology*, *15*(8), 442-451.

Cimini, D., Wan, X., Hirel, C. B., & Salmon, E. D. (2006). Aurora kinase promotes turnover of kinetochore microtubules to reduce chromosome segregation errors. *Current Biology*, *16*(17), 1711-1718.

Cimini, D., Moree, B., Canman, J. C., & Salmon, E. D. (2003). Merotelic kinetochore orientation occurs frequently during early mitosis in mammalian tissue cells and error correction is achieved by two different mechanisms. *Journal of cell science*, *116*(20), 4213-4225.

Collavin, L., Monte, M., Verardo, R., Pfleger, C., & Schneider, C. (2000). Cell-cycle regulation of the p53-inducible gene B99. *FEBS letters*, *481*(1), 57-62.

Compton, D. A. (2011). Mechanisms of aneuploidy. *Current opinion in cell biology*, *23*(1), 109-113.

Cong, L., Ran, F. A., Cox, D., Lin, S., Barretto, R., Habib, N., ... & Zhang, F. (2013). Multiplex genome engineering using CRISPR/Cas systems. *Science*, *339*(6121), 819-823.

Cross, M. K., & Powers, M. A. (2011). Nup98 regulates bipolar spindle assembly through association with microtubules and opposition of MCAK. *Molecular biology of the cell*, *22*(5), 661-672.

Cross, R. A., & McAinsh, A. (2014). Prime movers: the mechanochemistry of mitotic kinesins. *Nature reviews Molecular cell biology*, *15*(4), 257-271.

D'Assoro, A. B., Haddad, T., & Galanis, E. (2015). Aurora-A kinase as a promising therapeutic target in cancer. *Frontiers in oncology*, *5*.

David-Pfeuty, T., Erickson, H. P., & Pantaloni, D. (1977). Guanosinetriphosphatase activity of tubulin associated with microtubule assembly. *Proceedings of the National Academy of Sciences*, *74*(12), 5372-5376.

De Koninck, M., & Losada, A. (2016). Cohesin Mutations in Cancer. *Cold Spring Harbor Perspectives in Medicine*, a026476.

DeLuca, J. G., Dong, Y., Hergert, P., Strauss, J., Hickey, J. M., Salmon, E. D., & McEwen, B. F. (2005). Hec1 and Nuf2 Are Core Components of the Kinetochore Outer Plate Essential for Organizing Microtubule Attachment Sites. *Molecular Biology of the Cell*, *16*(2), 519–531.

DeLuca, M., Brunetto, L., Asteriti, I. A., Giubettini, M., Lavia, P., & Guarguaglini, G. (2008). Aurora-A and ch-TOG act in a common pathway in control of spindle pole integrity. *Oncogene*, *27*(51), 6539-6549.

Desai, A., & Mitchison, T. J. (1997). Microtubule polymerization dynamics. *Annual review of cell and developmental biology*, *13*(1), 83-117.

di Pietro, F., Echard, A., & Morin, X. (2016). Regulation of mitotic spindle orientation: an integrated view. *EMBO reports*, e201642292.

Domnitz, S. B., Wagenbach, M., Decarreau, J., & Wordeman, L. (2012). MCAK activity at microtubule tips regulates spindle microtubule length to promote robust kinetochore attachment. *J Cell Biol*, *197*(2), 231-237.

Dong, Y., VandenBeldt, K. J., Meng, X., Khodjakov, A., & McEwen, B. F. (2007). The outer plate in vertebrate kinetochores is a flexible network with multiple microtubule interactions. *Nature Cell Biology*, *9*(5), 516–522. http://doi.org/10.1038/ncb1576

Duellberg, C., Cade, N. I., Holmes, D., & Surrey, T. (2016). The size of the EB cap determines instantaneous microtubule stability. *Elife*, *5*, e13470.

Duijf, P. H. G., & Benezra, R. (2013). The cancer biology of whole-chromosome instability. *Oncogene*, *32*(40), 4727-4736.

Eliezer, D. (2006). Characterizing residual structure in disordered protein states using nuclear magnetic resonance. *Protein Folding Protocols*, 49-67.

Eliyahu, D., Raz, A., Gruss, P., Givol, D., & Oren, M. (1984). Participation of p 53 cellular tumour antigen in transformation of normal embryonic cells. *Nature*, *312*(5995), 646-649.

Ems-McClung, S. C., Hertzer, K. M., Zhang, X., Miller, M. W., & Walczak, C. E. (2007). The interplay of the N-and C-terminal domains of MCAK control microtubule depolymerization activity and spindle assembly. *Molecular biology of the cell*, *18*(1), 282-294.

Ems-McClung, S. C., Hainline, S. G., Devare, J., Zong, H., Cai, S., Carnes, S. K., Shaw, S.L. & Walczak, C. E. (2013). Aurora B inhibits MCAK activity through a phosphoconformational switch that reduces microtubule association. *Current Biology*, *23*(24), 2491-2499.

Ertych, N., Stolz, A., Stenzinger, A., Weichert, W., Kaulfuß, S., Burfeind, P., Aigner, A., & Bastians, H. (2014). Increased microtubule assembly rates influence chromosomal instability in colorectal cancer cells. *Nature cell biology*, *16*(8), 779-791.

Evans, T., Rosenthal, E. T., Youngblom, J., Distel, D., & Hunt, T. (1983). Cyclin: a protein specified by maternal mRNA in sea urchin eggs that is destroyed at each cleavage division. *Cell*, *33*(2), 389-396.

Eyers, P. A., Erikson, E., Chen, L. G., & Maller, J. L. (2003). A novel mechanism for activation of the protein kinase Aurora A. *Current Biology*, *13*(8), 691-697.

Flemming, W. (1882). Zellsubstanz, Kern und Zelltheilung (F. C. W. Vogel, Leipzig).

Foley, E. A., & Kapoor, T. M. (2013). Microtubule attachment and spindle assembly checkpoint signalling at the kinetochore. *Nature reviews Molecular cell biology*, *14*(1), 25-37.

Foltz, D. R., Jansen, L. E., Black, B. E., Bailey, A. O., Yates, J. R., & Cleveland, D. W. (2006). The human CENP-A centromeric nucleosome-associated complex. *Nature cell biology*, *8*(5), 458-469.

Foraker, A. B., Camus, S. M., Evans, T. M., Majeed, S. R., Chen, C. Y., Taner, S. B., Corrêa, I.R., Doxsey, S.J. & Brodsky, F. M. (2012). Clathrin promotes centrosome integrity in early mitosis through stabilization of centrosomal ch-TOG. *J Cell Biol*, *198*(4), 591-605.

Friel, C. T., & Howard, J. (2011). The kinesin-13 MCAK has an unconventional ATPase cycle adapted for microtubule depolymerization. *The EMBO journal*, *30*(19), 3928-3939.

Gaetz, J., & Kapoor, T. M. (2004). Dynein/dynactin regulate metaphase spindle length by targeting depolymerizing activities to spindle poles. *The Journal of cell biology*, *166*(4), 465-471.

Ganem, N. J., Upton, K., & Compton, D. A. (2005). Efficient mitosis in human cells lacking poleward microtubule flux. *Current biology*, *15*(20), 1827-1832.

Gell, C., V. Bormuth, G.J. Brouhard, D.N. Cohen, S. Diez, C.T. Friel, J. Helenius, B. Nitzsche, H. Petzold, J. Ribbe, E. Sch.ffer, J.H. Stear, A. Trushko, V. Varga, P.O. Widlund, M. Zanic, and J. Howard. (2010). Microtubule dynamics reconstituted in vitro and imaged by single-molecule fluorescence microscopy. *Methods Cell Biol. 95*, 221–245.

Gergely, F., Kidd, D., Jeffers, K., Wakefield, J. G., & Raff, J. W. (2000a). D-TACC: a novel centrosomal protein required for normal spindle function in the early Drosophila embryo. *The EMBO journal*, *19*(2), 241-252.

Gergely, F., Karlsson, C., Still, I., Cowell, J., Kilmartin, J., & Raff, J. W. (2000b). The TACC domain identifies a family of centrosomal proteins that can interact with microtubules. *Proceedings of the National Academy of Sciences*, *97*(26), 14352-14357.

Gergely, F., Draviam, V. M., & Raff, J. W. (2003). The ch-TOG/XMAP215 protein is essential for spindle pole organization in human somatic cells. *Genes & development*, *17*(3), 336-341.

Giam, M., & Rancati, G. (2015). Aneuploidy and chromosomal instability in cancer: a jackpot to chaos. *Cell division*, *10*(1), 3.

Gibson, D. G., Young, L., Chuang, R. Y., Venter, J. C., Hutchison, C. A., & Smith, H. O. (2009). Enzymatic assembly of DNA molecules up to several hundred kilobases. *Nature methods*, *6*(5), 343-345.

Goda, N., Shimizu, K., Kuwahara, Y., Tenno, T., Noguchi, T., Ikegami, T., Ota, M. and Hiroaki, H. (2015). A Method for Systematic Assessment of Intrinsically Disordered Protein Regions by NMR. *International journal of molecular sciences*, *16*(7), 15743-15760.

Good, M. C., Vahey, M. D., Skandarajah, A., Fletcher, D. A., & Heald, R. (2013). Cytoplasmic volume modulates spindle size during embryogenesis. *Science*, *342*(6160), 856-860.

Gregan, J., Polakova, S., Zhang, L., Tolić-Nørrelykke, I. M., & Cimini, D. (2011). Merotelic kinetochore attachment: causes and effects. *Trends in cell biology*, *21*(6), 374-381.

Gualberto, A., Aldape, K., Kozakiewicz, K., & Tlsty, T. D. (1998). An oncogenic form of p53 confers a dominant, gain-of-function phenotype that disrupts spindle checkpoint control. *Proceedings of the National Academy of Sciences*, *95*(9), 5166-5171.

Gutiérrez-Caballero, C., Burgess, S. G., Bayliss, R., & Royle, S. J. (2015). TACC3–ch-TOG track the growing tips of microtubules independently of clathrin and Aurora-A phosphorylation. *Biology open*, BIO201410843.

Hartwell, L. H., Culotti, J., & Reid, B. (1970). Genetic control of the cell-division cycle in yeast, I. Detection of mutants. *Proceedings of the National Academy of Sciences*, *66*(2), 352-359.

Hassold, T., & Hunt, P. (2001). To err (meiotically) is human: the genesis of human aneuploidy. *Nature Reviews Genetics*, *2*(4), 280-291.

Hauf, S., Cole, R. W., LaTerra, S., Zimmer, C., Schnapp, G., Walter, R., Heckel, A., Van Meel, J., Rieder, C.L. & Peters, J. M. (2003). The small molecule Hesperadin reveals a role for Aurora B in correcting kinetochore–microtubule attachment and in maintaining the spindle assembly checkpoint. *J Cell Biol*, *161*(2), 281-294.

Hégarat, N., Smith, E., Nayak, G., Takeda, S., Eyers, P. A., & Hochegger, H. (2011). Aurora A and Aurora B jointly coordinate chromosome segregation and anaphase microtubule dynamics. *J Cell Biol*, *195*(7), 1103-1113.

Helenius, J., Brouhard, G., Kalaidzidis, Y., Diez, S., & Howard, J. (2006). The depolymerizing kinesin MCAK uses lattice diffusion to rapidly target microtubule ends. *Nature*, *441*(7089), 115-119.

Hepler, P. K., McIntosh, J. R., & Cleland, S. (1970). Intermicrotubule bridges in mitotic spindle apparatus. *The Journal of Cell Biology*, *45*(2), 438.

Hill, V. K., Kim, J. S., & Waldman, T. (2016). Cohesin mutations in human cancer. *Biochimica et Biophysica Acta (BBA)-Reviews on Cancer*, *1866*(1), 1-11.

Hirokawa, N. (1998). Kinesin and dynein superfamily proteins and the mechanism of organelle transport. *Science*, *279*(5350), 519-526.

Hochegger, H., Hégarat, N., & Pereira-Leal, J. B. (2013). Aurora at the pole and equator: overlapping functions of Aurora kinases in the mitotic spindle. *Open biology*, *3*(3), 120185.

Holland, A. J., & Cleveland, D. W. (2009). Boveri revisited: chromosomal instability, aneuploidy and tumorigenesis. *Nature reviews Molecular cell biology*, *10*(7), 478-487.

Holmfeldt, P., Stenmark, S., & Gullberg, M. (2004). Differential functional interplay of TOGp/XMAP215 and the KinI kinesin MCAK during interphase and mitosis. *The EMBO journal*, *23*(3), 627-637.

Honnappa, S., Gouveia, S. M., Weisbrich, A., Damberger, F. F., Bhavesh, N. S., Jawhari, H., Grigoriev, I., van Rijssel, F.J., Buey, R.M., Lawera, A. & Jelesarov, I. (2009). An EB1-binding motif acts as a microtubule tip localization signal. *Cell*, *138*(2), 366-376.

Hood, E. A., Kettenbach, A. N., Gerber, S. A., & Compton, D. A. (2012). Plk1 regulates the kinesin-13 protein Kif2b to promote faithful chromosome segregation. *Molecular biology of the cell*, *23*(12), 2264-2274.

Hood, F. E., Williams, S. J., Burgess, S. G., Richards, M. W., Roth, D., Straube, A., Pfuhl, M., Bayliss, B., & Royle, S. J. (2013). Coordination of adjacent domains mediates TACC3–ch-TOG–clathrin assembly and mitotic spindle binding. *J Cell Biol*, *202*(3), 463-478.

Howard, J., & Hyman, A. A. (2003). Dynamics and mechanics of the microtubule plus end. *Nature*, *422*(6933), 753-758.

Howell, B. J., Moree, B., Farrar, E. M., Stewart, S., Fang, G., & Salmon, E. D. (2004). Spindle checkpoint protein dynamics at kinetochores in living cells. *Current biology*, *14*(11), 953-964.

Huang, Y., Jiang, L., Yi, Q., Lv, L., Wang, Z., Zhao, X., Zhong, L., Jiang, H., Rasool, S., Hao, Q,. & Guo, Z. (2012). Lagging chromosomes entrapped in micronuclei are not'lost'by cells. *Cell research*, *22*(5), 932.

Hubner, N.C., Bird, A.W., Cox, J., Splettstoesser, B., Bandilla, P., Poser, I., Hyman, A. and Mann, M. (2010). Quantitative proteomics combined with BAC TransgeneOmics reveals in vivo protein interactions. *The Journal of cell biology*, *189*(4), 739-754.

Hunter, A. W., Caplow, M., Coy, D. L., Hancock, W. O., Diez, S., Wordeman, L., & Howard, J. (2003). The kinesin-related protein MCAK is a microtubule depolymerase that forms an ATP-hydrolyzing complex at microtubule ends. *Molecular cell*, *11*(2), 445-457.

Hyman, A. A., & Karsenti, E. (1996). Morphogenetic properties of microtubules and mitotic spindle assembly. *Cell*, *84*(3), 401-410.

Indjeian, V. B., & Murray, A. W. (2007). Budding yeast mitotic chromosomes have an intrinsic bias to biorient on the spindle. *Current Biology*, *17*(21), 1837-1846.

Inoué, S., & Salmon, E. D. (1995). Force generation by microtubule assembly/disassembly in mitosis and related movements. *Molecular Biology of the Cell*, *6*(12), 1619-1640.

Janke, C., Ortiz, J., Lechner, J., Shevchenko, A., Shevchenko, A., Magiera, M. M., Schramm, C. & Schiebel, E. (2001). The budding yeast proteins Spc24p and Spc25p interact with

Ndc80p and Nuf2p at the kinetochore and are important for kinetochore clustering and checkpoint control. *The EMBO Journal*, *20*(4), 777-791.

Jenkins, J. R., Rudge, K., & Currie, G. A. (1984). Cellular immortalization by a cDNA clone encoding the transformation-associated phosphoprotein p53.
Jiang, K., Toedt, G., Gouveia, S. M., Davey, N. E., Hua, S., van der Vaart, B., Grigoriev, I., Larsen, J., Pedersen, L.B., Bezstarosti, K. & Lince-Faria, M. (2012). A Proteome-wide screen for mammalian SxIP motif-containing microtubule plus-end tracking proteins. *Current Biology*, *22*(19), 1800-1807.

Jin, J., & Pawson, T. (2012). Modular evolution of phosphorylation-based signalling systems. *Phil. Trans. R. Soc. B*, *367*(1602), 2540-2555.

Kabeche, L., & Compton, D. A. (2013). Cyclin A regulates kinetochore microtubules to promote faithful chromosome segregation. *Nature*, *502*(7469), 110-113.

Kapoor, T. M. (2017). Metaphase spindle assembly. *Biology*, *6*(1), 8.

Kevenaar, J. T., Bianchi, S., van Spronsen, M., Olieric, N., Lipka, J., Frias, C. P., Mikhaylova, M., Harterink, M., Keijzer, N., Wulf, P.S. & Hilbert, M. (2016). Kinesin-binding protein controls microtubule dynamics and cargo trafficking by regulating kinesin motor activity. *Current Biology*, *26*(7), 849-861.

Kinoshita, K., Noetzel, T. L., Pelletier, L., Mechtler, K., Drechsel, D. N., Schwager, A., Lee, M., Raff, J.W. & Hyman, A. A. (2005). Aurora A phosphorylation of TACC3/maskin is required for centrosome-dependent microtubule assembly in mitosis. *J Cell Biol*, *170*(7), 1047-1055.

Kline-Smith, S. L., Khodjakov, A., Hergert, P., & Walczak, C. E. (2004). Depletion of centromeric MCAK leads to chromosome congression and segregation defects due to improper kinetochore attachments. *Molecular biology of the cell*, *15*(3), 1146-1159.

Knowlton, A. L., Lan, W., & Stukenberg, P. T. (2006). Aurora B is enriched at merotelic attachment sites, where it regulates MCAK. *Current biology*, *16*(17), 1705-1710.

Kobayashi, T., Tsang, W. Y., Li, J., Lane, W., & Dynlacht, B. D. (2011). Centriolar kinesin Kif24 interacts with CP110 to remodel microtubules and regulate ciliogenesis. *Cell*, *145*(6), 914-925.

Kollu, S., Bakhoum, S. F., & Compton, D. A. (2009). Interplay of microtubule dynamics and sliding during bipolar spindle formation in mammalian cells. *Current Biology : CB*, *19*(24), 2108–2113.

Komarova, Y., De Groot, C. O., Grigoriev, I., Gouveia, S. M., Munteanu, E. L., Schober, J. M., Honnappa, S., Buey, R. M., Hoogenraad, C. C., Dogterom, M. and Borisy, G. G., Steinmetz M. O., & Akhmanova, A. (2009). Mammalian end binding proteins control persistent microtubule growth. *The Journal of cell biology*, *184*(5), 691-706.

Kronja, I., Kruljac-Letunic, A., Caudron-Herger, M., Bieling, P., & Karsenti, E. (2009). XMAP215–EB1 interaction is required for proper spindle assembly and chromosome segregation in Xenopus egg extract. *Molecular biology of the cell*, *20*(11), 2684-2696.

Kurinna, S., Stratton, S. A., Coban, Z., Schumacher, J. M., Grompe, M., Duncan, A. W., & Barton, M. C. (2013). p53 regulates a mitotic transcription program and determines ploidy in normal mouse liver. *Hepatology*, *57*(5), 2004-2013.

Lan, W., Zhang, X., Kline-Smith, S. L., Rosasco, S. E., Barrett-Wilt, G. A., Shabanowitz, J., Hunt, D.F., Walczak, C.E. & Stukenberg, P. T. (2004). Aurora B phosphorylates centromeric MCAK and regulates its localization and microtubule depolymerization activity. *Current Biology*, *14*(4), 273-286.

Lara-Gonzalez, P., Westhorpe, F. G., & Taylor, S. S. (2012). The spindle assembly checkpoint. *Current biology*, *22*(22), R966-R980.

Lawrence, C. J., Dawe, R. K., Christie, K. R., Cleveland, D. W., Dawson, S. C., Endow, S. A., ... & Malmberg, R. L. (2004). A standardized kinesin nomenclature. *The Journal of cell biology*, *167*(1), 19-22.

Lee, M. J., Gergely, F., Jeffers, K., Peak-Chew, S. Y., & Raff, J. W. (2001). Msps/XMAP215 interacts with the centrosomal protein D-TACC to regulate microtubule behaviour. *Nature cell biology*, *3*(7), 643-649.

Levine, M. S., Bakker, B., Boeckx, B., Moyett, J., Lu, J., Vitre, B., ... & Foijer, F. (2017). Centrosome amplification is sufficient to promote spontaneous tumorigenesis in mammals. *Developmental Cell*, *40*(3), 313-322.

Li, C., Zhang, Y., Yang, Q., Ye, F., Sun, S. Y., Chen, E. S., & Liou, Y. C. (2016). NuSAP modulates the dynamics of kinetochore microtubules by attenuating MCAK depolymerisation activity. *Scientific reports*, *6*, 18773.

Lin, C. H., Hu, C. K., & Shih, H. M. (2010). Clathrin heavy chain mediates TACC3 targeting to mitotic spindles to ensure spindle stability. *The Journal of cell biology*, *189*(7), 1097-1105.

Liu, D., Vader, G., Vromans, M. J., Lampson, M. A., & Lens, S. M. (2009). Sensing chromosome bi-orientation by spatial separation of aurora B kinase from kinetochore substrates. *Science*, *323*(5919), 1350-1353.

Lončarek, J., Kisurina-Evgenieva, O., Vinogradova, T., Hergert, P., La Terra, S., Kapoor, T. M., & Khodjakov, A. (2007). The centromere geometry essential for keeping mitosis error free is controlled by spindle forces. *Nature*, *450*(7170), 745-749.

Lukas, J., Lukas, C., & Bartek, J. (2004). Mammalian cell cycle checkpoints: signalling pathways and their organization in space and time. *DNA repair*, *3*(8), 997-1007.

MacNeal, R. K., & Purich, D. L. (1978). Stoichiometry and role of GTP hydrolysis in bovine neurotubule assembly. *Journal of Biological Chemistry*, *253*(13), 4683-4687.

Maiato, H., Sampaio, P., & Sunkel, C. E. (2004). Microtubule-associated proteins and their essential roles during mitosis. *International review of cytology*, *241*, 53-153.

Maiato, H., Gomes, A. M., Sousa, F., & Barisic, M. (2017). Mechanisms of chromosome congression during mitosis. *Biology*, *6*(1), 13.

Maney, T., Hunter, A. W., Wagenbach, M., & Wordeman, L. (1998). Mitotic centromere–associated kinesin is important for anaphase chromosome segregation. *The Journal of cell biology*, *142*(3), 787-801.

Maney, T., Wagenbach, M., & Wordeman, L. (2001). Molecular dissection of the microtubule depolymerizing activity of mitotic centromere-associated kinesin. *Journal of Biological Chemistry*, *276*(37), 34753-34758.

Manning, A. L., Ganem, N. J., Bakhoum, S. F., Wagenbach, M., Wordeman, L., & Compton, D. A. (2007). The kinesin-13 proteins Kif2a, Kif2b, and Kif2c/MCAK have distinct roles during mitosis in human cells. *Molecular biology of the cell*, *18*(8), 2970-2979.

Marumoto, T., Zhang, D., & Saya, H. (2005). Aurora-A—a guardian of poles. *Nature Reviews Cancer*, *5*(1), 42-50.

McClelland, S. E., Borusu, S., Amaro, A. C., Winter, J. R., Belwal, M., McAinsh, A. D., & Meraldi, P. (2007). The CENP-A NAC/CAD kinetochore complex controls chromosome congression and spindle bipolarity. *The EMBO journal*, *26*(24), 5033-5047.

McDonald, K. L., O'Toole, E. T., Mastronarde, D. N., & McIntosh, J. R. (1992). Kinetochore microtubules in PTK cells. *J. Cell Biol*, *118*(2), 369-383.

Mejillano, M. R., Barton, J. S., & Himes, R. H. (1990). Stabilization of microtubules by GTP analogues. *Biochemical and biophysical research communications*, *166*(2), 653-660.

Meunier, S., & Vernos, I. (2011). K-fibre minus ends are stabilized by a RanGTP-dependent mechanism essential for functional spindle assembly. *Nature Cell Biology*, *13*(12), 1406-1414.

Miki, H., Setou, M., Kaneshiro, K., & Hirokawa, N. (2001). All kinesin superfamily protein, KIF, genes in mouse and human. *Proceedings of the National Academy of Sciences*, *98*(13), 7004-7011.

Miki, H., Okada, Y., & Hirokawa, N. (2005). Analysis of the kinesin superfamily: insights into structure and function. *Trends in cell biology*, *15*(9), 467-476.
Mitchison, T., & Kirschner, M. (1984). Dynamic instability of microtubule growth. *nature*, *312*(5991), 237-242.

Mimori-Kiyosue, Y., Shiina, N., & Tsukita, S. (2000). The dynamic behavior of the APC-binding protein EB1 on the distal ends of microtubules. *Current biology*, *10*(14), 865-868.

Mitchison, T., & Kirschner, M. (1984a). Dynamic instability of microtubule growth. *nature*, *312*(5991), 237-242.

Mitchison, T., & Kirschner, M. (1984b). Microtubule assembly nucleated by isolated centrosomes. *Nature*, *312*, 232-237.

Mitelman Database of Chromosome Aberrations and Gene Fusions in Cancer (2017). Mitelman F, Johansson B and Mertens F (Eds.),
http://cgap.nci.nih.gov/Chromosomes/Mitelman

Monte, M., Collavin, L., Lazarevic, D., Utrera, R., Dragani, T. A., & Schneider, C. (2000). Cloning, chromosome mapping and functional characterization of a human homologue of murine gtse-1 (B99) gene. *Gene*, *254*(1), 229-236.

Monte, M., Benetti, R., Collavin, L., Marchionni, L., Del Sal, G., & Schneider, C. (2004). hGTSE-1 expression stimulates cytoplasmic localization of p53. *Journal of Biological Chemistry*, *279*(12), 11744-11752.

Monte, M., Benetti, R., Buscemi, G., Sandy, P., Del Sal, G., & Schneider, C. (2003). The cell cycle-regulated protein human GTSE-1 controls DNA damage-induced apoptosis by affecting p53 function. *Journal of Biological Chemistry*, *278*(32), 30356-30364.

Moore, A.T., Rankin, K.E., Von Dassow, G., Peris, L., Wagenbach, M., Ovechkina, Y., Andrieux, A., Job, D. and Wordeman, L. (2005). MCAK associates with the tips of polymerizing microtubules. *J Cell Biol*, *169*(3), 391-397.

Moore, A., & Wordeman, L. (2004). C-terminus of mitotic centromere-associated kinesin (MCAK) inhibits its lattice-stimulated ATPase activity. *Biochemical Journal*, *383*(2), 227-235.

Morgan, D. O. (1995). Principles of CDK regulation. *Nature*, *374*(6518), 131.
Musacchio, A., & Salmon, E. D. (2007). The spindle-assembly checkpoint in space and time. *Nature reviews Molecular cell biology*, *8*(5), 379-393.

Musacchio, A., & Desai, A. (2017). A molecular view of kinetochore assembly and function. *Biology*, *6*(1), 5.

Nicklas, R. B., & Ward, S. C. (1994). Elements of error correction in mitosis: microtubule capture, release, and tension. *The Journal of cell biology*, *126*(5), 1241-1253.

Nixon, F. M., Gutiérrez-Caballero, C., Hood, F. E., Booth, D. G., Prior, I. A., & Royle, S. J. (2015). The mesh is a network of microtubule connectors that stabilizes individual kinetochore fibers of the mitotic spindle. *Elife*, *4*, e07635.

Noda, Y., Sato-Yoshitake, R., Kondo, S., Nangaku, M., & Hirokawa, N. (1995). KIF2 is a new microtubule-based anterograde motor that transports membranous organelles distinct from those carried by kinesin heavy chain or KIF3A/B. *Journal of Cell Biology*, *129*(1), 157-168.

Nogales, E., Wolf, S. G., & Downing, K. H. (1998). Structure of the αβ tubulin dimer by electron crystallography. *Nature*, *391*(6663), 199-203.

Norbury, C., & Nurse, P. (1992). Animal cell cycles and their control. *Annual review of biochemistry*, *61*(1), 441-468.

O'Brien, L. L., Albee, A. J., Liu, L., Tao, W., Dobrzyn, P., Lizarraga, S. B., & Wiese, C. (2005). The Xenopus TACC homologue, maskin, functions in mitotic spindle assembly. *Molecular biology of the cell*, *16*(6), 2836-2847.

Ogawa, T., Nitta, R., Okada, Y., & Hirokawa, N. (2004). A common mechanism for microtubule destabilizers—M type kinesins stabilize curling of the protofilament using the class-specific neck and loops. *Cell*, *116*(4), 591-602.

Ohi, R., Coughlin, M. L., Lane, W. S., & Mitchison, T. J. (2003). An inner centromere protein that stimulates the microtubule depolymerizing activity of a KinI kinesin. *Developmental cell*, *5*(2), 309-321.

Ohi, R., Sapra, T., Howard, J., & Mitchison, T. J. (2004). Differentiation of cytoplasmic and meiotic spindle assembly MCAK functions by Aurora B-dependent phosphorylation. *Molecular biology of the cell*, *15*(6), 2895-2906.

Okada, M., Cheeseman, I. M., Hori, T., Okawa, K., McLeod, I. X., Yates, J. R., Desai, A. & Fukagawa, T. (2006). The CENP-H–I complex is required for the efficient incorporation of newly synthesized CENP-A into centromeres. *Nature cell biology*, *8*(5), 446-457.
Orr, B., & Compton, D. A. (2013). A double-edged sword: how oncogenes and tumor suppressor genes can contribute to chromosomal instability. *Frontiers in oncology*, *3*, 164.

Ovechkina, Y., Wagenbach, M., & Wordeman, L. (2002). K-loop insertion restores microtubule depolymerizing activity of a "neckless" MCAK mutant. *The Journal of cell biology*, *159*(4), 557-562.

Parada, L. F., Land, H., Weinberg, R. A., Wolf, D., & Rotter, V. (1984). Cooperation between gene encoding p53 tumour antigen and ras in cellular transformation.

Pardee, A. B. (1974). A restriction point for control of normal animal cell proliferation. *Proceedings of the National Academy of Sciences*, *71*(4), 1286-1290.

Paweletz, N. (2001). Walther Flemming: pioneer of mitosis research. *Nature Reviews Molecular Cell Biology*, *2*(1), 72-76.

Pearson, C. G., & Bloom, K. (2004). Dynamic microtubules lead the way for spindle positioning. *Nature Reviews Molecular Cell Biology*, *5*(6), 481-492.

Peng, Y., Chen, L., Li, C., Lu, W., & Chen, J. (2001). Inhibition of MDM2 by hsp90 contributes to mutant p53 stabilization. *Journal of Biological Chemistry*, *276*(44), 40583-40590.

Peset, I., & Vernos, I. (2008). The TACC proteins: TACC-ling microtubule dynamics and centrosome function. *Trends in cell biology*, *18*(8), 379-388.

Peset, I., Seiler, J., Sardon, T., Bejarano, L. A., Rybina, S., & Vernos, I. (2005). Function and regulation of Maskin, a TACC family protein, in microtubule growth during mitosis. *J Cell Biol*, *170*(7), 1057-1066.

Peters, J. M., Tedeschi, A., & Schmitz, J. (2008). The cohesin complex and its roles in chromosome biology. *Genes & development*, *22*(22), 3089-3114.

Petry, S. (2016). Mechanisms of mitotic spindle assembly. *Annual review of biochemistry*, *85*, 659-683.

Pines, J. (1991). Cyclins: wheels within wheels. *Cell growth & differentiation: the molecular biology journal of the American Association for Cancer Research*, *2*(6), 305-310.

Popov, A. V., Severin, F., & Karsenti, E. (2002). XMAP215 is required for the microtubule-nucleating activity of centrosomes. *Current biology*, *12*(15), 1326-1330.

Prosser, S. L., & Pelletier, L. (2017). Mitotic spindle assembly in animal cells: a fine balancing act. *Nature Reviews Molecular Cell Biology*, *18*(3), 187-201.

Przewloka, M. R., Venkei, Z., Bolanos-Garcia, V. M., Debski, J., Dadlez, M., & Glover, D. M. (2011). CENP-C is a structural platform for kinetochore assembly. *Current Biology*, *21*(5), 399-405.

Ran, F. A., Hsu, P. D., Wright, J., Agarwala, V., Scott, D. A., & Zhang, F. (2013). Genome engineering using the CRISPR-Cas9 system. *Nature protocols*, *8*(11), 2281-2308.

Rankin, K. E., & Wordeman, L. (2010). Long astral microtubules uncouple mitotic spindles from the cytokinetic furrow. *The Journal of cell biology*, *190*(1), 35-43.

Rieder, C. L. (1981). The structure of the cold-stable kinetochore fiber in metaphase PtK1 cells. *Chromosoma*, *84*(1), 145-158.

Rieder, C. L. (1982). The formation, structure, and composition of the mammalian kinetochore and kinetochore fiber. *International review of cytology*, *79*, 1-58.

Rieder, C. L., Schultz, A., Cole, R., & Sluder, G. (1994). Anaphase onset in vertebrate somatic cells is controlled by a checkpoint that monitors sister kinetochore attachment to the spindle. *Journal of Cell Biology*, *127*(5), 1301-1310.

Rieder, C. L., Cole, R. W., Khodjakov, A., & Sluder, G. (1995). The checkpoint delaying anaphase in response to chromosome monoorientation is mediated by an inhibitory signal produced by unattached kinetochores. *The Journal of cell biology*, *130*(4), 941-948.

Rieder, C. L. (2005). Kinetochore fiber formation in animal somatic cells: dueling mechanisms come to a draw. *Chromosoma*, *114*(5), 310-318.

Ritter, A., Sanhaji, M., Friemel, A., Roth, S., Rolle, U., Louwen, F., & Yuan, J. (2015a). Functional analysis of phosphorylation of the mitotic centromere-associated kinesin by Aurora B kinase in human tumor cells. *Cell cycle*, *14*(23), 3755-3767.

Ritter, A., Sanhaji, M., Steinhäuser, K., Roth, S., Louwen, F., & Yuan, J. (2015b). The activity regulation of the mitotic centromere-associated kinesin by Polo-like kinase 1. *Oncotarget*, *6*(9), 6641.

Ritter, A., Kreis, N. N., Louwen, F., Wordeman, L., & Yuan, J. (2016). Molecular insight into the regulation and function of MCAK. *Critical reviews in biochemistry and molecular biology*, *51*(4), 228-245.

Rizk, R. S., Bohannon, K. P., Wetzel, L. A., Powers, J., Shaw, S. L., & Walczak, C. E. (2009). MCAK and paclitaxel have differential effects on spindle microtubule organization and dynamics. *Molecular biology of the cell*, *20*(6), 1639-1651.

Rogers, S. L., Rogers, G. C., Sharp, D. J., & Vale, R. D. (2002). Drosophila EB1 is important for proper assembly, dynamics, and positioning of the mitotic spindle. *The Journal of cell biology*, *158*(5), 873-884.

Royle, S. J., Bright, N. A., & Lagnado, L. (2005). Clathrin is required for the functionof the mitotic spindle. *Nature* 434, 1152-1157.

Royle, S. J., & Lagnado, L. (2006). Trimerisation is important for the function of clathrin at the mitotic spindle. *Journal of cell science*, *119*(19), 4071-4078.

Sanhaji, M., Friel, C. T., Kreis, N. N., Krämer, A., Martin, C., Howard, J., Strebhardt, K. & Yuan, J. (2010). Functional and spatial regulation of mitotic centromere-associated kinesin by cyclin-dependent kinase 1. *Molecular and cellular biology*, *30*(11), 2594-2607.

Sanhaji, M., Ritter, A., Belsham, H. R., Friel, C. T., Roth, S., Louwen, F., & Yuan, J. (2014). Polo-like kinase 1 regulates the stability of the mitotic centromere-associated kinesin in mitosis. *Oncotarget*, *5*(10), 3130-3144.

Santaguida, S., & Musacchio, A. (2009). The life and miracles of kinetochores. *The EMBO journal*, *28*(17), 2511-2531.

Saxton, W. M., Stemple, D. L., Leslie, R. J., Salmon, E. D., Zavortink, M., & McIntosh, J. R. (1984). Tubulin dynamics in cultured mammalian cells. *J. Cell Biol*, *99*(2), 175-2.

Schmiesing, J. A., Gregson, H. C., Zhou, S., & Yokomori, K. (2000). A human condensin complex containing hCAP-C–hCAP-E and CNAP1, a homolog of Xenopus XCAP-D2, colocalizes with phosphorylated histone H3 during the early stage of mitotic chromosome condensation. *Molecular and cellular biology*, *20*(18), 6996-7006.

Schvartzman, J. M., Sotillo, R., & Benezra, R. (2010). Mitotic chromosomal instability and cancer: mouse modelling of the human disease. *Nature Reviews Cancer*, *10*(2), 102-115.

Scolz, M., Widlund, P.O., Piazza, S., Bublik, D.R., Reber, S., Peche, L.Y., Ciani, Y., Hubner, N., Isokane, M., Monte, M. and Ellenberg, J. (2012). GTSE1 is a microtubule plus-end tracking protein that regulates EB1-dependent cell migration. *PLoS One*, *7*(12), e51259.

Screpanti, E., De Antoni, A., Alushin, G. M., Petrovic, A., Melis, T., Nogales, E., & Musacchio, A. (2011). Direct binding of Cenp-C to the Mis12 complex joins the inner and outer kinetochore. *Current Biology*, *21*(5), 391-398.

Seetapun, D., Castle, B. T., McIntyre, A. J., Tran, P. T., & Odde, D. J. (2012). Estimating the microtubule GTP cap size in vivo. *Current Biology*, *22*(18), 1681-1687.

Shao, H., Huang, Y., Zhang, L., Yuan, K., Chu, Y., Dou, Z., Jin, C., Garcia-Barrio, M., Liu, X. and Yao, X. (2015). Spatiotemporal dynamics of Aurora B-PLK1-MCAK signaling axis orchestrates kinetochore bi-orientation and faithful chromosome segregation. *Scientific reports*, *5*, 12204.

Sharp, D. J., Rogers, G. C., & Scholey, J. M. (2000). Microtubule motors in mitosis. *Nature*, *407*(6800), 41-47.

Shipley, K., Hekmat-Nejad, M., Turner, J., Moores, C., Anderson, R., Milligan, R., Sakowicz, R. and Fletterick, R. (2004). Structure of a kinesin microtubule depolymerization machine. *The EMBO journal*, *23*(7), 1422-1432.

Spiegelman, B. M., Penningroth, S. M., & Kirschner, M. W. (1977). Turnover of tubulin and the N site GTP in Chinese hamster ovary cells. *Cell*, *12*(3), 587-600.

Srayko, M., Quintin, S., Schwager, A., & Hyman, A. A. (2003). Caenorhabditis elegans TAC-1 and ZYG-9 form a complex that is essential for long astral and spindle microtubules. *Current biology*, *13*(17), 1506-1511.

Stevermann, L., & Liakopoulos, D. (2012). Molecular mechanisms in spindle positioning: structures and new concepts. *Current opinion in cell biology*, *24*(6), 816-824.

Stirling, P.C., Bloom, M.S., Solanki-Patil, T., Smith, S., Sipahimalani, P., Li, Z., Kofoed, M., Ben-Aroya, S., Myung, K. and Hieter, P. (2011). The complete spectrum of yeast chromosome instability genes identifies candidate CIN cancer genes and functional roles for ASTRA complex components. *PLoS Genet*, *7*(4), e1002057.

Stout, J. R., Yount, A. L., Powers, J. A., LeBlanc, C., Ems-McClung, S. C., & Walczak, C. E. (2011). Kif18B interacts with EB1 and controls astral microtubule length during mitosis. *Molecular biology of the cell*, *22*(17), 3070-3080.

Talapatra, S. K., Harker, B., & Welburn, J. P. (2015). The C-terminal region of the motor protein MCAK controls its structure and activity through a conformational switch. *Elife*, *4*, e06421.

Tanenbaum, M. E., Macurek, L., van der Vaart, B., Galli, M., Akhmanova, A., & Medema, R. H. (2011a). A complex of Kif18b and MCAK promotes microtubule depolymerization and is negatively regulated by Aurora kinases. *Current Biology*, *21*(16), 1356-1365.

Tanenbaum, M. E., Medema, R., & Akhmanova, A. (2011b). Regulation of localization and activity of the microtubule depolymerase MCAK. *Bioarchitecture*, *1*(2), 80-87.

Tanenbaum, M. E., & Medema, R. H. (2011c). Localized Aurora B activity spatially controls non-kinetochore microtubules during spindle assembly. *Chromosoma*, *120*(6), 599–607. http://doi.org/10.1007/s00412-011-0334-9.

Thiru, P., Kern, D. M., McKinley, K. L., Monda, J. K., Rago, F., Su, K. C., Tsinman, T., Yarar, D., Bell, G.W. & Cheeseman, I. M. (2014). Kinetochore genes are coordinately up-regulated in human tumors as part of a FoxM1-related cell division program. *Molecular biology of the cell*, *25*(13), 1983-1994.

Thompson, S. L., & Compton, D. A. (2008). Examining the link between chromosomal instability and aneuploidy in human cells. *J Cell Biol*, *180*(4), 665-672.

Thompson, S. L., & Compton, D. A. (2010). Proliferation of aneuploid human cells is limited by a p53-dependent mechanism. *The Journal of cell biology*, jcb-200905057.

Thompson, S. L., & Compton, D. A. (2011). Chromosome missegregation in human cells arises through specific types of kinetochore–microtubule attachment errors. *Proceedings of the National Academy of Sciences*, *108*(44), 17974-17978.

Tournebize, R., Popov, A., Kinoshita, K., Ashford, A.J., Rybina, S., Pozniakovsky, A., Mayer, T.U., Walczak, C.E., Karsenti, E. & Hyman, A.A. (2000). Control of microtubule dynamics by the antagonistic activities of XMAP215 and XKCM1 in Xenopus egg extracts. *Nature cell biology*, *2*(1), 13-19.

Trowitzsch, S., Bieniossek, C., Nie, Y., Garzoni, F., & Berger, I. (2010). New baculovirus expression tools for recombinant protein complex production. *Journal of structural biology*, *172*(1), 45-54.

Uehara, R., Tsukada, Y., Kamasaki, T., Poser, I., Yoda, K., Gerlich, D. W., & Goshima, G. (2013). Aurora B and Kif2A control microtubule length for assembly of a functional central spindle during anaphase. *J Cell Biol*, *202*(4), 623-636.

Utrera, R., Collavin, L., Lazarević, D., Delia, D., & Schneider, C. (1998). A novel p53-inducible gene coding for a microtubule-localized protein with G2-phase-specific expression. *The EMBO Journal*, *17*(17), 5015-5025.

Vale, R. D., Reese, T. S., & Sheetz, M. P. (1985). Identification of a novel force-generating protein, kinesin, involved in microtubule-based motility. *Cell*, *42*(1), 39-50.

Vanneste, E., Voet, T., Melotte, C., Debrock, S., Sermon, K., Staessen, C., Liebaers, I., Fryns, J.P., D'hooghe, T. & Vermeesch, J. R. (2009). What next for preimplantation genetic screening? High mitotic chromosome instability rate provides the biological basis for the low success rate. *Human reproduction*, *24*(11), 2679-2682.

Van Stedum, S., & King, W. (2003). Basic FISH techniques and troubleshooting. *Molecular cytogenetics: protocols and applications*, 51-63.

Vitre, B., Coquelle, F. M., Heichette, C., Garnier, C., Chrétien, D., & Arnal, I. (2008). EB1 regulates microtubule dynamics and tubulin sheet closure in vitro. *Nature cell biology*, *10*(4), 415-421.

Walczak, C. E., Mitchison, T. J., & Desai, A. (1996). XKCM1: a Xenopus kinesin-related protein that regulates microtubule dynamics during mitotic spindle assembly. *Cell*, *84*(1), 37-47.

Walczak, C. E., Gan, E. C., Desai, A., Mitchison, T. J., & Kline-Smith, S. L. (2002). The microtubule-destabilizing kinesin XKCM1 is required for chromosome positioning during spindle assembly. *Current biology*, *12*(21), 1885-1889.

Wang, F., Dai, J., Daum, J. R., Niedzialkowska, E., Banerjee, B., Stukenberg, P. T., Gorbsky, G.J. & Higgins, J. M. (2010). Histone H3 Thr-3 phosphorylation by Haspin positions Aurora B at centromeres in mitosis. *Science*, *330*(6001), 231-235.

Wang, W., Shen, T., Guerois, R., Zhang, F., Kuerban, H., Lv, Y., ... & Wang, C. (2015). New insights into the coupling between microtubule depolymerization and ATP hydrolysis by kinesin-13 protein Kif2C. *Journal of Biological Chemistry*, *290*(30), 18721-18731.

Waters, J. C., Mitchison, T. J., Rieder, C. L., & Salmon, E. D. (1996). The kinetochore microtubule minus-end disassembly associated with poleward flux produces a force that can do work. *Molecular Biology of the Cell*, *7*(10), 1547-1558.

Weaver, B. A., & Cleveland, D. W. (2006). Does aneuploidy cause cancer?. *Current opinion in cell biology*, *18*(6), 658-667.

Weir, J. R., Faesen, A. C., Klare, K., Petrovic, A., Basilico, F., Fischböck, J., Pentakota, S., Keller, J., Pesenti, M. E., Pan, D., Wohlgemuth, S., Herzog, F., Musacchio, A. & Vogt, D. (2016). Insights from biochemical reconstitution into the architecture of human kinetochores. *Nature*.

Weisenberg, R. C., Broisy, G. G., & Taylor, E. W. (1968). Colchicine-binding protein of mammalian brain and its relation to microtubules. *Biochemistry*, *7*(12), 4466-4479.

Weisenberg, R. C., Deery, W. J., & Dickinson, P. J. (1976). Tubulin-nucleotide interactions during the polymerization and depolymerization of microtubules. *Biochemistry*, *15*(19), 4248-4254.

Wieczorek, M., Chaaban, S., & Brouhard, G. J. (2013). Macromolecular crowding pushes catalyzed microtubule growth to near the theoretical limit. *Cellular and Molecular Bioengineering*, *6*(4), 383-392.

Wieczorek, M., Bechstedt, S., Chaaban, S., & Brouhard, G. J. (2015). Microtubule-associated proteins control the kinetics of microtubule nucleation. *Nature cell biology*, *17*(7), 907-916.

Wigge, P. A., & Kilmartin, J. V. (2001). The Ndc80p complex from Saccharomyces cerevisiae contains conserved centromere components and has a function in chromosome segregation. *The Journal of cell biology*, *152*(2), 349-360.

Wilbur, J. D., & Heald, R. (2013). Mitotic spindle scaling during Xenopus development by kif2a and importin α. *Elife*, *2*, e00290.

Witt, P. L., Ris, H., & Borisy, G. G. (1981). Structure of kinetochore fibers: microtubule continuity and inter-microtubule bridges. *Chromosoma*, *83*(4), 523-540.

Wordeman, L., & Mitchison, T. J. (1995). Identification and partial characterization of mitotic centromere-associated kinesin, a kinesin-related protein that associates with centromeres during mitosis. *The Journal of cell biology*, *128*(1), 95-104.

Wordeman, L., Wagenbach, M., & Maney, T. (1999). Mutations in the ATP-binding domain affect the subcellular distribution of mitotic centromere-associated kinesin (MCAK). *Cell biology international*, *23*(4), 275-286.

Wordeman, L. (2005). Microtubule-depolymerizing kinesins. *Current opinion in cell biology*, *17*(1), 82-88.

Zanic, M., Stear, J. H., Hyman, A. A., & Howard, J. (2009). EB1 recognizes the nucleotide state of tubulin in the microtubule lattice. *PloS one*, *4*(10), e7585.

Zhai, Y., Kronebusch, P. J., & Borisy, G. G. (1995). Kinetochore microtubule dynamics and the metaphase-anaphase transition. *Journal of Cell Biology*, *131*(3), 721-734.

Zhai, Y., Kronebusch, P. J., Simon, P. M., & Borisy, G. G. (1996). Microtubule dynamics at the G2/M transition: abrupt breakdown of cytoplasmic microtubules at nuclear envelope

breakdown and implications for spindle morphogenesis. *Journal of Cell Biology*, *135*(1), 201-214.

Zhang, X., Lan, W., Ems-McClung, S. C., Stukenberg, P. T., & Walczak, C. E. (2007). Aurora B phosphorylates multiple sites on mitotic centromere-associated kinesin to spatially and temporally regulate its function. *Molecular biology of the cell*, *18*(9), 3264-3276.

Zhang, X., Ems-McClung, S. C., & Walczak, C. E. (2008). Aurora A phosphorylates MCAK to control ran-dependent spindle bipolarity. *Molecular biology of the cell*, *19*(7), 2752-2765.

Zhang, L., Shao, H., Huang, Y., Yan, F., Chu, Y., Hou, H., ... & Ding, X. (2011). PLK1 phosphorylates mitotic centromere-associated kinesin and promotes its depolymerase activity. *Journal of Biological Chemistry*, *286*(4), 3033-3046.

Zong, H., Carnes, S. K., Moe, C., Walczak, C. E., & Ems-McClung, S. C. (2016). The far C-terminus of MCAK regulates its conformation and spindle pole focusing. *Molecular biology of the cell*, *27*(9), 1451-1464.

Acknowledgements

First and foremost, I would like to thank my Ph.D. advisor Dr. Alex Bird. I am happy that he believed in me and gave me a chance to be his first Ph.D. student. Alex has always been very motivating and supportive and has given me the freedom to test my ideas. I sincerely appreciate his contribution of ideas and time that has made my Ph.D. productive. I would like to sincerely thank him for all his efforts and help in improving my presentation and writing skills.

I would like to thank all the past and present members of the Bird lab who have immensely contributed to my professional and personal life. I would like to sincerely thank all of them for creating and maintaining a very friendly and homely atmosphere in the lab. I would like to thank Brenda Aguero and Julian Berlitz for helping me getting started in Dortmund. I am thankful to Yu-Chih Lin who taught me several techniques in molecular biology and biochemistry and always provided nice tips and advices on improving experiments. I would like to acknowledge Arnaud Rondelet who has always been a good friend with whom I have had great scientific discussions. I very much appreciate his joyfulness, enthusiasm, willingness to always help, teach and advice me. I would like to sincerely thank him for introducing me to the field of BAC recombineering and Cas9 gene editing technique. I would like to thank Divya Singh, a dear friend, who stood besides me through thick and thin and made difficult times seem easy. I would also like to thank her for teaching me *in vitro* phosphorylation assays and pull-downs. I would like to thank Divya and Arnaud for proofreading my thesis. I am also grateful to Nadine Schmidt for her help in generating cell lines, cloning and purification of GTSE1 fragments. She is a very dear friend and has always helped me with difficult German bureaucratic work. I would also like to acknowledge Dominic Heinecke for his help with purifying GTSE1 fragments. I would like to thank all the master students and interns: Lisa Mazul, Julian Berlitz, and Vanessa Garius for helping me in my project.

I would like to acknowledge all the past and present members of the Vader group, especially, Gerben Vader, Lisa-Marie Kuhl, Janine Beermann, Maria-Ascension Villar-Fernandez, Vivek Raina (VBR), Richard Cardoso da Silva and Elisabeth Weir for their equal contribution in generating a joyful and friendly lab environment. Gerben's knowledge and

enthusiasm for research has always motivated me and I would like to express my sincerest gratitude towards him. I am grateful to Janine Beermann who patiently taught me protein purification from insect cells.

My sincere thanks to my TAC committee members: Dr. Gerben Vader and Dr. Leif Dehmelt for their time and helpful suggestions.

It has been a pleasure to work in department one, as it has been a constant source of collaborations and friendships. I would like to express my sincerest gratitude to Prof. Dr. Andrea Musacchio for being my official Ph.D. supervisor, and for his time and insightful discussions throughout my Ph.D. I would like to acknowledge Alex Faesen for teaching and helping me with microtubule sedimentation assays and protein purification. I sincerely appreciate Stefano Maffini's help with performing and analyzing photoactivation experiments and for suggesting ideas for experiments. I would also like to thank Marta Mattiuzzo for teaching me FISH, and Kerstin Killinger for helping with bacterial protein purification. I would like to thank Satyakrishna Pentakota for teaching and helping me with Size Exclusion Chromatography. I am very grateful to Katharina Overlack for her help with writing the Zusammenfassung. I would also like to thank the entire department one for making my time at the institute enjoyable.

I would like to express my sincere gratitude towards Conrad Hall and Dr. Gary Brouhard for providing us purified MCAK protein and for performing MCAK depolymerization assays in presence and absence of GTSE1 using TRIF. I would like to thank Dr. Duane Compton for providing the U2OS PA-GFP-tubulin and HCT116 p53-/- cell lines.

My Ph.D. work was supported by an IMPRS-CMB fellowship. I would like to thank Christa Hornemann for being my support system since the day I started working at the Max Planck Institute. I would also like to thank Antje Peukert and Lucia Sironi for helping with administrative and scientific difficulties. I would also like to thank the IMPRS-CMB for organizing retreats, symposiums and for providing funding for conferences.

I would especially like to thank all my friends and family who have always supported me when I needed them the most. My parents, sister and grandparents have always inspired me and I am eternally indebted to them for making me what I am today. I have come so far only because of their love, encouragement and their confidence in me.

Last but not the least, I want to thank Amogh for being very supportive, patient and for always encouraging me. I would also like to thank Amogh's family for their constant support.

Curriculum vitae

Der Lebenslauf ist in der Online-Version aus Gründen des Datenschutzes nicht enthalten.